universität wien

DIPLOMARBEIT / DIPLOMA THESIS

Titel der Diplomarbeit / Title of the Diploma Thesis

Biochemical characterization of the central carbohydrate metabolism in *Arabidopsis thaliana* during extended night exposure

verfasst von / submitted by

Lydia Sophie Priglinger

angestrebter akademischer Grad / in partial fulfilment of the requirements for the degree of

Magistra der Naturwissenschaften (Mag.rer.nat.)

Wien, 2017 / Vienna, 2017

Studienkennzahl lt. Studienblatt / degree programme code as it appears on the student record sheet:	A 190 445 299
Studienrichtung lt. Studienblatt / degree programme as it appears on the student record sheet:	Lehramtsstudium UF Biologie und Umweltkunde UF Psychologie und Philosophie
Betreut von / Supervisor:	Univ.-Prof. Dr. Wolfram Weckwerth
Mitbetreut von / Co-Supervisor:	Dipl.-Biol. Dr. Thomas Nägele

Acknowledgments

It fills me with great gratitude to realize how many people supported me throughout my studies, enhancing my life in various respects. I want to express my appreciation for all of them. I would like to thank the following persons in particular, as they played important roles in the process of writing my diploma thesis:

Wolfram for providing the opportunity to write at the MOSYS department

Thomas for taking the time to answer all my questions, for offering insights, and for providing support every step of the way

Alex, Lisa, Jana and Jakob for sharing meals, fruitful conversations and wine

My parents for their encouragement, for inspiring me to pursue whatever goal I have in life, and not least for their patience and financial support

Moritz for being a motivational role model

My roommate Amanda for keeping my dog, Rigo, company while I spent time at university

Rigo for his patience, never complaining about my absence but instead being the most faithful companion I could imagine

I am grateful for my long-lasting friendships with Anita, Lisa-Marie, Johann, Kerstin and Tanja. I am also thankful for a very enriching relationship with Stefan. The countless joyful hours with you are a truly important aspect of my life.

Further, I want to thank all the professors, lecturers and teachers who sustained my enthusiasm for the field of biology throughout my studies.

Abbreviations

µM	Micromolar; Micromol per litre
µmol	Micromol; 10^{-6} Mol
3-PGA	3-Phosphoglyceric acid
ABA	Abscisic acid
ADP	Adenosine diphosphate
AGPase	ADP-glucose pyrophosphorylase
Ami-RNA	Artificial microRNA
AMP	Adenosine monophosphate
AMPK	5' adenosine monophosphate-activated protein kinase
ATP	Adenosine triphosphate
BAMs	β-Amylases
BEs	Branching enzymes
bZIP	Basic leucine zipper
CCA1	Circadian Clock Associated 1
cDNA	Complementary DNA
cFBPase	Cytosolic fructose 1,6bisphosphatase
CH	Carbohydrate(s)
CO2	Carbon dioxide
cPGM	Cytosolic phosphoglucomutase
DBEs	Debranching enzymes
EN	Extended night
F2KP	Fructose-2-6-bisphosphatase
F6P	Fructose-6-phosphate
Fkin	Fructokinase
G1P	Glucose-1-phosphate
G6P	Glucose-6-phosphate

G6PDH	Glucose-6-phosphate dehydrogenase
GC-TOF	Gas chromatography coupled to time-of-flight mass spectrometry
gFW	Gram fresh weight
GI	Gigantea
Gkin	Glucokinase
GWD	α-glucan water dikinase
HK	Hexokinase
HMGR	3-hydroxymethyl-3-methylglutaryl-CoA reductase
IC-MS	Ion chromatography coupled to triple quadrupole mass spectrometry
Inv	Invertase
LHY	Late Elongated Hypocotyl
m/z ratio	Mass-to-charge ratio
min	Minutes
mM	Millimolar; Millimol per litre
mmol	Millimol; 10^{-3} Mol
NAD	Nicotinamide adenine dinucleotide
NADP	Nicotinamide adenine dinucleotide phosphate
NR	Nitrate reductase
PGI	Phosphoglucose-isomerase
P_i	Anorganic phosphate
PWD	Phosphoglucan water dikinase
rpm	Revolutions per minute
SnAK	SnRK1-activating kinase
SNF1	Sucrose non-fermenting 1 protein kinase
SnRK	SNF1-related protein kinase
SPP	Sucrose-phosphate phosphatase
SPS	Sucrose-phosphate synthase

SSs	Starch synthases
Suc	Sucrose
SuSy	Sucrose Synthase
T6P	Trehalose-6-phosphate
TCA cycle	Tricarboxylic acid cycle
T-DNA	Transfer DNA
TIC	Time for coffee (gene)
T-loop	Threonine residue at the activation site of the catalytic subunit of a protein kinase
TOR	Target of rapamycin
TPP	Trehalose-6-phosphate phosphatase
TPS	Trehalose-6-phosphate synthase
UDPG	Uridine diphosphate glucose
UGPase	UDP-glucose-phyrophosphorylase
$\mathbf{v_{max}}$	Maximum activity

Table of Contents

1 Introduction

1.1 The Central Carbohydrate Metabolism in Higher Plants

As photoautotrophic organisms, plants synthesize organic carbon molecules from atmospheric carbon dioxide (CO_2) in their chloroplasts. Photosynthesis is subdivided in primary and secondary reactions. Light reactions result in the generation of adenosine triphosphate (ATP) and reduced nicotinamide adenine dinucleotide phosphate (NADPH) through an electron transport chain and a proton gradient across the thylakoid membrane. In the secondary reactions, CO_2 is fixed in the Calvin-Benson cycle being located in the chloroplast stroma (Pribil, Leister 2016). The assimilated carbon is either used for starch synthesis within the chloroplast or exported to the cytosol in the form of triose phosphates for sucrose synthesis (Figure 1) and/or subsequent distribution to heterotrophic organs and tissues (Flugge 1999; Zeeman et al. 2007).

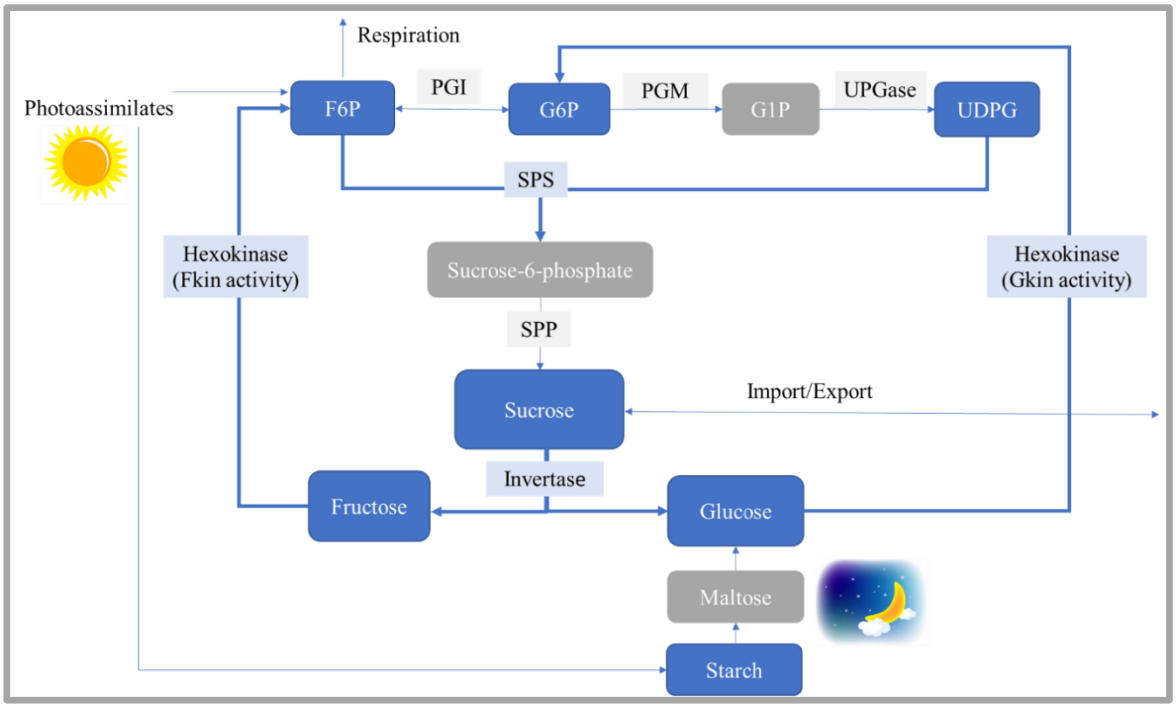

Figure 1 **Model of the central carbohydrate metabolism** in Arabidopsis; blue boxes indicate that the metabolite concentration and enzyme activity was quantified in the present study. SPS = sucrose phosphate synthase, SPP = sucrose phosphate phosphatase, F6P = fructose-6-phosphate, Fkin = fructokinase, G6P = glucose-6-phosphate, Gkin = glucokinase, UDPG = UDP-glucose, UGPase = UDP-glucose-phyrophosphorylase, G1P = glucose-1-phosphate, PGM = phosphoglucomutase, PGI = phosphoglucose-isomerase.

Carbohydrates (CH) are constantly needed to fuel glycolysis and the tricarboxylic acid (TCA) cycle for the synthesis of ATP and NADH. Furthermore, carbon skeletons are substrate for diverse biosynthetic reactions, e.g. for organic acids, amino acids and polysaccharides. Under specific situations, secondary metabolites are synthesized to enhance stress resistance, e.g. against abiotic stress or pathogens or herbivores (Sturm 1999). Efficient carbon partitioning is vital for plant growth and thus should be tightly regulated (Kolling et al. 2015; Sturm 1999; Smith, Stitt 2007). The central carbohydrate metabolism of plants (Figure 1) is a complex network including various branching points, subcellular compartmentalization and futile cycles (Nägele et al. 2010).

Sucrose metabolism

Sucrose represents a main transport sugar in higher plants, and, hence, its allocation has to be tightly regulated with regard to the actual need of specific tissues (Sturm 1999). In source tissue, sucrose-phosphate synthase (SPS) catalyses the rate limiting step of sucrose biosynthesis. In this reaction, sucrose-6-phosphate (S6P) is synthesized from uridine 5'-diphosphoglucose (UDPG) and fructose-6-phosphate (F6P). Subsequently, S6P is rapidly converted to sucrose by sucrose-phosphate phosphatase (SPP) releasing inorganic phosphate, P_i (Ruan 2014). For a long time, SPS alone was considered the rate limiting step in sucrose biosynthesis, but recent studies reveal a controversial, and possibly also regulatory impact of SPP (Albi et al. 2016). The kinetic properties of SPS are well characterized: Glucose-6-phosphate (G6P) acts as an allosteric activator, while Pi represents an inhibitor. Both effectors alter substrate affinity, thereby influencing the kinetic properties of the enzyme. Additionally, SPS is regulated by reversible phosphorylation on multiple serine residues (Huber, Huber 1996).

Trehalose, another non-reducing disaccharide, is also synthesized in two enzymatic steps. In a first step, trehalose-6-phosphate is synthesised from UDP-glucose and glucose-6-phosphate. This reaction is catalysed by trehalose-6-phosphate synthase (TPS). In a second step, T6P is dephosphorylated by trehalose-6-phosphate phosphatase (TPP) (Ruan 2014). Trehalose, as well as T6P, are present *in vivo* at very low micromolar concentrations. T6P has been discussed to play a central role in sucrose sensing, as its level correlates with sucrose content across a wide range of physiological concentrations (Lunn et al. 2014).

Sucrose cleavage is catalysed by invertase and sucrose synthase (SuSy). The difference consists in the products of cleavage: sucrose synthase degrades sucrose into UDP-glucose and fructose, while invertase activity results in glucose and fructose (Ruan 2014). A debate about the physiological role of invertase in mature leaves, as well as the differentiation from SuSy function, is still ongoing. SuSy yields UDP glucose, which can fuel respiration without the ATP consuming pathway of hexose phosphorylation. This feature is especially important under oxygen limitation (Koch 2004). While some authors conclude just a minor role of SuSy based on lower activities measured (Kingston-Smith et al. 1999), a recent study argued in favour of an important function of SuSy for starch and cell wall synthesis in Arabidopsis (Baroja-Fernandez et al. 2012).

As their substrate sucrose as well as the reaction products (hexoses) have a dual function in being nutrients and important signalling molecules, invertase enzymes are key players in plant development and reaction to environmental cues (Roitsch, Gonzalez 2004). Invertases manifest a higher potential to alter sugar signalling, as they produce twice as much free hexoses than SuSy. Furthermore, catalytic activity of specific invertase isoforms in the vacuole could play a role in the regulation of sucrose compartmentalization (Koch 2004). Pools of vacuolar sucrose were shown to constitute a transient sugar storage besides starch (Kingston-Smith et al. 1999). While SuSy is known to be active in the cytoplasm, more distinct invertase isoforms exist which are located at different compartments and vary in terms of their biochemical properties (Sturm 1999). Vacuolar invertases are soluble proteins with a pH optimum of 4.5 to 5. Cell-wall bound invertases exhibit similar biochemical properties, as they cleave sucrose at comparably acidic conditions and also cleave sucrose at its fructose residue. These two acid invertases are thus classified as fructofuranosidases. They also cleave other oligosaccharides containing fructose, like raffinose or stachyose. In contrast, the third group, the neutral invertases, are restrained to sucrose cleavage. They show a more alkaline pH optimum of 7 to 7.8. They are not inhibited by heavy metal ions, but share the feature of sensitivity to inhibition by glucose and fructose with the acid invertases. For acid invertases, glucose was suggested as a non-competitive inhibitor, while the type of interaction with fructose was classified as competitive (Sturm, 1999).

In plants, each isoform of the enzyme is encoded by a different gene (Sturm 1999). Although the multiple forms can be roughly classified into acid and alkaline invertases as

described above, the existence of numerous genes facilitates a fine regulation of sucrose cleavage already at the genetic level. Gene expression for the isoforms varies significantly depending on tissue, growth stage and plant species, even amongst the individual members of an isoform, e.g. cell-wall bound invertases (Tymowska-Lalanne, Kreis 1998).

Hexose phosphorylation

In order to be available for metabolic processes, glucose and fructose are activated by phosphorylation. Particularly in the processes of carbohydrate mobilization from sucrose or starch at night or in sink tissues, hexose phosphorylation is indispensable for plant metabolism. Furthermore, hexokinase has been shown to play a crucial role in sugar sensing (Granot et al. 2014). Free hexoses, resulting from sucrose cleavage, are phosphorylated in plants by two enzyme families: Fructokinase only phosphorylates fructose, while hexokinases can use different sugar substrates, including both glucose and fructose (Granot 2008). *In vivo*, fructose is suggested to be primarily phosphorylated by fructokinase, as the affinity of hexokinases for fructose is distinctly lower. Hexokinase activity is non-competitively inhibited by the product G6P, but the degree of sensitivity varies strongly between isoforms (Claeyssen, Rivoal 2007). Fructose phosphorylation might likewise be inhibited by F6P (Nägele, Weckwerth 2014).

A repeated cleavage and resynthesis of sucrose, termed ‘futile cycling’ was described already decades ago (see e.g. Huber 1989). Although this procedure is energetically wasteful as re-phosphorylation of released hexoses consumes ATP, it might provide accurate control over carbohydrate partitioning and could constitute a necessary factor for inhibition of photosynthesis at light.

So far, fructokinase has not been shown to act in fructose sensing (Granot et al. 2014), but a hexokinase-based glucose-sensing pathway is well established (Moore et al. 2003; Sheen 2014). Experiments with Arabidopsis mutants lacking hexokinase 1 revealed an essential role of hexokinases in sensing the plants glucose levels, furthermore interconnecting its nutrient status, light conditions and hormone signalling. This signalling function was found to act independently of the enzymes catalytic activity, pointing towards a dual role of hexokinases (Moore et al. 2003).

As indicated in the illustration of the central CH metabolism (Figure 1), F6P can be transformed to G6P and *vice versa*. This isomerisation reaction is catalysed by phosphoglucose isomerase (PGI). Cytosolic phosphoglucomutase (cPGM) converts G6P into G1P, which is the substrate for UDP-glucose synthesis by the enzyme UDP-glucose phyrophosphorylase (UGPase) (Stitt et al. 2010). Via these intermediate reactions, F6P can for instance fuel the UDP-glucose pool, making an interpretation of functional connections between changes in pool size and pathway activities very difficult (Claeyssen, Rivoal 2007). Nevertheless, hexose phosphates are discussed as an indicator for the general carbon status of a plant, and a distinct decrease is associated with carbohydrate limitation (Usadel et al. 2008). F6P and G6P are predominantly located in the cytosol, but are also present in plastids due to their connection to leaf starch synthesis (Szecowka et al. 2013).

The physiological importance of glucose-6-phosphate is often emphasized, as it is situated at the intersection of several important pathways. It supplies glycolysis and thus mitochondrial respiration, provides substrate for sucrose or starch synthesis, as well as for trehalose synthesis. Conversely, it is also the product of photosynthetic carbohydrate synthesis and carbohydrate degradation (Sulpice et al. 2014; Granot 2008). Although photosynthesis massively increases the flux into G6P, its levels respond with a slight decrease, probably because of an activation of SPS (Sulpice et al. 2014). Due to the possibility of interconversion, the roles of F6P and G6P cannot be fully distinguished. It should be noted, that F6P holds a likewise central position. Indeed, during photosynthesis, the interconversion of assimilated triose phosphates to sucrose is mainly limited by the transformation of fructose-1,6-bisphosphate to F6P, catalysed by the enzyme cytosolic fructose 1,6bisphosphatase (cFBPase) (Strand et al. 2000). Finally, F6P is the direct entrance point of carbohydrates into glycolysis (Schopfer, Brennicke 2010).

In context of the present experimental approach, the terms glucokinase, fructokinase and hexokinase will be used differently: hexokinase activity designates the phosphorylation of hexoses, irrespective of the specific enzyme catalysing this reaction *in vivo*. In the same manner, glucokinase activity describes the interconversion of glucose to glucose-6-phosphate, and fructokinase activity refers to fructose phosphorylation.

Transitory starch

Due to their autotrophic lifestyle, plants are subject to diurnal fluctuations in carbohydrate availability, as photosynthesis is restricted to the light phase. Like most higher plants, Arabidopsis synthesises the glucose homopolymer starch on a daily basis, to maintain energy supply for growth and vital processes at night. In contrast to amyloplastic "storage starch" fuelling early growth processes, Arabidopsis leaf starch is a short-term reserve, therefore often referred to as "transitory starch" (Streb, Zeeman 2012). Early perceptions viewed leaf starch as an overflow pool, when photosynthesis provides more carbohydrates than required for export and vacuolar storage. This proved to be not the case for Arabidopsis. Even under conditions of restrained photosynthesis, a part of the photoassimilates is directed into starch synthesis (ibid.). The relative amount of assimilates partitioned into starch was found to be even higher under short day conditions, probably to maintain growth processes at night (Smith, Stitt 2007).

Starch mainly consists of two glucose polymers: Amylose is a linear molecule, in which the glycosyl units are composed in chains via α-1,4-glycosidic bonds. It accounts for 10-30% of granule assemblage, while the residual majority of mass is made up from amylopectin, the second glucan. Herein, the chains are additionally joined via α-1,6-glucosidic bonds, forming branch points every 20-25 glucose units. Amylopectin configures a semicrystalline structure, making the starch granules insoluble and very stable (Streb, Zeeman 2012).

The pathway of leaf **starch biosynthesis** takes place in the chloroplast. Its direct substrate in higher plants is ADP-glucose, which is generated from glucose-1-phosphate and ATP by the enzyme ADP-glucose pyrophosphorylase (AGPase). The activity of AGPase is considered to be a limiting step in carbon partitioning, being regulated on various levels (Streb, Zeeman 2012). The Calvin cycle intermediate 3-phosphoglyceric acid (3-PGA) allosterically activates the enzyme, providing a means of activating starch synthesis when photoassimilates accumulate. Additionally, AGPase is inhibited by inorganic phosphate, Pi (Iglesias et al. 1993). The enzyme has been shown to be a heterotetrameric complex, and reversible formation of a disulphide bridge between the small subunits changes substrate affinity (Fu et al. 1998). The redox state defines the conformation, i.e. reduction leads to the break of the disulphide bridge thereby activating the enzyme. Changing light

conditions and metabolite levels can induce a shift in the conformation (Streb, Zeeman 2012). Hexokinase was suggested to implement glucose signals (Tiessen et al. 2003), while sucrose levels influence AGPase redox state probably via a SnRK1 pathway (ibid) and/or T6P signalling (Kolbe et al. 2005).

Molecules of ADP-glucose are linked into linear chains by starch synthases (SSs). In the case of amylopectin, branching enzymes (BEs) cut and transfer segments of at least 6 glucose residues to another chain, connecting them via α-1,6 linkage. In the current understanding, a third step involving debranching enzymes (DBEs) is necessary for proper formation of starch granules (Streb, Zeeman 2012). They probably remove inappropriate branch points in order to facilitate double helix formation and subsequent crystallization (Myers et al. 2000).

Under regular diurnal conditions, nocturnal **starch breakdown** takes place at a nearly constant rate, degrading almost the whole starch reserve until dawn. Glucose and maltose, representing the main products of degradation, are then exported into the cytosol (Zeeman et al. 2007). The enzymatic breakdown of transient chloroplast starch occurs via a different pathway than that known from germinating cereal endosperm (Streb, Zeeman 2012). The semi-crystalline surface of the granules is solubilized as a prerequisite for degradation. This happens via the two enzymes α-glucan water dikinase (GWD) and phosphoglucan water dikinase (PWD), phosphorylating glucosyl residues of amylopectin at different carbon positions. Phosphorylated glucans are then accessible for degradation by hydrolytic enzymes (ibid.). The balance of enzymatic phosphorylation and dephosphorylation events controls the phosphate content of granules, which defines specific properties of the starch (Santelia et al. 2011). Phosphorylated residues interfere with β-amylase (Takeda, Hizukuri 1981), highlighting the importance of specific amylopectin phosphorylation patterns for starch functionality. Linear glucans can be dissected into maltose molecules by β-amylases (BAMs), but these enzymes are unable to hydrolyse α-1,6 branch points (Streb, Zeeman 2012). To further degrade amylopectin, debranching enzymes (DBEs) are necessary. Although BAMS and DBEs are constitutive for the bulk of chloroplast starch degradation in Arabidopsis, further enzymes, namely α-amylase, α-glucan phosphorylase and disproportionating enzyme “attack” glucans. The various enzymatic pathways might be partially redundant and their relative influence in Arabidopsis probably varies depending on the type of tissue (Streb, Zeeman 2012). The

main products of starch degradation, maltose and glucose, are exported to the cytosol via specific transporters (Niittyla et al. 2004). Aside from that, G1P can originate from starch breakdown, being metabolised instantly within the chloroplast (Zeeman et al. 2007).

Recent studies address the question how the **balance** of starch accumulation during the day and starch degradation at night is achieved on a molecular level. Plant productivity is largely based on the correct adjustment of depletion of carbohydrate reserves to the onset of dawn (Graf et al. 2010). In short day conditions, the percentage of carbon used for starch synthesis was found to be higher, going along with reduced degradation at night and a lowered growth rate. In this way, the rate of carbon consumption is adjusted to its availability over the diurnal cycle (Stitt et al. 2007). Signalling must be triggered by small changes in the carbohydrates status, to allow adaptations in starch turnover, growth and metabolism before acute carbon starvation occurs (ibid.). Sugar levels decrease when starch reserves are depleted (Usadel et al. 2008). Under natural conditions, the rate of starch degradation is fine-tuned to maintain stable sugar levels until the actual dawn. The circadian clock components LATE ELONGATED HYPOCOTYL (LHY) and CIRCADIAN CLOCK ASSOCIATED 1 (CCA1) have been shown to be involved in anticipating that specific time (Graf et al. 2010). The circadian regulation of starch degradation assures optimal carbohydrate availability during the whole night, preventing starvation responses (ibid.). While diurnal fluctuations of sucrose and hexose levels are thereby kept moderate (Bläsing et al. 2005), more severe depletion of carbohydrates occurs in a period of extended darkness acutely limiting metabolism already within the first hours (Bläsing et al. 2005; Stitt et al. 2007; Usadel et al. 2008).

1.2 The Plant Energy Homeostasis

ATP is the main transport currency of energy within cells, providing a means to contribute energy for the several endergonic processes essential for metabolic function (Schopfer, Brennicke 2010). Living cells need to sustain a high ATP/ADP ratio. Catabolism and photosynthesis transform adenosine diphosphate (ADP) and inorganic phosphate into ATP, while the majority of cellular processes hydrolyse ATP. To stay alive, cells need to balance their energy expenditure with the rate of catabolism and photosynthesis to maintain the essential ATP/ADP ratio (Hardie 2007).

Carbohydrates are the primary photoassimilates constituting the largest quantity of substrate for energy generation in plants. In the multi-step process of glycolysis taking place in plastids and cytoplasm, mainly glucose is dissimilated into two molecules of pyruvate. In sum, 2 molecules of ATP are produced out of each glucose molecule. Pyruvate is channelled into the mitochondria, and further used in the TCA cycle to gain reducing equivalents and 1 molecule ATP each. The TCA cycle additionally plays an important role in the biosynthesis of amino acids, providing carbon skeletons for transamination reactions. The released reducing equivalents (NADH & $FADH_2$) are fed into the respiratory electron transport chain. In course of the oxidative phosphorylation, the reductive potential is finally transformed into phosphorylation potential by proton pumps at the inner mitochondrial membrane (Schopfer, Brennicke 2010). If this acquisition of energy is critically limited, damage can occur to single cells, or whole tissues and organs (Tome et al. 2014).

Various reasons for **energy deficits** in plants are known (summarized by Baena-Gonzalez, Sheen 2008; Tome et al. 2014). One of them is an altered day-night cycle, which can occur naturally as a result of shading or due to an experimentally induced extension of the night. Extreme environmental conditions like temperature stress, water deficit or flooding also perturb fundamental metabolic processes as photosynthesis or respiration. Pathogens likewise divert carbohydrates from their host plants. Furthermore, tissue specific limitations can result from competition for photoassimilates between sink organs like roots and fruits. As sessile organisms, plants show specific adaptations in their stress response. Under suboptimal conditions, energy consumption and conservation must be coordinated efficiently in all tissues (Baena-Gonzalez et al. 2007). Source leaves are often constrained in photosynthesis and respiration, which results in reduced sugar export to sink tissues. The emanating energy deficiency shows similar characteristics for different environmental stresses (Baena-Gonzalez, Sheen 2008). Alterations of the cellular energy status caused by various stress conditions require and induce a reprogramming of metabolism. To describe the central energy preserving response in higher plants, the term “low energy syndrome” was established (Tome et al. 2014). Figure 2 provides an overview about the phenotypical effects of restricted energy conditions, referred to as low energy syndrome.

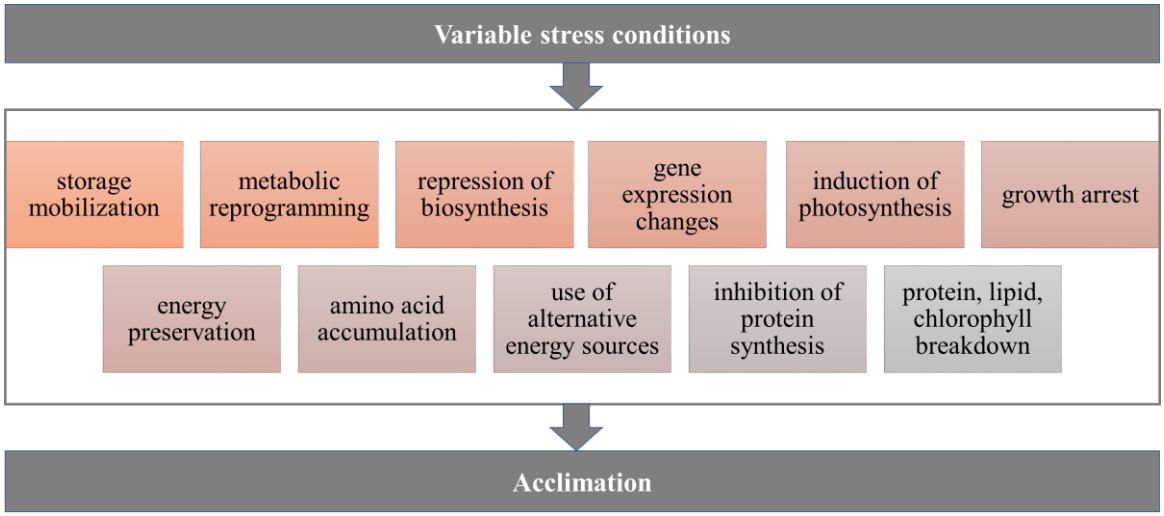

Figure 2 Low energy syndrome is an assemblage of universal phenotypical consequences in reaction to stress conditions (modified from Tome et al. 2014).

To regulate the energy homeostasis, environmental signals have to be sensed and integrated in cellular signalling pathways (Polge, Thomas 2007). Various signalling pathways have been shown to be involved in a plants response to energy deficiency. In this context, two highly conserved protein kinases, SnRK1 and TOR, are known to play central and antagonistic roles in balancing energy demanding versus energy preserving processes (Tome et al. 2014). The Sucrose non-Fermenting-1 Related protein Kinase 1, SnRK1, has been shown to induce vast metabolic changes towards energy conservation under energy deprivation. The reprogramming takes place on several levels, comprising phosphorylation of target proteins, modified gene expression and reduction of energy consuming translation (Baena-Gonzalez et al. 2007). The following chapter provides further detailed information about SnRK1, discussing its structure, regulation, and function in plant metabolism.

In contrast, TOR (=Target of Rapamycin), a conserved serine/threonine kinase, affects plant metabolism in a converse manner. TOR is activated under conditions of sufficient energy and nutrient availability, promoting anabolic processes like growth and protein synthesis (Robaglia et al. 2012). TOR and SnRK1 act antagonistically in the control of several nutrient-dependent processes. For example, while SnRK1 promotes autophagy under starvation to mobilize nutrients, TOR restricts this process under energy-repletion (ibid.). A recent work on phosphoproteomics and metabolomics provided evidence for a regulatory crosstalk between SnRK1 and TOR signalling (Nukarinen et al. 2016). A fluorescence assay showed *in vivo* interaction between SnRK1α proteins and

RAPTOR1B, a domain of the Arabidopsis TOR-complex. The ability of SnRK1 to phosphorylate RAPTOR1B was proven *in vitro* by a kinase assay. These findings indicate an inhibition of TOR signalling under energy deprivation via phosphorylation of RAPTOR in plants.

1.3 SnRK1

SnRK1 is the plant homolog of SNF1 (=sucrose non-fermenting 1) in yeast and AMPK (=AMP activated protein kinase) in mammals (Hardie 2007, Polge, Thomas (2007). These kinases perform a fundamental function in integrating nutrient status, stress signals and energy consumption (Halford, Hardie 1998). Having a central role in maintaining energy homeostasis, the mammalian orthologue is a sensor for the cellular adenosine monophosphate (AMP):ATP ratio (Hardie 2007). Alderson et al. (1991) first provided evidence for the conserved function of the plant SnRKs in their role of a regulator of energy metabolism. In their experiment, a rye complementary DNA (cDNA) showing strong sequence similarity to yeast SNF1, could substitute lacking SNF1 activity in a yeast mutant. The ability of yeast to metabolize glycerol and ethanol was restored, indicating a similar function in carbohydrate metabolism. Since then, SnRK1 genes of many plant species have been described (Halford, Hardie 1998). Within the Arabidopsis SnRK superfamily, SnRK1 is not the only protein kinase. It is classified into three distinct subgroups labelled SnRK1, SnRK2 and SnRK3, based on sequence similarity and structure of active sites (ibid.). The catalytic domains of SnRK2 and SnRK3 show less amino acid sequence similarity to SNF1 and AMPK (42-45%), but can be clearly placed within the SnRK family (Halford et al. 2003). In Arabidopsis, 3 genes encode SnRK1, 10 encode SnRK2 and there are 25 SnRK3 genes (Hrabak et al. 2003). The latter two are described as plant-specific gene subfamilies being relatively diverse in comparison to SnRK1. SnRK2 kinases play a role in abscisic acid (ABA) signalling, drought tolerance, and chilling response. SnRK3 may act in a calcium-dependent manner and could be involved in salt resistance (Halford et al. 2003).

The complex

In yeast and mammals, SNF1 and AMPK operate as heterotrimeric enzyme complexes, including the catalytically active alpha subunit and further beta and gamma subunits performing regulative functions (Hardie 2007). In *A. thaliana*, the catalytic subunits

SnRK1α1 and SnRK1α2 are sometimes also termed AKIN10 and AKIN11 (Baena-Gonzalez et al. 2007). Bouly and co-workers characterized cDNA sequences for β- and γ-subunits of plant SnRK1 (Bouly et al. (1999). The β- and γ- subunits bear a resemblance to the yeast SIP1/SIP2/GAL83 and respectively SNF4 proteins, which are known to be necessary for SNF1 catalytic functionality. This similarity indicated the existence of heterotrimeric complexes of SnRK1 in plants. Interactions resembling each other in plants, mammals and yeast provide evidence for the evolutionary conserved role of the heterotrimeric complex in eukaryotes. Differences of the SNF1-related complexes between the kingdoms appear with respect to the mechanisms of interaction among the subunits. In addition, plants show higher structural diversity of the subunits, including Akinβ3 and Akinβγ proteins (Polge, Thomas 2007). The plant specific βγ subunit was shown to be involved in heterotrimeric SnRK1 complexes in the cytoplasm and nucleus (Gissot et al. 2006). The authors suggested a role in pathogen resistance. Plant specific variants of SnRK1 complexes could perform specialised functions adapted to plant lifestyle (Gissot et al. 2004).

The role of SnRK1 signalling in plant metabolism

SnRK1 signalling plays a role in response to several abiotic stresses like flooding, exceptional temperatures, drought, and extended darkness. These harsh conditions cause energy depletion and thus elicit SnRK1 signalling (Baena-Gonzalez, Sheen 2008). SnRK1 can furthermore be involved in response to pathogen attack, as infection potentially leads to changes in plant metabolism and energy status (Margalha et al. 2016).

Early studies on SnRK1 indicated a conserved role in controlling metabolism via enzyme phosphorylation and transcriptional regulation. An overview of enzymes and other target molecules interacting with SnRK1 is provided by Margalha et al. (2016): among the enzymes, SPS, NR (nitrate reductase), HMGR (3-hydroxymethyl-3-methylglutaryl-CoA reductase), F2KP (fructose-2-6-bisphosphatase) and class II TPS (T6P synthase) proteins are phosphorylated by SnRK1. The enzyme SPS is inactivated upon phosphorylation by SnRK1 (Sugden et al. 1999), pointing towards the relevance of SnRK1 for the central carbohydrate metabolism. Moreover, F2KP activity determines the levels of fructose-2-6-bisphosphate, which in turn is an important effector controlling the partitioning of carbon between starch and sucrose synthesis (Stitt 1990). A recent study suggested that SnRK1

activity alters the flux of carbon into the TCA cycle as an instant response to energy deficiency via phosphorylation of F2KP (Nukarinen et al. 2016).

Purcell and colleagues suggested a regulatory function of SnRK1 in carbohydrate metabolism on the transcriptional level (Purcell et al. (1998). A SnRK1 antisense-induced drop of sucrose synthase transcript levels and enzyme activity in potato tubers was observed. In contrast to control lines, the transgenic plants lacked inducibility of SuSy gene expression by sucrose treatment. Laurie (2003) examined a possible regulatory role of SnRK1 on α-amylase promoter activity in wheat embryos. Their results show a full suppression of the α-amylase promoter activity by co-bombardment with SnRK1 antisense sequence**.** SnRK1 might play a crucial role in the activation of α-amylase genes under low cellular glucose conditions. Beyond these examples, SnRK1 activity induces a broad transcriptional reprogramming to maintain energy homeostasis. Among the genes activated by SnRK1, many are involved in catabolism of alternative nutrient sources like amino acids, lipids, cell wall and polysaccharides (Baena-Gonzalez, Sheen 2008). Besides activating catabolism, under low energy conditions SnRK1 activity simultaneously represses transcription of several enzymes of biosynthetic pathways. A transcriptional response of AKIN 10 influenced genes occurs already under regular night conditions or in the early phase of an extended night treatment. This suggests that SnRK1 sets up transcriptional reprogramming in reaction to small shifts in carbon levels (Usadel et al. 2008).

The expression of SnRK1 target genes is altered partially via basic leucine zipper (bZIP) transcription factors (Baena-Gonzalez et al. 2007), but the vast effect of SnRK1 on transcript regulation in its entirety requires involvement of other downstream-effectors and therefore further research (Tome et al. 2014). Recently, micro-RNAs were shown to participate in the SnRK1 signalling cascade. These short RNA sequences are post-transcriptional regulators, possibly reducing selected cellular processes in the SnRK1 mediated stress response (Confraria et al. 2013).

Apart from an affected catabolism in SnRK1 mutant lines, a reduced capacity for leaf starch degradation was observed. Starch persisted at higher levels at the end of the night in AKIN10/11 mutants, which is probably one of the main reasons for restricted growth of the mutants. The finding that starch mobilization - a crucial process for autotrophic

diurnal lifestyle - is impaired, points to an essential role of SnRK1 also under natural non-stress conditions (Baena-Gonzalez et al. 2007). SnRK1 is an important signalling link between metabolic conditions and plant growth. The induction of several developmental programs, including root growth, fruit growth, leaf shape and germination are depending on energy availability. Manipulation of SnRK1 activity fundamentally alters these processes (for a detailed overview, see e.g. Margalha et al. 2016). SnRK1 was even suggested to play a role in upholding proper cell cycles, irrespective of its role in stress response (Guérinier et al. 2013).

The effect of SnRK1 activity varies strongly between different tissues and cell types, which complicates the understanding of its already diverse functions. Differential composition of the subunits forming the SnRK1 complex could provide the molecular ground for contrasting downstream signalling (Margalha et al. 2016).

Regulation of the kinase

The specific stress signals activating SnRK1 are not known in their entirety, yet it is suggested that SnRK1 is modulated by sugars at several levels (Margalha et al. 2016). For example, the activity of a *Vicia faba* SnRK1 promoter expressed in Arabidopsis protoplasts was induced by sucrose depletion (Radchuk et al. 2010). Downstream effectors of SnRK1, like bZIP transcription factors, also change in response to carbohydrate availability. bZIP63 is phosphorylated by SnRK1α1 in response to starvation, affecting its dimerization (Mair et al. 2015).

On a functional level, SnRK1 kinases of plants are regulated by several post-translational modifications, affecting their catalytic activity, localization or the stability of the complex (Margalha et al. 2016). A conserved mechanism, also known for AMPK and SNF1, is the phosphorylation of a threonine residue at the activation site (T-loop) of the catalytic subunit. Two upstream kinases, SnAK1&2 (or GRIK1/2), were found to activate SnRK1 by T-loop phosphorylation (Crozet et al. 2010). *Vice versa*, SnRK1 phosphorylates SnAK1/2 on their activation loop, resulting in inactivation. This negative feedback loop points to a rigid regulation of SnRK1 activity (ibid.). In contrast to mammals, the role of T-loop phosphorylation *in vivo* is still under discussion for plants. Under stress conditions inducing a comprehensive SnRK1-induced transcriptional reprogramming, the

phosphorylation state of the T-loop did not significantly differ from control conditions (Baena-Gonzalez et al. 2007). It was suggested that only α-subunits incorporated into a complex are increasingly phosphorylated on their activation site upon stress (Nunes et al. 2013). Nevertheless, T-loop phosphorylation is not the only regulatory mechanism influencing SnRK1 activity under stress conditions (Robaglia et al. 2012). Several further phosphorylation sites on the catalytic, as well as on the regulatory subunits, were identified, but their functional role is not yet clear (Margalha et al. 2016).

Two PPC2 phosphatases were shown to dephosphorylate and hence inactivate SnRK1α1, suggesting a connection with ABA signalling. The concerned phosphatases PP2CA and ABI1 are inactivated upon ABA binding. The repression of these upstream inhibitors could lead to a SnRK1 activation in response to ABA (Rodrigues et al. 2013). Crozet et al. (2016) recently postulated the regulation of SnRK1 activity by SUMOylation, leading to ubiquitination and finally proteosomal degradation. In their studies, only active SnRK1 was degraded, while inactive SnRK1 accumulated. This led to the hypothesis of a negative feedback loop, in which SnRK1 activity enhances its own degradation, preventing hyper-activation of stress responses. The composition of the heterotrimeric complex is likely to be one further mechanism of regulation, as subtle peculiarities of the subunits could affect the localization of the complex, adapting it to functional demands of specific tissues or developmental stages (Crozet et al. 2014).

Several metabolites constitute allosteric effectors, having an impact on kinase activity (Robaglia et al. 2012). Unlike the mammalian homolog AMPK, SnRK1 lacks binding sites for adenine nucleotides and is therefore not allosterically regulated by ADP or ATP (Emanuelle et al. 2015). However, SnRK1 is allosterically inhibited by T6P, G6P and G1P, each attaching to different sites of the SnRK1 complex. The regulatory effect of T6P requires an unknown intermediary factor not present in mature leaves (Zhang et al. 2009), and such one could also be required for the effects of G6P and G1P (Nunes et al. 2013). Each of these metabolites is capable of discrete inhibition of the kinase, showing different kinetic parameters. Under concentrations comparable to conditions of high carbon availability in *A. thaliana* tissue, T6P and G1P show synergistic inhibition. T6P may be needed to inhibit SnRK1 activity under stress conditions without carbon starvation, e.g. cold stress going along with sugar accumulation (Lunn et al. 2014). The functional extent of the interaction between SnRK1 and T6P is not fully understood yet.

In one scenario, the function of T6P in activating biosynthesis and inhibiting catabolism is restricted to allosterically inhibit SnRK1 activity. In an alternative scenario, SnRK1 and T6P affect plant metabolism via separate pathways. In that case, the inhibition of SnRK1 by T6P would convey an interaction between these distinct pathways. The observation that T6P levels track sucrose levels across a great range of concentrations, far away from carbohydrate starvation, suggests a discrete role of T6P in sucrose sensing (Lunn et al. 2014).

1.4 Aim

The present study intends to characterize differences between *Arabidopsis thaliana* wildtype plants and *snrk1α1α2* double mutants, focusing on extended night-induced dynamics of the central carbohydrate metabolism. The motivation of this study derives from a previous study, reporting on strongly deviating sucrose levels between wildtype and *snrk1α1α2* plants during 6 hours of extended night exposure (Nukarinen et al. 2016). Nukarinen and colleagues revealed stress-induced differences in hexose levels which were, however, not as severe as for sucrose. Sucrose concentration of *snrk1α1α2* plants was observed to be reduced by half at the end of the regular night, and, consequently, it was hypothesized that the mutant plants cannot properly control the consumption of carbohydrate reserves under energy limitation. To shed light on processes leading to such divergent sucrose levels, the present study complements the characterization of the carbohydrate status with measurement data for starch, G6P, F6P and UDPG. Furthermore, the role of key enzymes (namely glucokinase, fructokinase, SPS and invertase) in stabilizing carbohydrate levels under energy limitation is investigated.

2 Material and Methods

2.1 Material, Software and Technical Devices

The following tables cover all chemicals and enzymes used for the experiments (Table 1), a list of repeatedly used chemical solutions and buffers (Table 2), technical devices employed for the measurements (Table 3), licensed software used for data processing and evaluation (Table 4), as well as a list of utilized consumable material (Table 5).

Table 1 Chemicals and enzymes

SHORT NAME	FULL DESCRIPTION	MANUFACTURER	ORDER NUMBER
Ethanol denatured	Ethanol Prima 96% incompletely denatured	AustrAlco	AAAH-5000-07322-190116
NaOH	Sodium hydroxide	Roth	P031.1
HCl	Hydrochloric acid 37%	AnalaR Normapur	20252.290
TRIS Pufferan	Tris(hydroxymethyl)-aminomethane	Roth	AE15.3
Glycerol	Glycerol Rotipuran 99.5% anhydrous	Roth	3783.1
Amyloglucosidase	Amyloglucosidase from *Aspergillus niger*	Sigma-Aldrich	10115-1G-F
Glucose Oxidase	Glucose Oxidase from *Aspergillus niger*	Sigma-Aldrich	G6125-10KU
Peroxidase	Peroxidase from horseradish	Sigma-Aldrich	P8125-5KU
o-Dianisidin HCl	o-Dianisidine dihydrochloride	Sigma-Aldrich	F5803-50MG
Glucose	D(+)-Glucose anhydrous	Merck	1.08337.0250
Wheat starch	Starch (from wheat)	Merck	1.11685.0250
Pyridine	Pyridine anhydrous	Sigma-Aldrich	270970
MeOH	Methoxyamine hydrochloride	Sigma-Aldrich	226904
MSTFA	N-Methyl-N-trimethylsilyl trifluor(o) acetamid(e)	Macherey-Nagel	701270.201
$MgCl_2$	Magnesium chloride (anhydrous for synthesis)	Merck	8.14733.0100
EDTA	Ethylenediamine tetraacetic acid dipotassium salt dihydrate	Roth	3053.1
Triton X-100	4-(1,1,3,3-Tetramethylbutyl)phenyl-polyethylene glycol	Sigma-Aldrich	X100-500ML
DTT	DL-Dithiothreitol	Sigma-Aldrich	43819-5G
HEPES	2-[4-(2-Hydroxyethyl)-1-piperazinyl]-ethanesulfonic acid	Merck	1.10110.0250

ATP	Adenosine 5′-triphosphate disodium salt hydrate	Sigma-Aldrich	A2383-5G
NADP+	β-Nicotinamide adenine dinucleotide phosphate disodium salt	Roth	AE13.1
G6PDH	Glucose-6-phosphate Dehydrogenase from baker's yeast (*S. cerevisiae*)	Sigma-Aldrich	G7877-500UN
PGI	Phosphoglucose Isomerase from *S. cerevisiae*	Sigma-Aldrich	P5381-1KU
Hexokinase	Hexokinase from *S. cerevisiae*	Sigma-Aldrich	H4502-1KU
Glucose	D(+)-Glucose monohydrate	Roth	6887.1
Glucose	D(+)-Glucose anhydrous	Merck	1.08337.025
Fructose	D(-)-Fructose	Merck	1.04007
Sucrose (powdered)	D(+)-Saccharose powdered	Roth	9286.1
KOH	Potassium hydroxide pellets	Merck	1.05029.1000
UDP-GluNcose	Uridine 5′-diphosphoglucose disodium salt hydrate from *Saccharomyces cerevisiae*	Sigma Aldrich	U4625
Fructose-6-Phosphat	D-Fructose 6-phosphate disodium salt hydrate	Sigma Aldrich	F3627
Glucose-6-Phosphat	D-Glucose 6-phosphate disodium salt hydrate	Sigma Aldrich	G7250
Anthrone	Anthrone for analysis	AppliChem	132441.1605
Sulfuric acid	Sulfuric acid 98% for analysis EMSURE®	Merck	1.12080.1000
PMSF	Phenylmethanesulfonyl fluoride	Sigma Aldrich	P7626
Sucrose	D+(-)Saccharose	Roth	4621.2
Na-Acetat	Sodium acetate (ACS) anhydrous	Roth	6773.2
Acetic acid	Acetic Acid 100% AnalR normapur	VWR Chemicals	20104.323

Table 2 Chemical solutions and buffers

NAME OF SOLUTION	COMPOSITION
SPS Assay	
Anthrone reagent	0.14 % (w/v) Anthrone in 14.6 M H_2SO_4 (98% H_2SO_4 = 18.4 M -> dilute 4:1)
Extraction buffer	50 mM HEPES-KOH pH 7.5 10 mM $MgCl_2$ 1 mM EDTA

	2.5 mM DTT 10 % (v/v) Glycerol 0.1 % (v/v) Triton X-100 H_2O
Reaction buffer	50 mM HEPES-KOH pH 7.5 15 mM MgCl2 2.5 mM DTT 35 mM UDP-glucose 35 mM Fructose-6-phosphat 140 mM Glucose-6-phosphat H_2O
Sucrose standard	5 mM Sucrose 10 mM HEPES-KOH pH 7.5
Invertase Assay	
Extraction buffer	50 mM HEPES-KOH pH 7.5 5 mM $MgCl_2$ 2 mM EDTA 1 mM PMSF 5 mM DTT 0.1 % Triton X-100 10 % Glycerin
Neutral reaction buffer	20 mM HEPES-KOH pH 7.5 100 mM Sucrose
Acidic reaction buffer	20 mM Na-Acetate pH 4.7
Invertase well-plate mixture	90 µl Hexokinase reaction buffer 4 µl ATP (100mM) 2 µl $NADP^+$ 2 µl Hexokinase enzyme (0.25u/µl) 2 µl G6PDH enzyme (0.25u/µl) (=total volume of 100µl)
Hexokinase reaction buffer	100 mM HEPES-KOH pH 7.5 10 mM $MgCl_2$
Hexokinase Assay	
Extraction buffer	50 mM TRIS-HCl pH 8 0.5 mM MgCl2 1 mM EDTA 1% Triton 2.5 mM DTT

Reaction buffer	100 mM HEPES-KOH pH 7.5 10 mM $MgCl_2$
Hexokinase well-plate mixture	140 µl Reaction buffer 4 µl ATP (100mM)– not in blank 2 µl NADP (100mM) 1 µl PGI (0.5 u/µl) – only in FKin batch 1 µl G6PDH (0.5 u/µl) 20 µl Plant extract 20 µl Sugar-solution (1µl 1M Glc or Fru + 19 µl Reaction buffer) (= total volume of 188µl)
Starch Assay	
Standard acetate buffer	200 ml 1N acetic acid 100 ml 1N NaOH Fill up to 1 L with H_2O
Amyloglucosidase reagent	1mg Amyloglucosidase dissolved in 1ml standard acetate buffer
Methoximation reagent	30 mg Methoxyaminhydrochlorid in 750 µl Pyridine
Only used for glucose-oxidase/peroxidase method	
Tris-glycerin buffer pH 7	61g TRIS dissolved in 85ml 5N HCl Fill up to 1 L with H_2O Add 660 ml Glycerin Adjust pH to 7 with 5N HCl
Glucoseoxidase reagent	15 mg Glucoseoxidase 1.5 mg Peroxidase 5 mg Dianisidine-HCl in 50 ml Tris-Glycerin buffer pH 7

Table 3 Technical devices

NAME	MANUFACTURER
Thermo-shaker	DITABIS Digital Biomedical Imaging Systems AG, Pforzheim, Germany; Eppendorf AG, Hamburg, Germany
Microlitercentrifuge 'Heraeus'	Thermo Scientific, Waltham, Massachusetts, USA
Vacuum Evaporator 'Scanspeed 40'	LaboGene ApS, Lynge, Denmark
Microcentrifuge	Fisher Scientific (Austria) GmbH, Wien
Spectrophotometer 'Multiscan Spectrum'	Thermo Scientific, Waltham, Massachusetts, USA
Microwave 'Whirlpool'	Philips Austria GmbH, Wien, Austria
Agilent 6890 gas chromatograph	Agilent Technologies®, Santa Clara, CA, USA
LECO Pegasus® 4D GCxGC-TOF mass spectrometer	LECO Corporation, St. Joseph, MI, USA

Table 4 Software

NAME	SOFTWARE PUBLISHER
Matlab® Version R2015a	The MathWorks, Inc www.mathworks.com
Systems Biology Toolbox 2	Henning Schmidt, henning@sbtoolbox2.org www.sbtoolbox2.org/main.php
Microsoft® Office 2016	Microsoft® www.microsoft.com
R Version 3.3.2	The R Foundation for Statistical Computing www.r-project.org
Leco® ChromaTOF-GC Software v4.50.8.0	www.leco.com
Chromeleon™ Chromatography Data System Software	Thermo Scientific Dionex www.dionex.com

Table 5 Consumable material

LABEL	MANUFACTURER
Pipette tips 100 - 1000µl	Greiner Bio-One International GmbH, Kremsmünster, Österreich
Pipette tips 10 - 200µl	Greiner Bio-One International GmbH, Kremsmünster, Österreich
Pipette tips 0.5 - 10 µl	Greiner Bio-One International GmbH, Kremsmünster, Österreich
Flat bottomed photometer well-plates (340nm, µClear®)	Greiner Bio-One International GmbH, Kremsmünster, Österreich
Photometer well-plates	Greiner Bio-One International GmbH, Kremsmünster, Österreich
Glass vials	MACHEREY-NAGEL GmbH & Co. KG, Düren, Germany
Crimp caps for gas chromatography	IVA Analysentechnik GmbH & Co. KG, Meerbusch, Germany
Crimp caps for ion chromatography	MACHEREY-NAGEL GmbH & Co. KG, Düren, Germany
Micro-inserts for glass vials	Markus Bruckner Analysentechnik, Linz, Austria
Eppendorf Tubes (2ml safelock)	Eppendorf Austria GmbH, Wien
Eppendorf Tubes (1.5ml)	Eppendorf Austria GmbH, Wien
Eppendorf Tubes (2ml)	Eppendorf Austria GmbH, Wien
Falcon Tubes (50ml)	Greiner Bio-One International GmbH, Kremsmünster, Österreich
Falcon Tubes (15ml)	Greiner Bio-One International GmbH, Kremsmünster, Österreich
Centrifuge Tube Filters (0.45µm, 2ml)	COSTAR Spin X (8170)

2.2 Plant Material

All plant material used for this project was obtained from the Department of Molecular Biology and Plant Biotechnology at the Julius-Maximilians-Universität Würzburg, headed by Prof. Dr. Wolfgang Dröge-Laser. All steps of plant growth and sampling were described recently by Nukarinen and colleagues (Nukarinen et al. 2016). In brief, plants with a deficiency in both catalytically active subunits α1 and α2 of the protein kinase SnRK1 were generated by β-estradiol inducible amiRNA (= artificial microRNA) against the α2 subunit in the genetic background of a transfer DNA (T-DNA) insertional mutant of the α1 subunit (*snrkα1/α2*). Four week old plants were sprayed with 10 μM β - estradiol, 0.1% DMSO and 0.005% Silwet for 6 days. Extended night (EN) treatment and harvesting followed on the 7th day (Nukarinen et al. 2016).

Wildtype (Col-0) and mutant (*snrkα1/α2*) plants were cultivated and harvested under equal conditions. They were grown in a 12/12h day/night cycle for 5 weeks, and finally exposed to a 6-hour extended night, i.e. in total 18h darkness. Harvesting time points were in the middle of the day, i.e. after 6 hours of light on, and after 0/20/40/60/80/100/120/180/360 minutes (min) of extended night (ibid.). If not stated otherwise, 80-100mg of frozen and finely ground leaf material were used for experimental analysis. The light samples were only used for testing the starch assay.

2.3 Concentrations of Fructose, Glucose, and Sucrose

Time series data for concentrations of fructose, glucose and sucrose were taken from a previous study (Nukarinen et al. 2016). The authors accomplished extraction and derivatization for a diverse range of primary metabolites as previously described (Doerfler et al. 2013). Gas chromatography was performed on an Agilent 6890 gas chromatograph. An Agilent HP5MS column (length: 30m, diameter: 0.25mm, film: 0.25μm) was used for separation of the compounds. The chromatograph was coupled to a GCxGC-TOF mass spectrometer (LECO Pegasus® 4D). Deconvolution of the total ion chromatograms was performed using the LECO Chromatof® software. Absolute quantification of metabolite concentrations was performed by comparing peak areas in the samples to those of a calibration curve (ibid.).

2.4 Hexose Phosphates and UDP-Glucose

Concentrations of glucose-6-phosphate, fructose-6-phosphate and uridine diphosphate glucose were quantified on a Dionex ion chromatography coupled to a triple quadrupole mass spectrometer (IC-MS) (Thermo Fisher Scientific Inc., Waltham, Massachusetts). Samples were analysed after 0, 20, 60, 120 and 360 minutes of extended night, each with three biological replicates.

Protocol

A hot-water extraction was applied as described previously (Sekiguchi et al. 2004). Frozen samples were immediately quenched by adding 500µl of heated water (95°C). Heating the samples was necessary to prevent enzymatic transformation or breakdown of the highly reactive sugar phosphates (Sekiguchi et al. 2004). Subsequently, samples were mixed for 5 minutes at 95°C.

After leaving the samples for two minutes at room temperature, they were put to the microwave to enhance the extraction efficiency. The microwave was switched on five times, each for 3 seconds, followed by a 5 seconds break. Samples were centrifuged for 5 minutes at 13,000 revolutions per minute (rpm) and 400µl of the supernatant were transferred into centrifuge tube filters (0.45µm). Filtration was accomplished by putting the samples into a microcentrifuge for 30 seconds. 180µl of the cleared extract were transferred to glass vials with micro-inserts and closed with crimp caps for IC analysis. Standard mix solutions containing G6P, F6P and UDPG at four different concentrations (0, 10, 25, 50µM) were also filled to glass vials.

Measurement was performed using a Dionex ion chromatography coupled to triple quadrupole mass spectrometry, which gives a good separation of different compounds. The settings were adjusted as described by (Hardy et al. 2010) via the Chromeleon® software package.

The basic principle of ion chromatography is the interaction between charged particles. At high pH values, molecules become negatively charged. Anion exchange chromatography uses a positive surface, called stationary phase, that attracts and separates negatively charged molecules. On the stationary phase, competition for oppositely charged groups takes place between sample ions and ions of the eluent. To

become attached to the stationary phase on the column, the analyte of interest needs to displace the counterions. Over the time, a pH gradient is applied (Table 7) which increases the competition between the eluent (here: OH^-) and analytes. Different molecules elute at different stages of the gradient, resulting in separation of the components (Velickovic et al. 2012). Further detailed settings of the chromatographic separation are described in Table 6.

Table 6 Chromatographic conditions

Column: Dionex IonPac AS11-HC-4µm, RFIC, Capillary 0.4 × 250 mm	
Flow Rate	100 µL/min
Injection Volume	15 µL
Column Temperature	40°C

Table 7 KOH gradient for IC elution

Time-frame [min]	KOH concentration of the mobile phase at the end of the interval [mM]
0	2
5	10
15	50
20	100
25	120
30	120

The electrospray ionization for mass spectrometry was set to negative mode with an ion-spray voltage of 2500V and a capillary temperature of 270°C. Nitrogen was utilized as collision gas.

A triple quadrupole instrument contains three linear quadrupoles (Q), each consisting of four rod electrodes arranged in a square. The opposing ones are always held at the same potential at a time. The applied current consists of a direct current and an alternating current component. Oscillating electric fields are used to select or scan specific ions from the continuous ion beam going through. Only ions that fulfil a characteristic mass-to-

charge (m/z) ratio stay on a stable trajectory and reach the detector. All other ions collide with the electrodes due to unstable oscillations (Gross 2013, pp. 162ff).

For the applied tandem mass spectrometry, the first and the third quadrupole (Q1 & Q3) are subject to radio-frequency current, while the one in between serves as collision chamber. Here, ions are fragmented by collision with a gas (here N_2) (Gross 2013, p.471f). Table 8 shows the selected m/z ratios for both quadrupoles (Q1 & Q3) as well as the applied potentials (Heinzel and Rolletschek, 2011).

Table 8 Instrumental settings (filtered masses and potentials) for triple quadrupole MS; DP = Declustering Potential, EP = Entrance Potential, CE = Collision Energy, CXP = Collision Cell Exit Potential

	Q1 Mass	Q3 Mass	DP	EP	CE	CXP
Glucose-6-Phosphate	258.8	96.8	-50	-10	-22	-5
Fructose-6-Phosphate	258.8	78.9	-55	-10	-60	-5
UDP-Glucose	281.9	111.0	-30	-10	-22	-7

For absolute quantification of each substance, the slope of the standard curve (peak area versus concentration in µM) was calculated using linear regression analysis. The quantified peak areas of the samples were divided through the corresponding standard slope value to get the concentrations (µM) of G6P, F6P and UDPG for each measured sample. These values were further divided by 2 to get the amount of substance per sample in nmol (total volume: 500µl). Finally, dividing through the sample fresh weight (FW) in [g] resulted in the concentration of the respective sugar in [nmol/gFW].

$$c\left[\frac{nmol}{g\ FW}\right] = \frac{A}{k} * \frac{1}{2} * \frac{1}{FW[g]} \qquad \text{(Eqn. 1)}$$

A…peak area
k…slope value in µmol/L

2.5 Sucrose-Phosphate Synthase Assay

The maximum enzyme velocity of SPS, v_{max}, was measured by quantifying the synthesised sucrose with the colorimetric anthrone method. The protocol was kindly provided by the Department of Plant Biotechnology, University of Stuttgart, Germany. It follows the quantification of the fructose moiety of sucrose at 40°C, which was described earlier by Van Handel et al. (1972).

Samples of 80-100mg frozen and finely ground rosette leaves were incubated for 10 minutes on ice with 750µl extraction buffer. Subsequently, they were centrifuged for 5 minutes at 13,000 rpm in a 4°C precooled centrifuge. The supernatant was transferred to new reaction tubes and again centrifuged for 2 minutes at the same settings. In general, samples were kept on ice between all steps to prevent the enzymes from denaturation.

One sample's supernatant was split in 8 fractions: four different time points of incubation (0, 10, 15, 20 minutes) were analysed, each with two technical replicates. 50µl of the crude extract were pipetted into each reaction mixture. Then 20µl of reaction buffer containing the substrates for SPS were added and incubated for the indicated time periods. For the step of adding the reaction buffer, it was crucial to mix the solutions by pipetting up and down a few times. Samples were incubated at 25°C mixing with 250 rpm. For stopping the enzyme reaction and destroying all sugars but sucrose, 70µl 30% (w/v) KOH were added immediately, then samples were heated to 95°C under constant shaking. A sucrose calibration row (Table 9) was prepared and treated equally from this step onwards.

Table 9 Preparation of sucrose standard row for the SPS assay; * the components of the sucrose-HEPES/KOH standard are explained in Table 2

Suc-HEPES/KOH standard [µl]*	0	0,5	1	2	4	10	20	30
H_2O [µl]	70	69,5	69	68	66	60	50	40
Suc concentration [mmol/L]	0	0,036	0,071	0,143	0,286	0,714	1,429	2,143
Suc in 70µl [µmol]	0	0,00252	0,00497	0,01001	0,02002	0,04998	0,10003	0,15001

After boiling with KOH, the samples were left for acclimation to room temperature. Samples were centrifuged for 1 minute at 13.000 rpm. 120µl of the supernatant were transferred to a new tube. The samples were placed in ice-water and 720µl of anthrone reagent were added. Following this, the tubes were carefully mixed, put on 40°C,

continuously mixed at 300rpm for 30 minutes. After incubation samples were mixed shortly. 200µl of each sample were transferred into a flat bottomed, pre-warmed (40°C) photometer 96 well-plate. Extinction was measured at a wavelength of 620 nm.

In each batch, a glucose calibration curve was included. The slope (*k)* per µmol sucrose in 70µl was calculated from the standards, using the *SLOPE* function in Microsoft Excel. Linear regression was applied to the mean values of enzyme measurements. Dividing the sample slope value through the calibration slope value resulted in the amount of sucrose produced in 50µl plant extract in one hour. Multiplication with the factor 15 (15*50µl = 750µl) and division through the fresh weight in [g] led to the maximum enzyme activity, v_{max}, in [µmol/g*h].

$$y = \boldsymbol{k} * x + d \qquad \text{(Eqn. 2)}$$

$$v_{max}\left[\frac{\mu mol}{g * h}\right] = \frac{k_{\mu mol}}{k_{hour}} * \text{ f } * \frac{1}{FW[g]} \qquad \text{(Eqn. 3)}$$

$k_{\mu mol}$…slope value per µmol Suc, calculated for the standard row of each batch
k_{hour} …. slope value per hour, calculated for each natural replicate
f…….. factor considering the fractional part of the total plant extract, here: 15

If the time course of the sucrose formation did not fit a straight line due to a single problematic value, this replicate was excluded. The values were boxplotted, outliers were identified and removed for calculation of mean values.

Assay optimization

The classical anthrone protocol for sucrose determination comprises the incubation of the extract solution at 95°C (see e.g. Nägele et al. 2010). The anthrone reagent indicates different sugars by a specific colour change which is sensitive to temperatures and incubation time. Therefore, testing and optimization of the new protocol (incubation temperature 40°C) with 70µl KOH or 70µl H_2O was done for the sugars fructose, glucose, sucrose, glucose-6-phosphate, fructose-6-phosphate and UDP-glucose. It was observed that the determination of sucrose remained intact irrespective of the KOH

treatment. The calibration curve showed a linear correlation in all cases and staining was stable for two hours on ice (Figure 3).

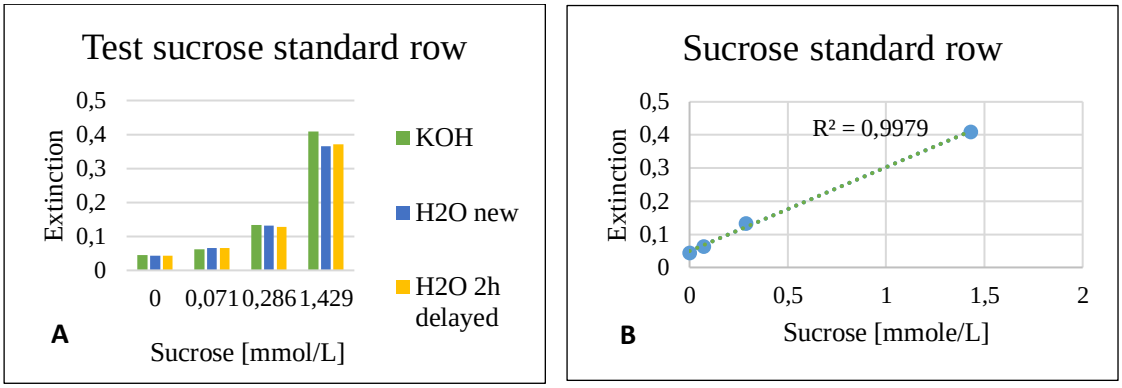

Figure 3 A: Stability of the sucrose calibration curve; B: Linearity of the anthrone signal for different sucrose concentrations

Fructose was shown to be detected by anthrone at 40°C but was completely destroyed by the KOH treatment. Glucose showed a minimal coloration at high concentrations, which was extinguished by KOH treatment. The tests of UDP-glucose (UDPG), glucose-6-phosphate (G6P) and fructose-6-phosphate (F6P) showed that only F6P could be fully detected. All of them were fully destroyed by KOH treatment (Figure 4). As sucrose was the only sugar for which a signal remained after the KOH treatment, and only fructose could be detected with anthrone at 40°C incubation temperature, this indicated that the obtained coloration correlates proportionally with the fructose moiety of the sucrose content in the sample. For the calculation, the amount of sucrose was considered equivalent to the detected amount of fructose.

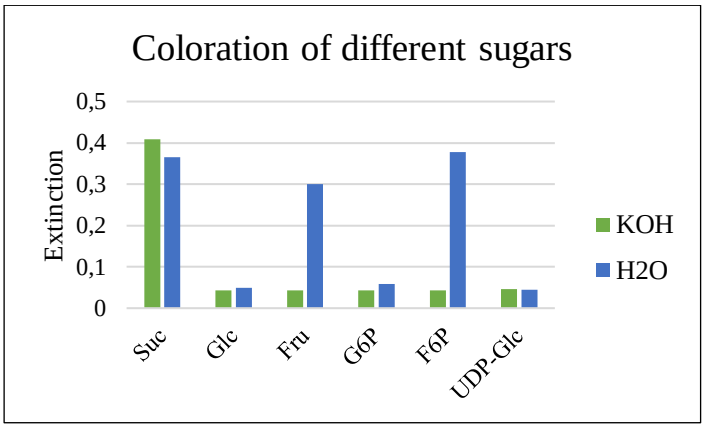

Figure 4 Stability of different sugars to KOH treatment & detectability with anthrone reaction at 40°C and 620nm; moderate differences in maximum extinction values between Suc, Fru and F6P are due to inaccuracy of the standard solutions

The first test with plant material was done with *snrk1α1α2* material from the end of the night. As described in the original protocol, 450 µl of extraction buffer were used. This turned out to be critical because the obtained amount of supernatant was slightly too little for the 8 aliquots needed. Following the given protocol, the enzyme reaction was stopped at 0, 4, 10 and 20 minutes. For each incubation time, two technical replicates were done. The obtained coloration was not sufficiently linear with regards to the incubation-time.

To increase the linearity, a higher volume of 750µl extraction buffer was taken. This advanced the purity of the extract, as it was easier to take down enough supernatant without material. A second step of 2 minutes centrifugation was introduced to remove the last material residues that could influence the photometric extinction. The incubation intervals were extended to 0, 10, 15, 20 minutes in order to reduce technical variance due to time limitation in pipetting.

Another explanation for the observed low linearity could be invertase activity in the extract counteracting SPS activity. TRIS buffer is known to inhibit invertase activity in *Pisum sativum L.* (Kim et al. 2010), hence a test with equivalent concentrations of TRIS-HCl instead of HEPES-KOH was done. Problematically, the activity of SPS was clearly reduced in the TRIS extract (Figure 5). TRIS may besides invertase also inhibit SPS activity and is therefore not applicable in this enzyme assay. A moderate inhibition of about 35% was already described previously in *Spinacia oleracea* (Amir, Preiss 1982).

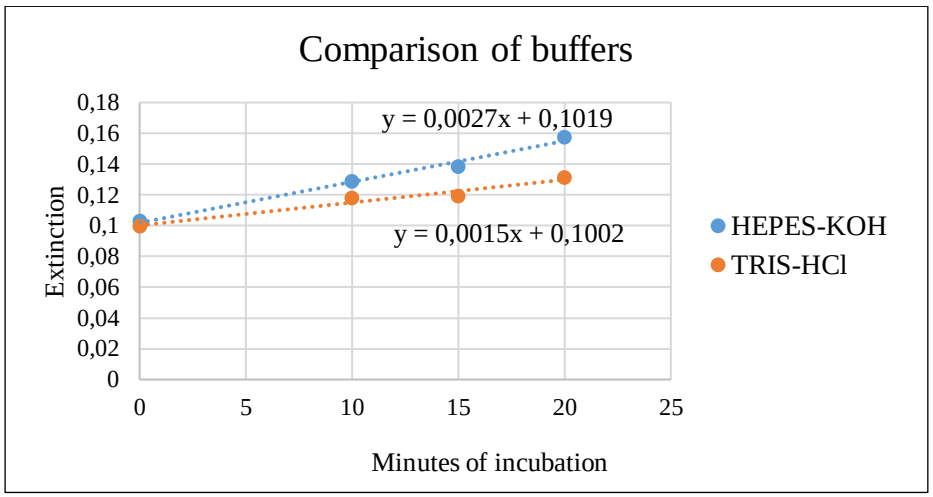

Figure 5 Test of different extraction buffers on the SPS anthrone assay. Results indicate that Tris-HCl buffer inhibits the activity of SPS

The most effective improvement concerning linearity was obtained by mixing the extract with the 20µl of reaction buffer properly before incubation. As the extraction buffer contained 10% glycerol, pipetting up and down several times was necessary to get a homogenous solution. Careful mixing was also important when adding 70µl KOH to immeadiately stop the incubation. Occasionally, single values did not fit the linear regression. These potential outliers were excluded if the other technical replicate fitted the line with the other values.

2.6 Invertase Assay

The maximum activity of soluble acid invertase (pH 4.7) and neutral invertase (pH 7.5) was measured by quantifying the amount of product (glucose) formed by the enzyme in a defined period. The measurement was finally done by converting glucose to glucose-6-phosphate via hexokinase. The enzyme glucose-6-phosphate-dehydrogenase further catalysed the reaction of G6P to 6-phosphogluconate resulting in the reduction of its co-substrate $NADP^+$ to NADPH in an equimolar amount. The increase of absorbance at 340nm could be measured on the photometer (Bisswanger 2012, p. 153).

Experimental protocol

Frozen and finely ground leaf material was incubated on ice with 500µl invertase extraction buffer for 10 minutes. To mix the plant material thoroughly with the buffer, the tubes were pivoted a few times. Centrifugation for 5 minutes followed with 13,000rpm and 4°C. The supernatant was transferred to new tubes and the pellet was discarded. To get rid of pellet leftovers, a second centrifugation step was done for 1 minute at the same settings and the supernatant was again transferred.

For each biological sample, four reaction tubes were prepared for the assay to detect soluble acid invertase with its corresponding blank and neutral invertase with its corresponding blank. Each tube was filled with 50µl of crude extract. The blanks were directly put to 95°C for 3 minutes to denaturate the enzymes. Then 100µl of acidic or neutral reaction buffer were added to each sample and were carefully but quickly blended by pipetting up and down a few times. The timer period for incubation was 15 minutes at 30°C. Subsequently all samples were immediately put on 95°C for three minutes to stop the invertase reaction. The samples were left to acclimate to room temperature.

The samples for acid invertase had to be pH neutralized for the later enzymatic conversion by hexokinase. 5µl 1.5% (w/v) KOH were added which resulted in a pH of 7.5. Following this, all samples were centrifuged at 13,000 rpm for 1 minute. 60µl (neutral invertase) or 30µl (acid invertase) of supernatant were transferred to new tubes. For dilution, doubly-distilled water (H_2O_{dd}) was added to a total volume of 120µl per sample.

The glucose quantification by a coupled hexokinase (HK) - glucose-6-phosphate dehydrogenase (G6PDH) assay was carried out in flat bottomed photometer well-plates (µClear®) specifically laminated for absorption at 340nm wavelength. 100µl of the diluted extract from the Eppendorf tubes were pipetted to 100µl of invertase assay hexokinase mixture (see Table 2) in the well-plate. The solutions were mixed by pipetting up and down a few times. The plates were incubated for 15 minutes at room temperature. Then the extinction was measured photometrically at 340nm.

Calculation of maximum activity

To calculate the concentration of NADPH from the measured extinction values, Lambert Beer's law was employed (Eqn. 4). First, the difference of extinction between blank and sample was determined, each for neutral and acid invertase. This change of absorption was divided by the molar extinction coefficient for NADPH multiplied with the layer thickness of the medium in the photometer well (1.1 cm). Next it was multiplied with 200 for the number of µl to get the amount of glucose in the well in µmol. A further dilution factor was 1.2 due to taking 100µl solution from the whole 120µl that were taken out after the last centrifugation step. Different factors 2.5 or 5.16667 were applied for either neutral invertase (60µl out of 150µl digested) or acid invertase (30µl out of 155µl digested & neutralized). This accounted for the dilution step done to get a proper amount of glucose that resulted in an extinction of below 1.0 in the photometer. Multiplication with 4, to get the turnover per hour, with 10 to get the activity for the whole extract and division through the sample weight in gram fresh weight finally resulted in the activity in $[\frac{\mu mol}{g*h}]$.

$$c\left[\frac{\mu mol}{\mu l}\right] = \frac{A}{\mathcal{E} * d}$$ Lambert Beer's law (Bisswanger 2012, p. 64) (Eqn. 4)

$$v_{max}\left[\frac{\mu mol}{g*h}\right] = \frac{\Delta A}{6220*1.1} * 200 * 1.2 * 2.5 \; or \; 5.16667 * 4 * 10 * \frac{1}{FW\,[g]}$$ (Eqn. 5)

c…..concentration
A….absorption value, Δ A: difference between sample and blank
Ɛ….molar absorption coefficient, NADPH (340nm): $\mathcal{E} = 6220\,\frac{L}{mol*cm}$
d… layer thickness

Detecting glucose moieties in assay solution

An alternative possibility for quantifying glucose moieties was measuring glucose via GC-ToF-MS. However, in a test batch the high concentration of the reaction substrate sucrose in the reaction buffer complicated the chromatographic analysis. Moreover, a first test showed that the pellet did not dry sufficiently in the vacuum concentrator, as the extraction buffer contained 10% glycerol. This would have interfered with the derivatization process.

Finally, in the present study, glucose was quantified photometrically by a coupled hexokinase/G6PDH enzyme assay. With using a completely new, intact hexokinase enzyme, the concentrations of a glucose standard row could be calculated correctly from the change of extinction by applying Lambert-Beer's law (Eqn. 4). 15 minutes of incubation in the photometer well-plate resulted in full conversion.

Table 10 Testing of the glucose standard row for Invertase assay

Glc concentrations [µM]	Resulting nmol/well	ΔExtinction	Calculated nmol/well
0	**0**	0	**0**
10	**1**	0,029529657	**0,863187867**
50	**5**	0,169988394	**4,968967971**
100	**10**	0,344029846	**10,05641176**
200	**20**	0,682329871	**19,94533386**

A possible negative interference of the mixture of invertase assay extraction- and reaction buffers with the hexokinase/G6PDH reaction was checked, yet no interference was observed. The acid invertase assay had to be pH neutralized. The protocol for the glucose-oxidase assay suggested to take 20µl 1M NaH_2PO_4, which did not result in the required pH of 7-7.5. It also turned out that a 1:1 mixture of extraction buffer and acid reaction buffer did not result in the needed pH of 5 for the acid invertase to work at maximum velocity. The protocol was consequently adjusted to taking only 50µl extract and adding 100µl of reaction buffer. The neutralization step for acid invertase was done with 5µl 1.5% (w/v) KOH.

The incubation time of the reaction buffer with the plant extract was set to 15 minutes. Further, samples for neutral invertase were diluted 1:2 with water after the last centrifugation step, for acid invertase with higher activity, a dilution of 1:4 was necessary to keep the extinction in a linear detection range.

2.7 Glucokinase & Fructokinase Assay

Maximum activities under substrate saturation for hexose phosphorylation were determined photometrically in a coupled enzyme assay. Glucokinase and fructokinase enzymes catalyse the phosphorylation of hexoses. Hexose phosphates then represent the substrate for the enzymatic interconversion catalysed by G6PDH. In the latter reaction, the co-substrate $NADP^+$ is reduced and the formed NADPH can be measured at 340nm. Finally, the extinction should change proportionally to the turnover of glucose/fructose by hexokinases. The substrate of G6PDH is glucose-6-phosphate, and, thus, to enable fructokinase activity measurement, the enzyme PGI had to be added additionally interconverting fructose-6-phosphate into glucose-6-phosphate.

Experimental protocol

To each sample of 80-100mg frozen and ground leaf material, 1ml extraction buffer was added. The samples were incubated for 10 minutes on ice. They were carefully pivoted a few times to make sure all material is suspended. Samples were centrifuged for 20 minutes at 4°C with 13,000 rpm. The supernatant was transferred to new tubes.

For each sample the activity of glucokinase and fructokinase was measured. 140µl of reaction buffer were pipetted into each well of the photometer well-plate. The other

components including the crude extract were added accordingly (see Table 2). ATP was not added to the blank and PGI was only added in the fructokinase batch. As a last step, the substrate, i.e. either glucose or fructose diluted in reaction buffer, was added. By pipetting up and down carefully, the solutions were mixed. Measurement started immediately after addition of the substrate. The measurement intervals were set to 15 seconds over a period of 15 minutes. The temperature inside the photometer was in a range of 25-27°C.

Calculation of maximum activity

For slope calculation, only samples without strong blank shift were taken. Slope calculation always started at the second measurement point (15sec), and ended where the reference began to rise distinctly.

Applying Lambert Beer's law (Eqn. 4) the final concentration of NADPH was calculated per µl. This was then multiplied with the factor 188 [µl] to account for the total amount of substance per well and with 50, accounting for the fraction of total extract used. To normalise the maximum enzyme activity to hours and gram fresh weight, results were multiplied with 60 (min->h) and divided by the fresh weight of the samples.

$$\mathcal{V}max\ [\frac{\mu mol}{g*h}] = \frac{\Delta\ A}{6220*1.1}\ * 188 * 50 * 60 * \frac{1}{FW\ [g]} \qquad \text{(Eqn. 6)}$$

ΔA = change of absorption per minute (= slope value)

The most critical part in this coupled assay was the lack of linearity in the recorded slope. If using cleaned up enzyme solutions under optimum conditions, the amount of NADPH should rise linearly for some minutes until substrate runs short. The blank extinction should stay the same over the whole time course. Only the linear part without blank shift is then used for activity calculation. But as crude enzyme extract actually contains a lot of ions and other interfering substances, perfectly linear graphs were the exception.

The performance of the coupled assay per se was tested with purchased hexokinase from bakers' yeast. The maximum velocity increased proportionally (within the first 4 minutes) to the deployed enzyme amount, indicating that the method worked properly (Figure 6).

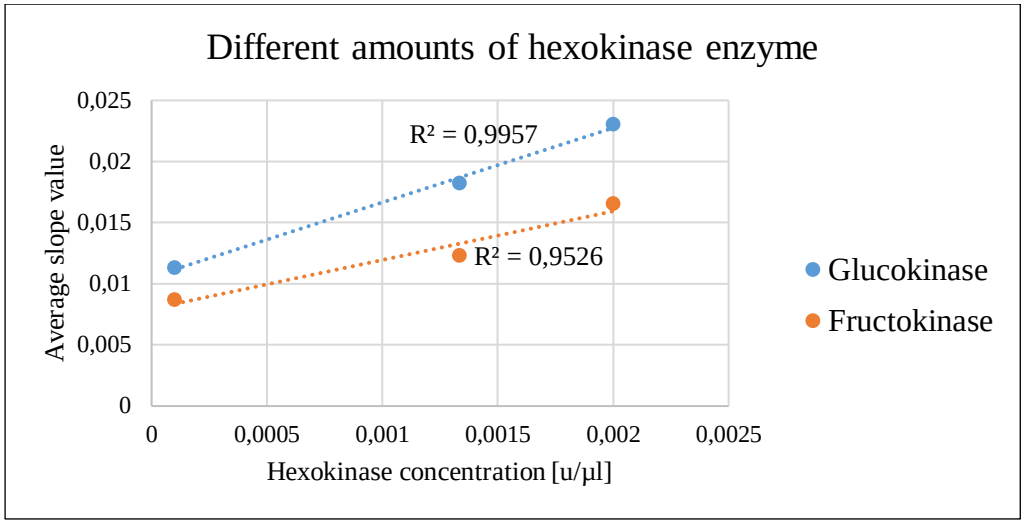

Figure 6 Dilution effect in photometric hexokinase activity analysis.

An equivalent test was done for the *A. thaliana* enzyme extracts. Different amounts of crude extract (20/30/40µl) were pipetted to the well-plate. The volume was compensated by varied amounts of reaction buffer (total volume: 188 µl). The different quantities of plant extract resulted in correspondingly distinct slope-values. The calculation of the activity [µmol/(g*h)], considering the different volumes of enzyme extract, revealed very similar values for all three variants. The shown proportionality of enzyme amount and slope proved the validity of the assay (Table 11).

Table 11 Proportionality of the amount of crude extract and slope values

	Glucokinase		
	20µl	30µl	40µl
Slope	0,00509	0,00813	0,01082
Vmax	4,932	5,253	5,239

	Fructokinase		
	20µl	30µl	40µl
Slope	0,00441	0,00629	0,00796
Vmax	4,275	4,064	3,854

As enzyme purification would have been too time consuming, the presence of interfering components in the crude extract could not be excluded. The linearity of the recorded slope could nevertheless be improved by enhancing solution mixing in the well-plates. For this purpose, a higher volume of more diluted substrates (1µl Sugar standard + 19µl HK reaction buffer) was pipetted as a final step.

2.8 Starch Quantification

For the determination of starch content, all soluble sugars were extracted from the plant material by adding 400µl 80% ethanol to each sample containing 80-100 mg frozen leaf material. Five biological replicates were done for each timepoint. Samples were incubated at 80°C / 400rpm on a thermoshaker for 30 minutes, afterwards centrifuged for 10 minutes at a speed of 13,000 rpm. The supernatant was discarded and the extraction was repeated a second time.

1ml of 0.5M NaOH was added to the pellet for alkaline hydrolysis of the starch granules. Samples were incubated on the shaker for 60 minutes at 95°C with 400rpm. Closing caps and safe lock tubes were utilized to safely lock the tubes. After cooling to room temperature, the solution was neutralized with 1ml 1N acetic acid. 500µl were transferred to a new tube. 500µl of amyloglucosidase reagent were added followed by incubation at 55°C for at least two hours for complete digestion to glucose.

200µl of each digested sample were transferred to a new tube and dried completely in vacuum concentrator at 0.001mbar. The dried samples were then kept at -20°C until measurement. Before derivatization they were put to room temperature for 20 minutes to avoid condense water being trapped in the tubes which would interfere with GC analysis.

20 µl of methoximation-reagent were pipetted to each sample. Incubation followed for 30 minutes on a thermoshaker at 30°C and 900rpm. 80µl of MSTFA were added and samples were incubated for 30 minutes at 37°C / 900rpm. Samples were centrifuged with 14,000rpm for 4 minutes and the supernatant was transferred to GC-microvials with micro-inserts which were closed immediately with crimp caps.

Glucose was detected on an Agilent 6890 gas chromatograph coupled to a LECO Pegasus® 4D GCxGC-TOF mass spectrometer. The column used for separation was an Agilent HP5MS (length: 30 m, diameter: 0.25 mm, film: 0.25 µm). The applied GC oven temperature ramp is described in the following (Table 12).

Table 12 Applied GC oven temperature ramp

Rate [°C/min]	Target Temperature [°C]	Duration [min]
0	70	1.00
18.00	330	6.00

Data processing and calculation

Deconvolution of the raw data was performed with the Leco Pegasus Chromatof® software. Standard processing without retention index was applied, glucose main- and by-product were set to the reference list (m/z ratio = 319). Peaks were manually checked for proper integration. For calculation of the glucose amount, the peak areas of main- and by-product were summed up and compared to calibration curves.

To reveal the concentration of starch per gram fresh weight, the calculated amount of glucose on the column was multiplied with the factor 100 which was the injection ratio (1µl out of 100µl sample). The second factor was 20, taking into account that only ¼ of the total volume (1/4*2000µl = 500µl) had been taken for digestion and again only 1/5 (1/5*500µl = 100µl) of the digested sample had been analysed via GC-MS. The glucose amount (in picomol) was divided through one million to get the unit of micromol. This total amount of starch-derived glucose moieties in the plant material was then divided through the sample weight in gram to get the amount of starch per gram fresh weight (Eqn. 8).

$$c\ (Starch)\left[\frac{\mu mol\ Glc}{g\ FW}\right] = \frac{x * 100 * 20}{1{,}000{,}000 * [g]\ FW} \qquad \text{(Eqn. 7)}$$

2.9 Functional Time Series Analysis

For merging experimental time series data of enzyme activities and metabolite levels into a coherent functional picture on the biological level, a mathematical approach was applied. Using the recently published FEMTO graphical user interface for Matlab® (Nägele et al. 2016), potential time points of regulatory perturbation were identified for both genotypes and then compared to each other. This should reveal differences in biochemical regulation due to a deficiency in SnRK1 activity.

To connect the discrete measurement points into continuous information, the FEMTO tool offers a range of interpolation methods. Here, a cubic spline interpolation was applied.

Based on the time-continuous spline interpolations, ratios of time-dependent derivative functions were built, suggesting an estimate of metabolic interactions. The first-order derivative f_x**'** *(t)* represents the metabolic function of metabolite x, i.e. the time-dependent change of a metabolite's concentration. This dynamic is the sum of all reactions producing or consuming a metabolite. The second-order derivative f_x**''** *(t)* of a metabolite's interpolation describes the time-dependent changes in its metabolic function. The final function ω always represents the ratio of a metabolic function (1st derivative) and a biochemically related 2nd derivative (Eqn. 8). (ibid.)

$$\omega\,(a \rightarrow b, t) = \frac{\frac{d}{dt}\,f(b)}{f(a)} \qquad \text{(Eqn. 8)}$$

A simplified reaction model comprising the known interactions between the measured metabolites is prerequisite for applying the FEMTO analysis. The stoichiometric matrix N of a metabolic model can be read-out from the model with the software Matlab. It contains information about dependencies of metabolic functions on specific metabolite concentrations. In ω(a → b, t), ω indicates changes in the metabolic function of metabolite b in context of concentration changes of metabolite a. The metabolite a might represent a substrate, inhibitor or activator molecule. The resulting time course of |ω(t)| gives information about possible time-points of deregulation. Time points of perturbation suggested by high |ω(t)| values might indicate changes in enzyme regulation or abundance (ibid.). Moreover, a shift in the metabolic function can be due to a modification in a consuming reaction. For the present work, interest was directed towards a potential correlation between the FEMTO-output and the measured time course of v_{max} enzyme activities.

The validity of the FEMTO approach presumes adequate sampling intervals, that lead to a meaningful regression analysis. The long intervals between the last sampling points, respectively the smaller number of measurement points for G6P, F6P and UDPG therefore constituted potential constraints for the interpretability of the FEMTO outcome.

3 Results

3.1 Metabolite Concentrations and Enzyme Activities

To further explore the impact of lacking SnRK1 catalytic activity under low energy conditions, one important part of the performed extended night experiment was the measurement of several key enzyme activities. To unravel biochemical regulation, enzyme data was kinetically connected with substrate and product concentration. The presented data for sucrose, fructose and glucose was taken from a previously published study (Nukarinen et al. 2016). The organisation of the *Results* chapter follows the model of central carbohydrate metabolism (Figure 1), shown in the chapter *Introduction*.

Sucrose biosynthesis: SPS activity is fluctuating stronger in the wild type than in *snrk1α1α2* plants at the beginning of the extended night

The measurement of maximum SPS activity in Col-0 (Figure 7) revealed a mean value of 4.38 µmol/(g*h) at the end of the night. A significant (t-test p = 0.006) upregulation to an average of 6.97 µmol/(g*h) occurred within the first 20 min of the extended night. The high value of v_{max} was maintained until 80 min of extended night, when a noteworthy decrease ensued. For the later time points, no significant changes were recorded.

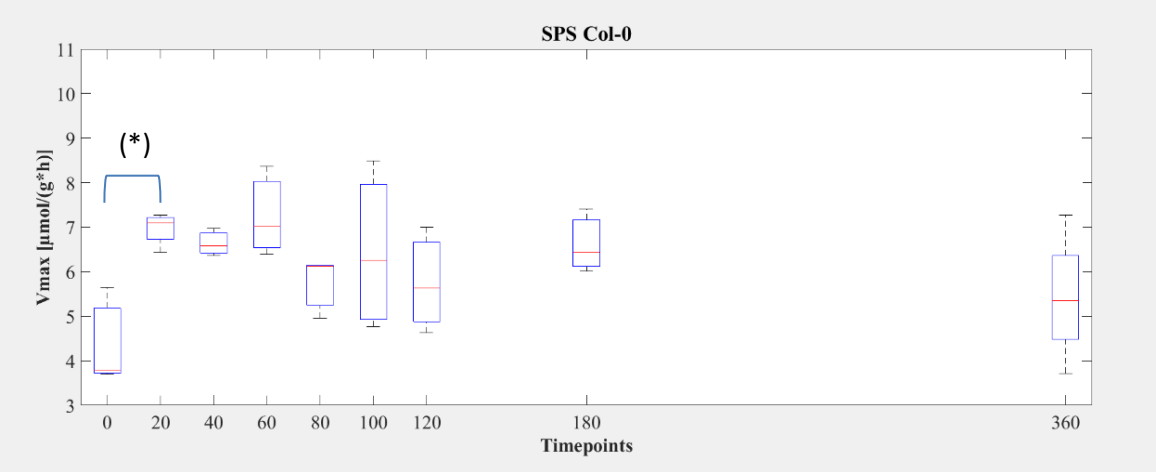

Figure 7 Time series of sucrose phosphate synthase maximum activity (v_{max}) for Col-0; Asterisks (*) indicate a significant difference between time points (t-test p<0.05)

The SPS data of *snrk1α1α2* (Figure 8) showed a higher biological variance and no significant changes over the time course. A moderate trend of downregulation could be observed between 80 and 180 min of extended night. After 180 min, the mean value of v_{max} was lower than at the beginning of the extended night.

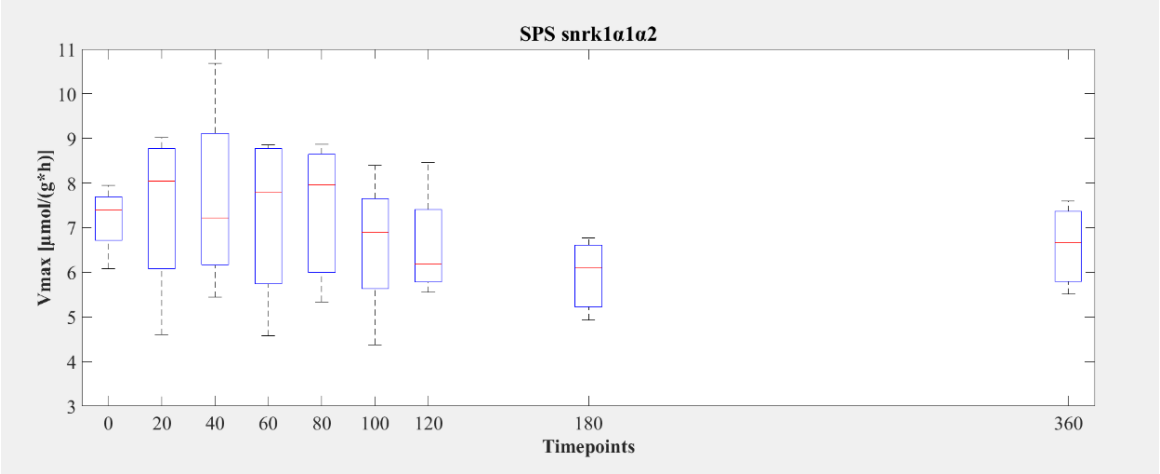

Figure 8 Time series of sucrose phosphate synthase maximum activity (v_{max}) for *snrk1α1α2*

The comparison of the time course of v_{max} values between the genotypes (Figure 9) revealed significant differences (ANOVA, p=0.0224). This divergence consisted mainly in the distinct values at the very beginning of the extended night, when upregulation took place within the first 20 min in the wildtype but not in *snrk1α1α2*. In the further course, mean values were similar.

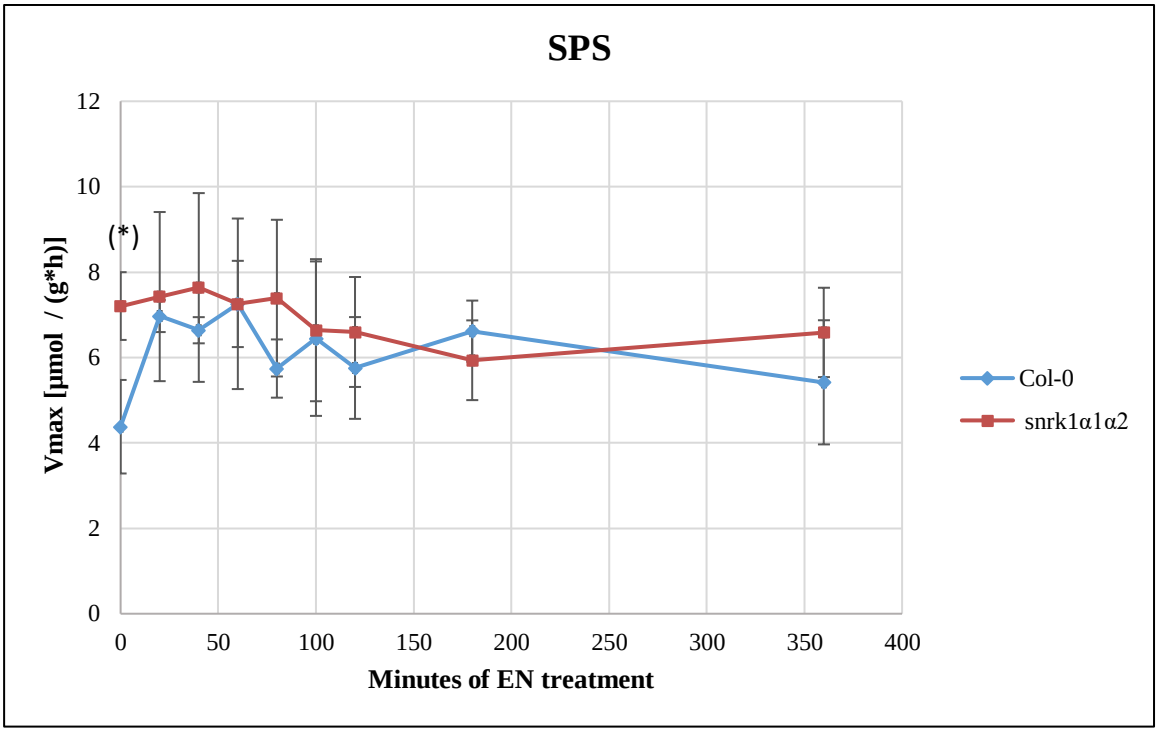

Figure 9 Comparison of sucrose phosphate synthase maximum activities (v_{max}) between Col-0 and *snrk1α1α2.* Data points are mean values of 3-5 biological replicates; error bars show standard deviation; Asterisks (*) indicate a significant difference between genotypes at that time point (t-test p<0.05)

The *snrk1α1α2* mutant has lowered fructose-6-phosphate levels at the end of the night

Generally, Col-0 showed higher F6P levels than *snrk1α1α2* except after one hour of extended night. Although differences were not significant, the genotypes showed an apparently distinct course of concentrations for this metabolite. Wildtype plants showed a mean value of ~0.03µmol /gFW at the end of the night, decreasing by 66% from 20 min to 120 min of extended night. Yet, after 360 min, Col-0 showed a moderately higher mean value again. In the *snrk1α1α2* mutant, the F6P concentration increased considerably during the first 20 min of extended night treatment and was still high after one hour. Between 60 min and 120 min, a significant decrease (t-test, p=0.03) occurred, approximating Col-0 levels. After 360 min, F6P content remained constantly low, resulting in notably different levels between genotypes at the end of the extended night treatment (see Figure 10).

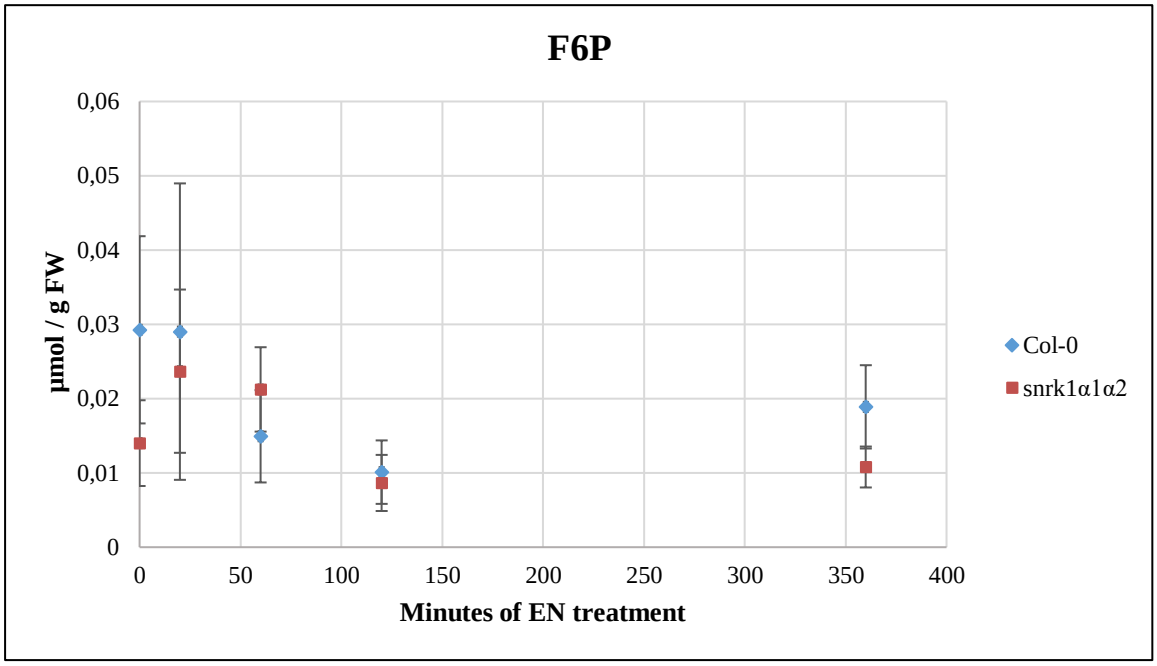

Figure 10 Fructose-6-phosphate concentrations of Col-0 and *snrk1α1α.2* plants in extended night treatment. Data points are mean values of 3 natural replicates; error bars show standard deviation

UDP-glucose concentrations do not differ significantly between wild type and *snrk1α1α2* plants

For UDP-glucose, no significant differences between time points and genotypes were observed. Overall, Col-0 showed slightly higher UDPG concentrations than the *snrk1α1α2* mutant. The average value increased by 20% during the first 20 min of the extended night in Col-0, then decreased again and remained constant over the time course. Compared to the wild type, *snrk1α1α2* contained equal concentrations of UDPG at the beginning of the extended night. The concentration was constant for the first 20 min, but slightly decreased after 60 min. The level recovered again after 2 hours, and subsequently decreased towards the end of the extended night exposure. The average value after 360 min was nearly twice as high in Col-0 (~0.055 µmol/gFW) compared to *snrk1α1α2* (~ 0.03 µmol/gFW) (Figure 11).

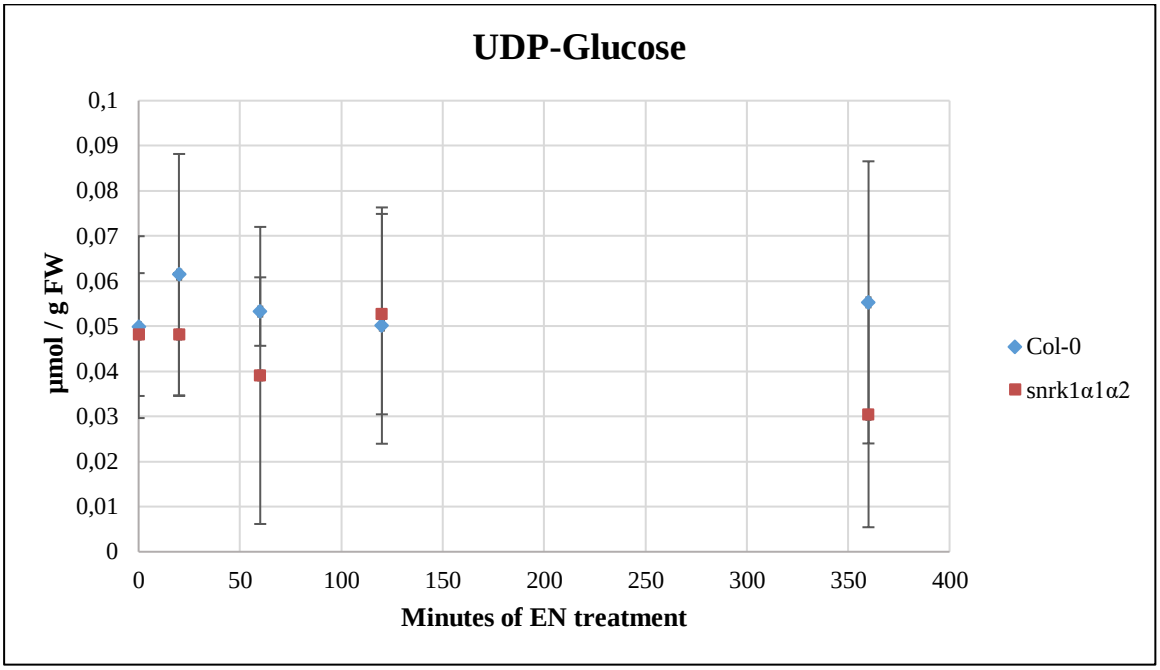

Figure 11 UDP-glucose concentrations of Col-0 and *snrk1α1α.2* plants in extended night treatment. Data points are mean values of 3 biological replicates; error bars show standard deviation

Col-0 maintains higher sucrose levels than the *snrk1α1α2* mutant throughout the whole extended night treatment

Sucrose concentrations were analysed and published by Nukarinen et al (2016). From all metabolites studied in this experiment, sucrose showed the most pronounced differences between the genotypes (ANOVA, $p<0.001$). Sucrose levels of Col-0 started at 0.95µmol/g

FW and showed a steady decline in the first hour of the extended night. After a slight accumulation between 60 and 80 min, degradation continued until 180 min. At that time in the middle of the treatment, sucrose concentration was signficantly lower than at the end of the night (Tukey HSD p = 0.022). In the second half of the extended night, the mean value slightly increased.

In the *snrk1α1α2* mutant line, a significant (t-test, p<0.001) drop took place between 20 and 40 min, when sucrose concentration decreased to a very low level (0.06µmol/g FW). In the following interval between 40 and 60 min, the sucrose level partially recovered (t-test p=0.01), showing a constant level until 120 min. During the third hour of the extended night treatment, the concentration declined considerably, staying constantly low until 6 hours of extended night.

Over the whole extended night time course, wildtype plants showed clearly higher sucrose levels. After 40 min and 80 min, this difference was signficiant in the Tukey HSD test. The average sucrose concentration at the end of the night in Col-0 was twice as high as in the *snrk1α1α2* mutant. The mean value in Col-0 after 6 hours of extended night resembled the sucrose concentration in *snrk1α1α2* plants at the very beginning of the treatment.

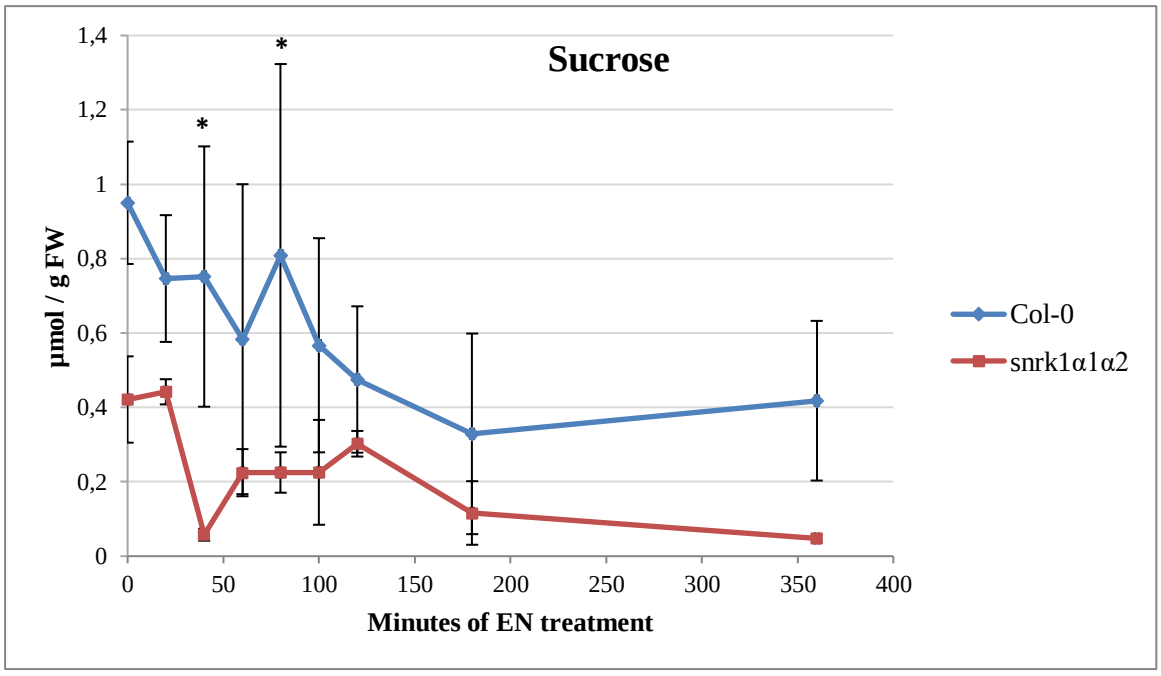

Figure 12 Sucrose concentrations of Col-0 and *snrk1α1α.2* plants during extended night treatment. Data points are mean values of 3-5 biological replicates; error bars show standard deviation; asterisks indicate significant differences between genotypes at each time point (*p< 0.05, **p< 0.01, ***p< 0.001)

Sucrose cleavage: maximum invertase activity is gradually upregulated in the wildtype during extended night exposure

Concerning the total invertase activity (sum of neutral and soluble acid invertase v_{max} activities), Col-0 started at a relatively low average activity of 26.71 µmol/(g*h) (Figure 13). A significant upregulation (t-test p=0.0097) was observed within the first 20 minutes, followed by a distinct decline after 40 min (t-test p= 0.038). In the interval between 40 and 120 min, the increase was linear, subsequently flattening from 120 to 180 min. The value of v_{max} after 6 hours was significantly (Tukey HSD p<0.05) higher than during the first 100 minutes of the extended night.

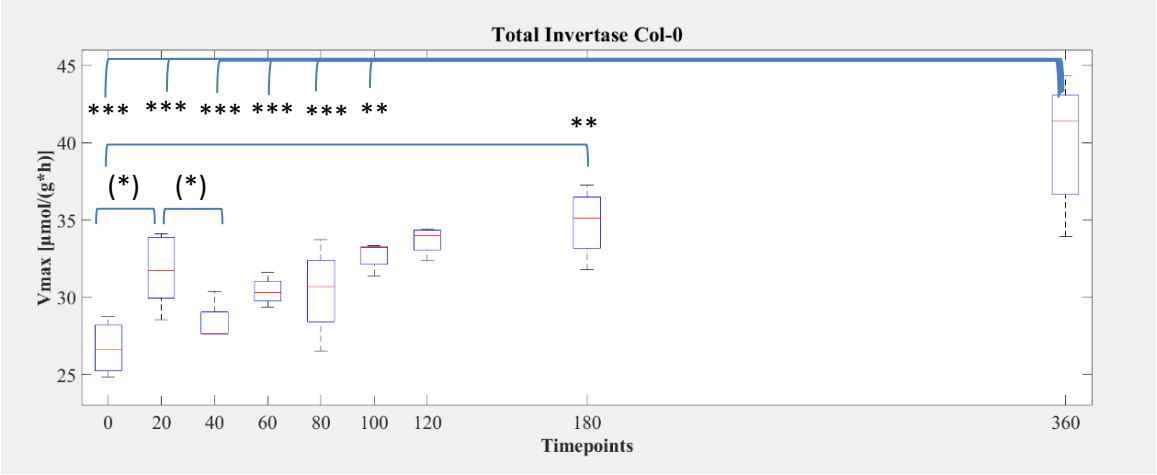

Figure 13 Time series of total invertase (= sum of acid and neutral Inv.) maximum activity (v_{max}) for Col-0; asterisks indicate significant differences between time points (Tukey HSD *p< 0.05, **p< 0.01, ***p< 0.001; t-test (*) p<0.05)

Snrk1α1α2 (Figure 14) showed a very high activity of 37.95 µmol/(g*h) when compared to the wildtype at the end of the night. Between 40 and 60 min, activity dropped from 37 to 32 µmol/(g*h). Subsequently, in the ensuing interval from 60 to 80 min, the activity increased significantly (p=0.037). From 80 to 120 min, the activity decreased constantly. This was followed by a significant rise during the third hour of the extended night exposure (p=0.00037).

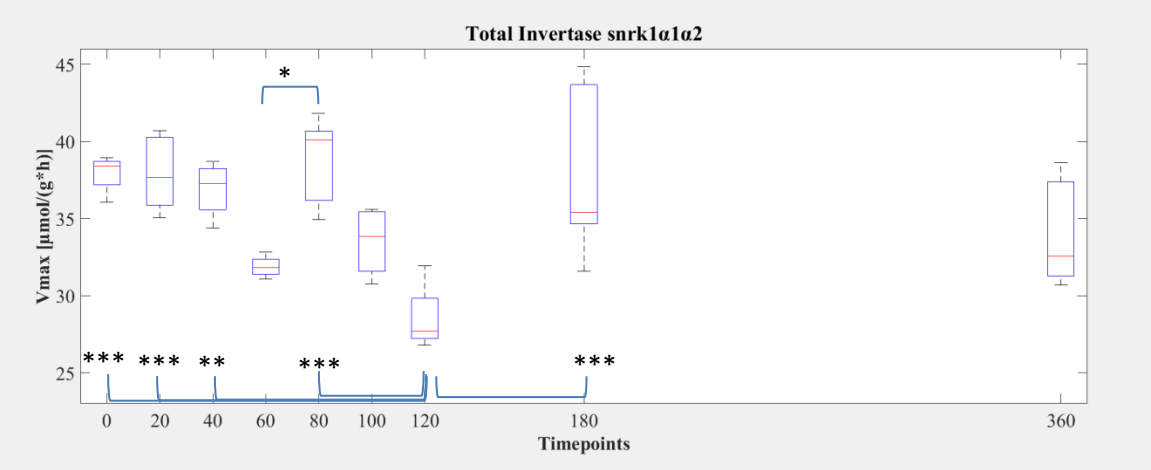

Figure 14 Time series of total invertase (= sum of acid and neutral Inv.) maximum activity (v_{max}) for *snrk1α1α2*; asterisks indicate significant differences between time points (*p< 0.05, **p< 0.01, ***p< 0.001)

The clear difference in the general dynamics between the two genotypes (Figure 15) was depicted by ANOVA giving a highly significant p-value of < 0.001. The difference was most pronounced at the end of the night, but even until 100 min, the wildtype showed constantly lower values than *snrk1α1α2*.

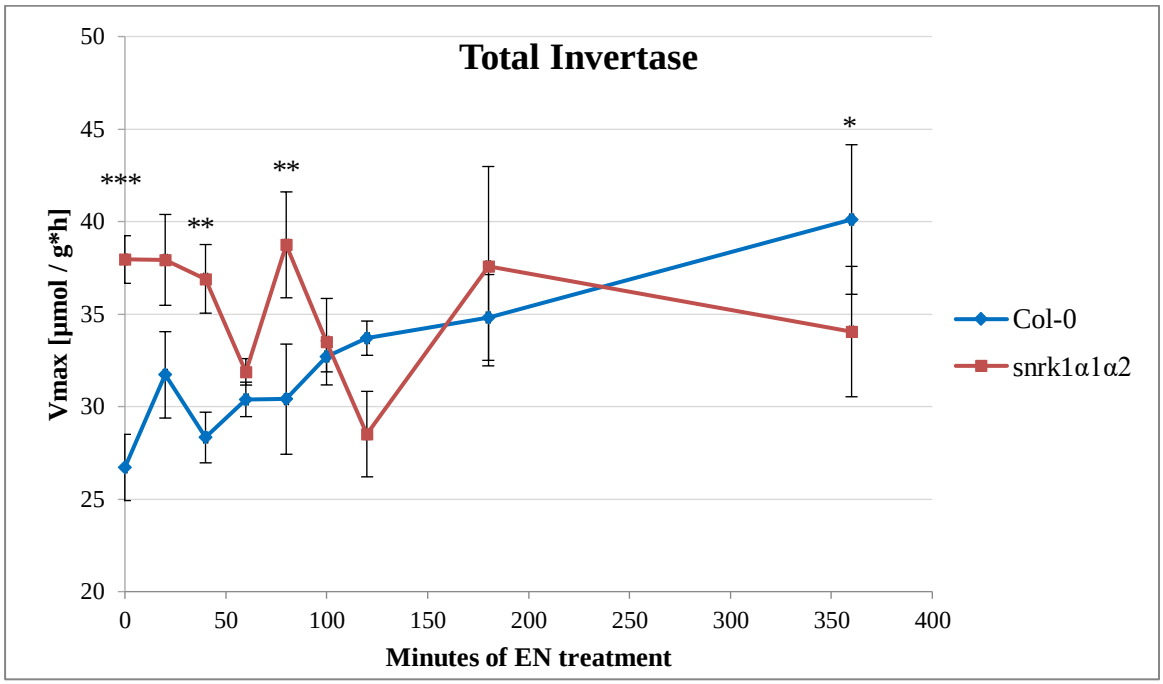

Figure 15 Comparison of total invertase (= sum of acid and neutral invertase) activities (v_{max}) between Col-0 and *snrk1α1α2* Data points are mean values of 4-5 biological replicates; error bars represent standard deviation. Asterisks indicate significant differences between genotypes at each time point (Tukey HSD *p< 0.05, **p< 0.01, ***p< 0.001).

The single invertase isoenzymes showed a trend like that of total invertase in each genotype. The activities measured for neutral invertase were low (5-10 µmol/(g*h)) when compared to acid invertase. Absolute values for each isozyme are plotted in *Appendix 6.3.*

Sucrose cleavage: Hexose levels are fluctuating stronger in *snrk1α1α2* than in Col-0

During the first 40 min of the extended night, average values of glucose levels were highly similar for both genotypes. Glucose content increased within the first 20 min and subsequently declined again to the same extent until 40 min. In the interval from 40 to 80 min, Col-0 showed a moderate increase. In the same interval, a clearly more pronounced and significant rise of the glucose level was observed in *snrk1α1α2* (t-test, p=0.034). From 80 to 180 min, glucose levels steadily decreased in the wildtype. In the second half of the extended night, a minimal recovery was observed. The *snrk1α1α2* mutant showed different dynamics with a significant drop by 80 % taking place between 80 and 100 min (Tukey HSD p=0.045). From 100 to 180 min, glucose significantly increased (Tukey HSD p=0.019), reaching the mean value of ~0.21 µmol/gFW which it had after 80 min, again. In the second half of the extended night time course, glucose concentration decreased, resulting in very similar concentrations for both genotypes after 360 minutes.

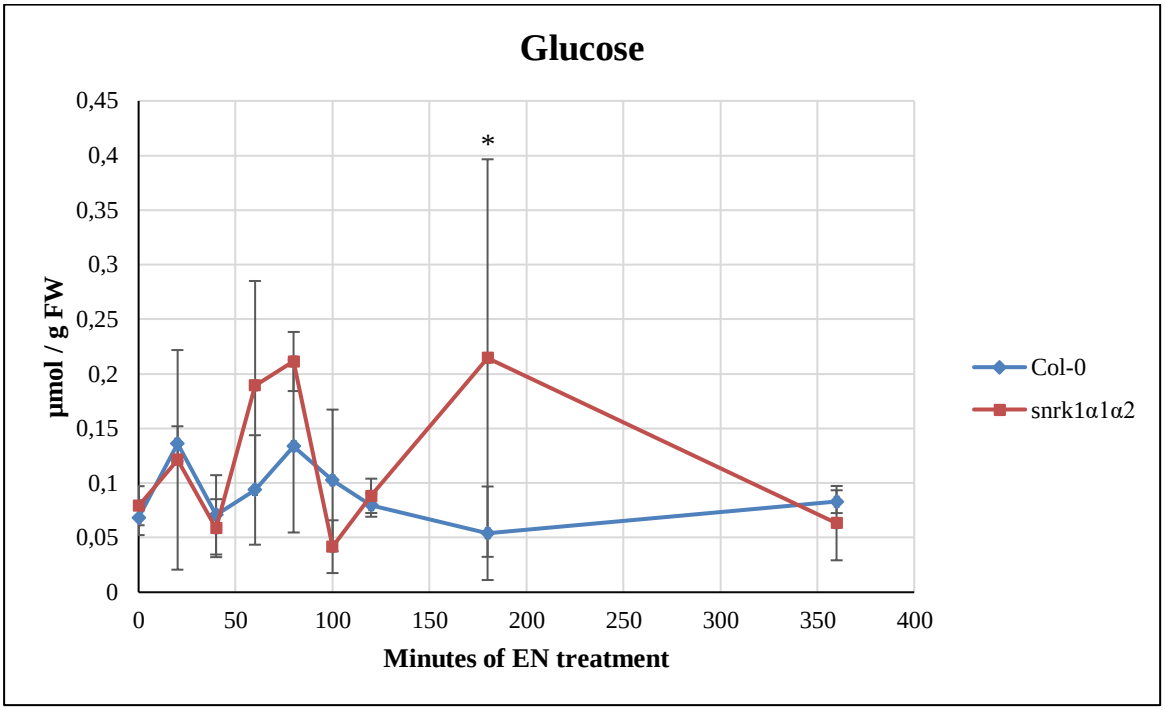

Figure 16 Glucose concentrations of Col-0 and *snrk1α1α.2* plants during extended night treatment. Data points are mean values of 3-5 biological replicates; error bars represent standard deviation. Asterisks indicate significant differences between genotypes at each time point (*p< 0.05, **p< 0.01, ***p< 0.001)

Fructose levels differed between both genotypes at the beginning of the extended night, showing higher concentrations in Col-0. Fructose decreased in the wildtype from within the first 40 min, but in the subsequent interval until 60 min, the concentration rose again. In the second hour of the extended night treatment, fructose content decreased constantly. From 2 hours onwards, the level was constantly low at 0.04 µmol /gFW. The fructose concentration in the *snrk1α1α2* mutant started at a lower value than in Col-0, and subsequently increased slightly within the first 20 minutes of extended night exposure. Significant depletion of the fructose pool was recorded in the interval from 20 to 40 min (t-test, p=0.0105), followed by a fast recovery to previous levels until 80 min. Between 80 and 100 min, fructose content moderately decreased and remained constant until 120 min. A possible rise was observed in the third hour, but due to high variance of the data after 180 min, the average value should not be over-interpreted. In the second half of the extended night treatment, levels decreased below wildtype levels until 360 min. The concentration in the *snrk1α1α2* mutant at the last time point was significantly lower than after 20 and 80 min.

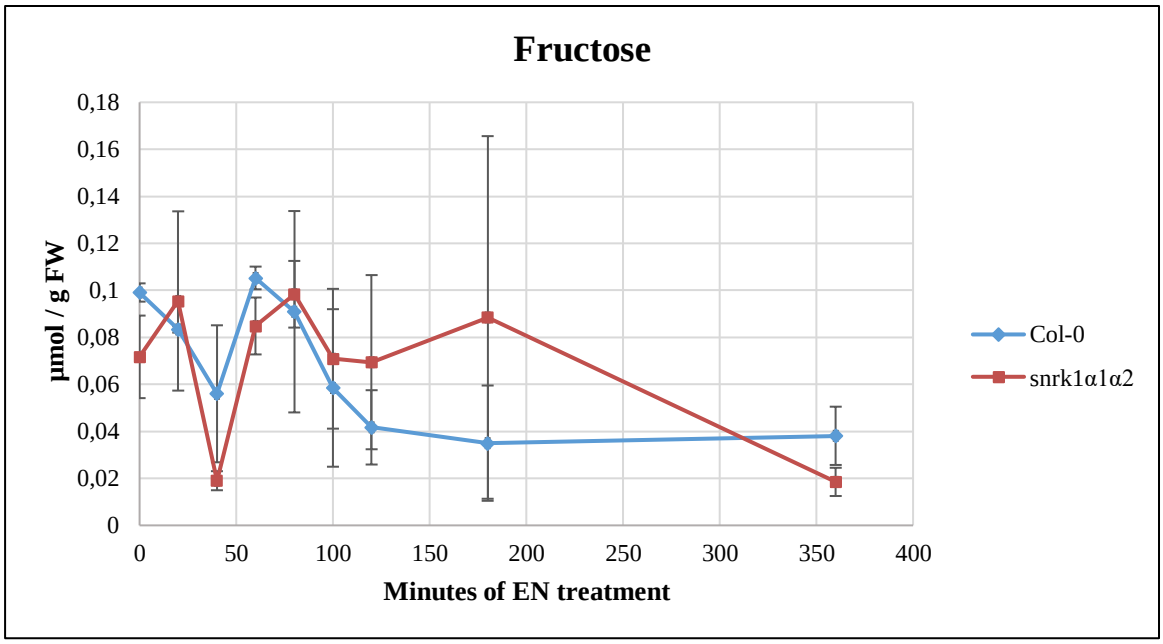

Figure 17 Fructose concentrations of Col-0 and *snrk1α1α.2* plants during extended night treatment. Data points are mean values of 3-5 biological replicates; error bars represent standard deviation.

Glucokinase activity is fluctuating stronger in the wild type than in *snrk1α1α2* plants

At the end of the night, low values of v_{max} for glucokinase were observed in the wild type, followed by an increase from ~4.6 to ~9.0 µmol/(g*h) within the first 20 minutes. In the subsequent interval, the maximum activity decreased significantly (t-test, p=0.0091). In the further time course, differences were not significant due to high variance of the enzyme assay data (Figure 18).

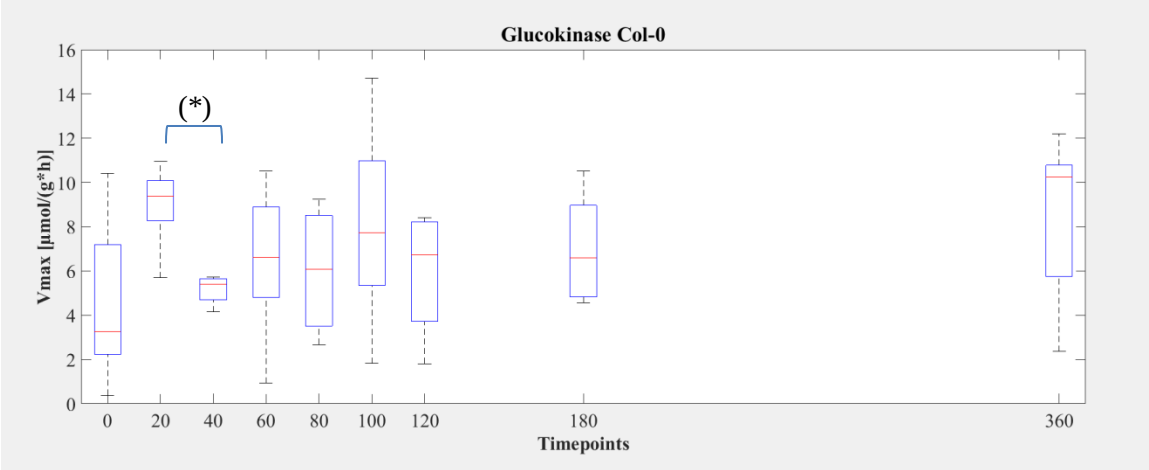

Figure 18 Time series of glucokinase maximum activity (v_{max}) for Col-0; asterisks indicate significant differences between time points (t-test (*) p< 0.05)

The *snrk1α1α2* mutant line (Figure 19) showed high values from the beginning of extended night exposure. After 40 min, a decrease was observed similarly to the wildtype. A trend of decreasing activity occurred in the later extended night between 120 and 360 min. In contrast, Col-0 showed a moderate increase in the same interval. The differences between the genotypes were not found to be significant (ANOVA). Interestingly, the time course of maximum enzyme activities was very similar between both genotypes within the first 100 minutes of the extended night, except for the increase in the wildtype during the first 20 minutes (Figure 20).

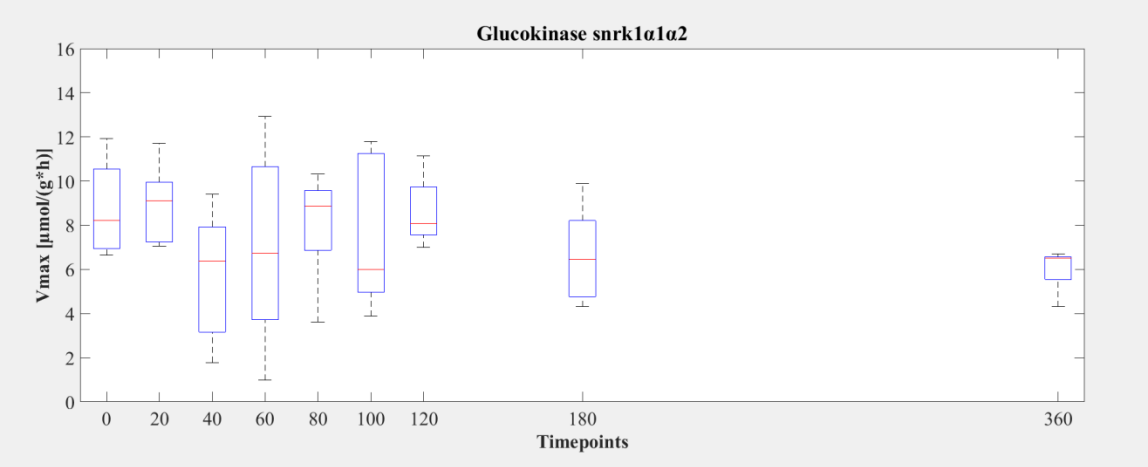

Figure 19 Time series of glucokinase maximum activity (v_{max}) for *snrk1α1α2*; asterisks indicate significant differences between time points (*p< 0.05, **p< 0.01, ***p< 0.001)

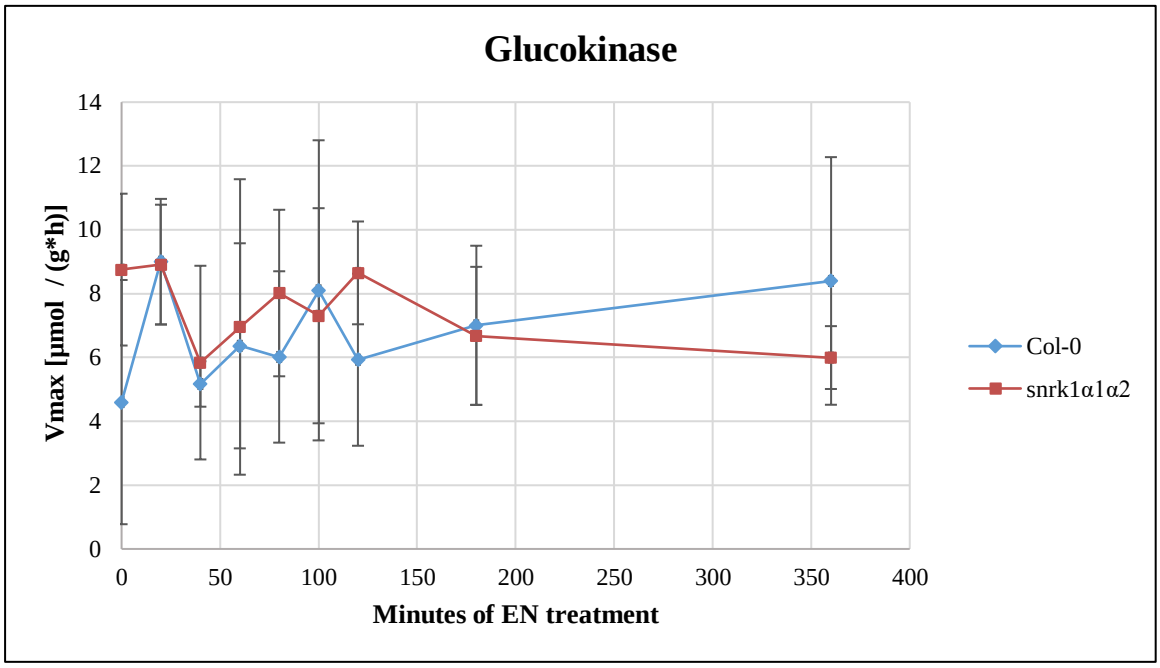

Figure 20 Comparison of glucokinase maximum activities (v_{max}) between Col-0 and *snrk1α1α.2.* Data points are mean values of 4-6 biological replicates; error bars represent standard deviation.

Glucose-6-phosphate levels are higher in the wildtype throughout the EN treatment

For glucose-6-phosphate, ANOVA confirmed significant differences between the analysed genotypes ($p<0.01$). The average values of Col-0 were continuouosly higher during the whole extended night time course (Figure 21). In the wildtype, the concentration decreased between within the first 20 minutes, followed by an accumulation until 120 min. In the second half of the treatment, the concentration

declined again. In *snrk1α1α2*, a rise occurred within the first hour of the extended night, while, subsequently, the concentration decreased again.

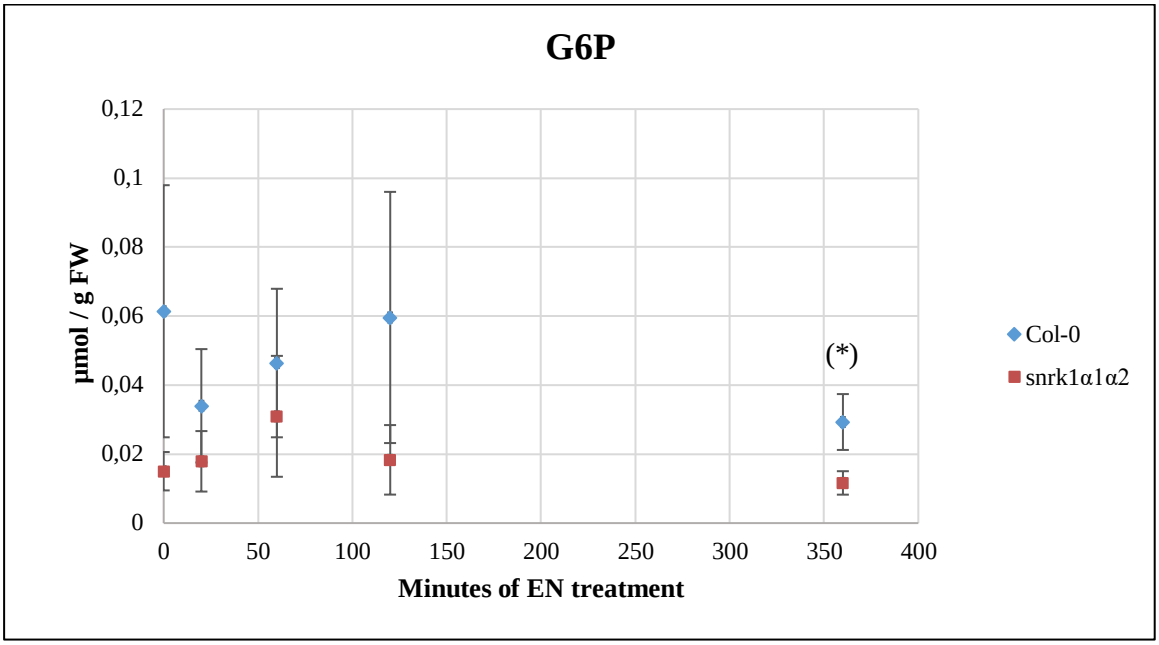

Figure 21 Glucose-6-phosphate concentrations of Col-0 and *snrk1α1α2* plants during extended night treatment. Data points are mean values of 3 biological replicates; error bars represent standard deviation. (*) indicates a significant difference between genotypes at that time point (t-test $p<0.05$)

Fructokinase is lower in the wildtype at the beginning and at the end of the EN treatment

For fructokinase, a similar pattern was observed as for glucokinase during the first 20 minutes: the wildtype had a lower activity at the end of the night, followed by a strong increase (t-test $p=0.0048$) (Figure 22).

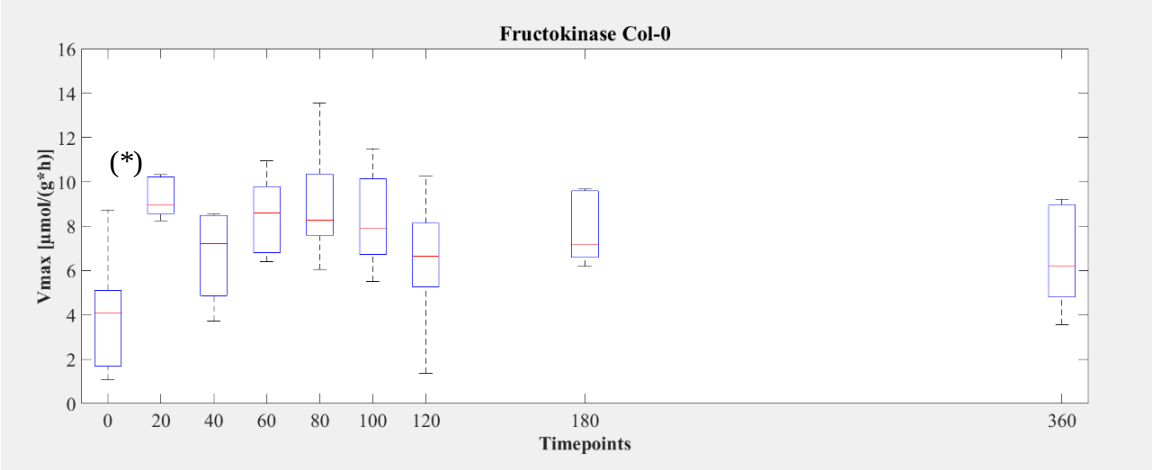

Figure 22 Time series of fructokinase maximum activity (v_{max}) for Col-0; asterisks indicate significant differences between time points (t-test $p<0.05$)

In contrast, the *snrk1α1α2* mutant, showed a constantly high value at the beginning of the extended night (Figure 23). A moderate decrease was observed in *snrk1α1α2* between 20 and 60 min, followed by a significantly higher value after 80 min (t-test p= 0.0307). The pattern in this interval was very similar for both genotypes, although the downregulation in the first hour was less distinct in Col-0 (Figure 24). Between 80 and 120 min, the average values of both genotypes behaved nearly identically. After 6 hours, Col-0 had lower activity than *snrk1α1α2*, revealing a contrasting picture between both genotypes in the second half of the extended night.

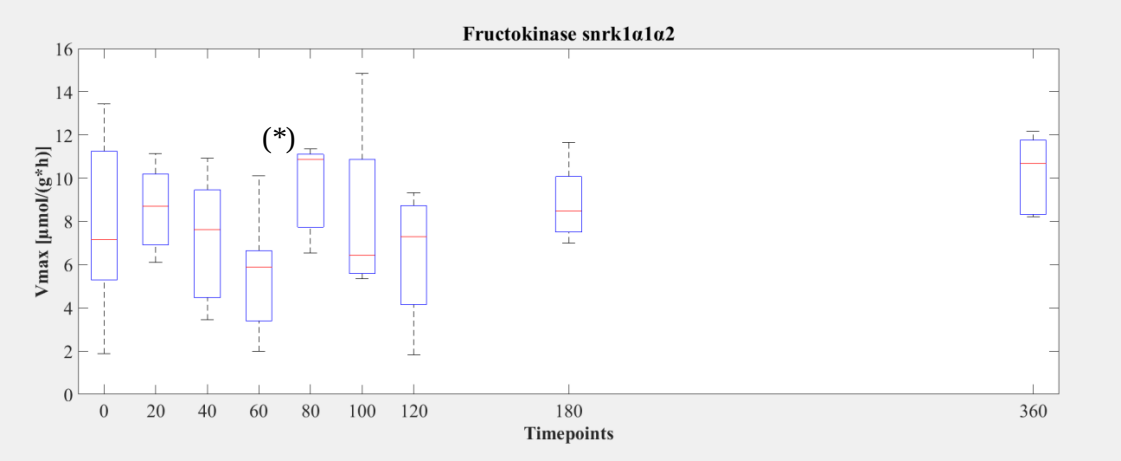

Figure 23 Time series of fructokinase maximum activity (v_{max}) for *snrk1α1α2*; asterisks indicate significant differences between time points (t-test p<0.05)

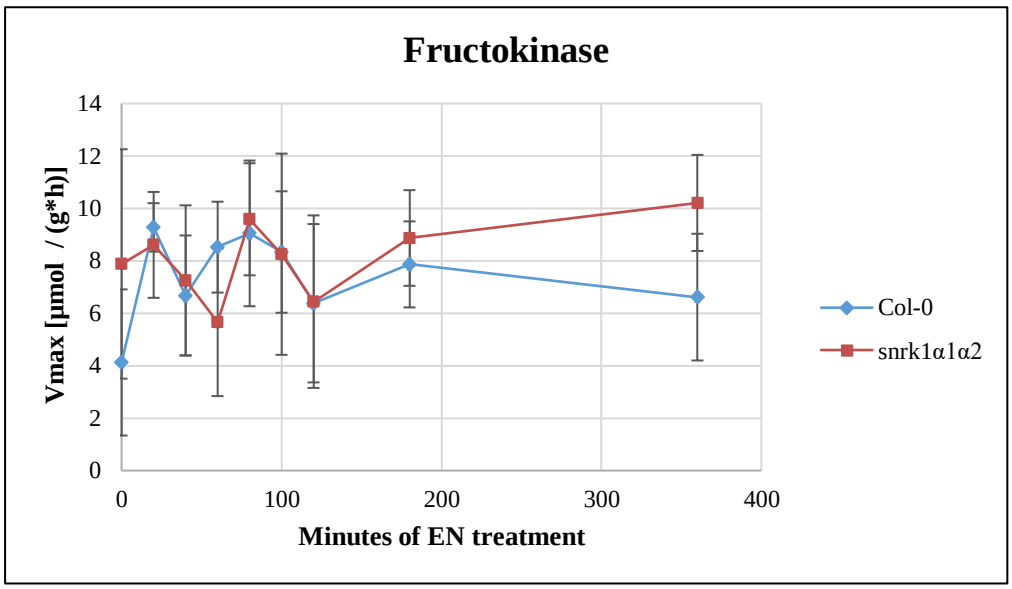

Figure 24 Comparison of glucokinase maximum activities (v_{max}) between Col-0 and *snrk1α1α.2.* Data points are mean values of 4-6 biological replicates; error bars represent standard deviation.

Degradation of transitory starch is affected by the *snrk1α1α2* mutation

In Col-0, starch content reduced by half within the first 20 minutes of the extended night and declined further until 40 min. In the interval between 40 and 60 min, a slight increase of the starch level was observed, but the content immediately decreased again in the following interval until 80 min. Subsequently, the starch level was constant at ~0.25 µmol C6/gFW. After 6 hours, the starch level was lowest (~0.2 µmol C6/gFW) (Figure 25).

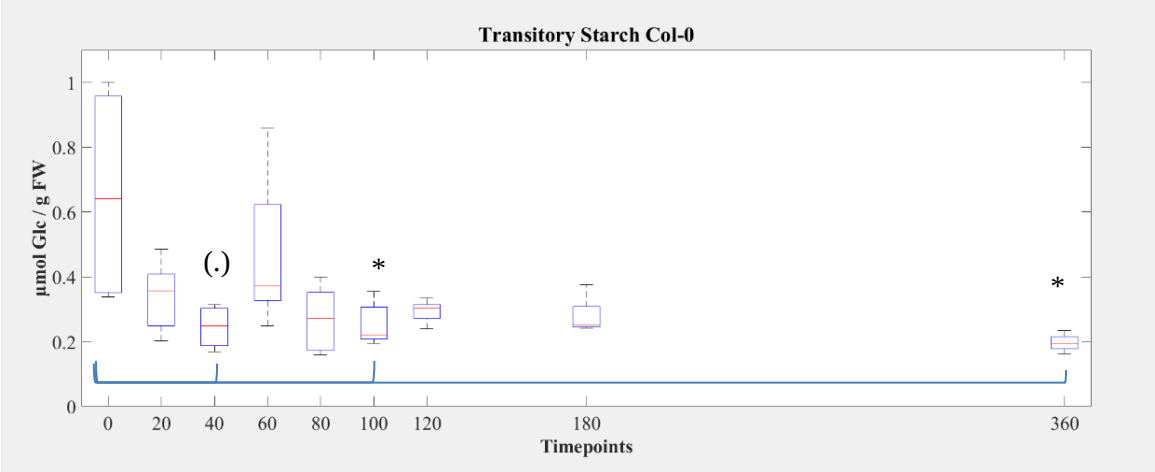

Figure 25 Time series of starch content (given as glucose equivalents) for Col-0; asterisks indicate significant differences between time points (*p< 0.05, **p< 0.01, ***p< 0.001, (.)p<0.1)

In *snrk1α1α2* (Figure 26) the initial value at the beginning of extended night exposure was similar to that of the wild type. The starch content showed only a minor decrease within the first hour (-13%). In the interval between 60 and 80 min, starch accumulated to 0.8 µmol/g FW, exceeding the initial value. From 80 to 120 min, starch was degraded and the value reduced by half, showing the lowest starch content of 0.36 µmol C6/g FW. Until the end of the extended night exposure, no additional significant changes were observed.

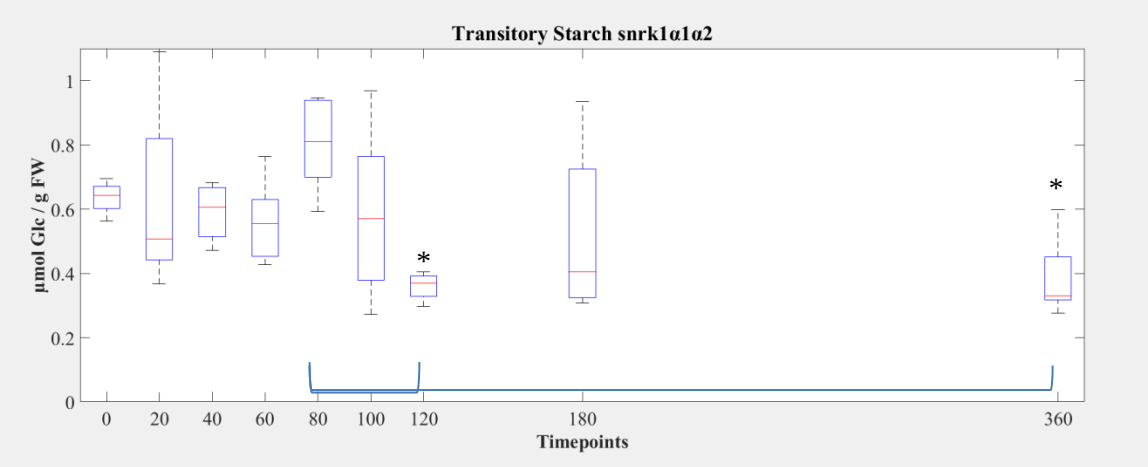

Figure 26 Time series of starch content (given as glucose equivalents) for *snrk1α1α2*; asterisks indicate significant differences between time points (*p< 0.05, **p< 0.01, ***p< 0.001)

ANOVA confirmed a highly significant difference between the genotypes (p =4.04*e-08) (Figure 27). Starch degradation in the *snrk1α1α2* mutant was obviously impaired at the beginning of the extended night. The short-time accumulation of starch occurred in both genotypes to the same extent (C: +0.23 vs S: +0.25µmol/g FW), but the increase happened 20 minutes later in *snrk1α1α2*. Due to a high value before the accumulation, *snrk1α1α2* reached after 80 min even higher levels of starch than at the end of the night. This was not the case for the wildtype. Both genotypes immediately degraded starch again in the following 20 minutes. Only in the *snrk1α1α2* mutant, further degradation took place. After 120 min, *snrk1α1α2* approximated Col-0 levels.

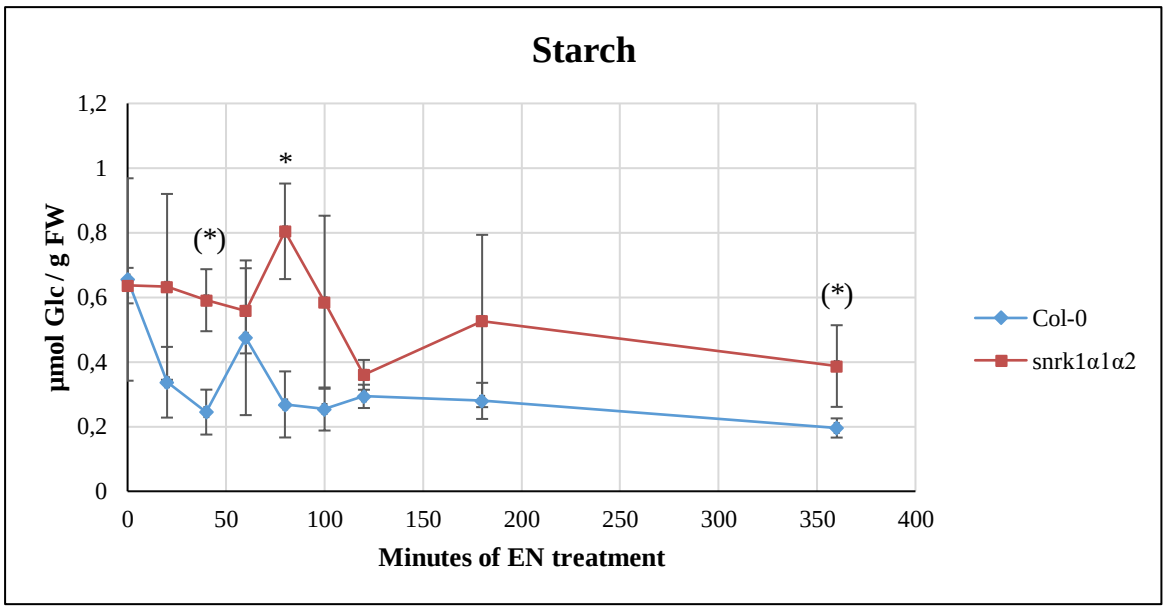

Figure 27 Starch content (given as glucose equivalents) of Col-0 and *snrk1α1α.2* plants in extended night treatment. Data points are mean values of 4-5 biological replicates; error bars represent standard deviation. Asterisks indicate significant differences between genotypes at each time point (Tukey HSD *p< 0.05, **p< 0.01, ***p< 0.001; t-test (*) p<0.05)

The *snrk1α1α2* mutant showed reduced carbohydrate levels and strong metabolic fluctuations between 20 and 60 minutes

Figure 28 summarizes average concentrations of sucrose, glucose, fructose, and starch in Col-0 and *snrk1α1α2*. Concentrations of hexose phosphates and UDP-glucose were excluded in this overview due to fewer measurement points. In both genotypes, the amount of carbohydrates decreased with proceeding extended night treatment. In general, the calculated CH content was lower in the mutant line. But within the first half of the treatment, Col-0 showed a stronger reduction in sugar content than *snrk1α1α2* plants.

The trend revealed an accumulation in Col-0 after 80 min. The increase was due to high sucrose and fructose levels. However, considering the high variance, mean values should not be over-interpreted. Noteworthy, the decrease of carbohydrates stopped after three hours, resulting in a very similar value after 6 hours. While starch was moderately degraded in the second half of the extended night, sucrose and glucose levels increased slightly.

In *snrk1α1α2*, a distinct decrease of CH levels was observed between 20 and 40 min, followed by an increase from 40 to 80 min. The increase consisted in combined recovery of sucrose, glucose, and fructose levels together with starch accumulation. In the following, carbohydrate levels decreased between 80 and 100 min. During this period, mainly glucose declined. Starch degradation also took place between 80 and 120 min. From 100 min onwards, the carbohydrate level decreased constantly.

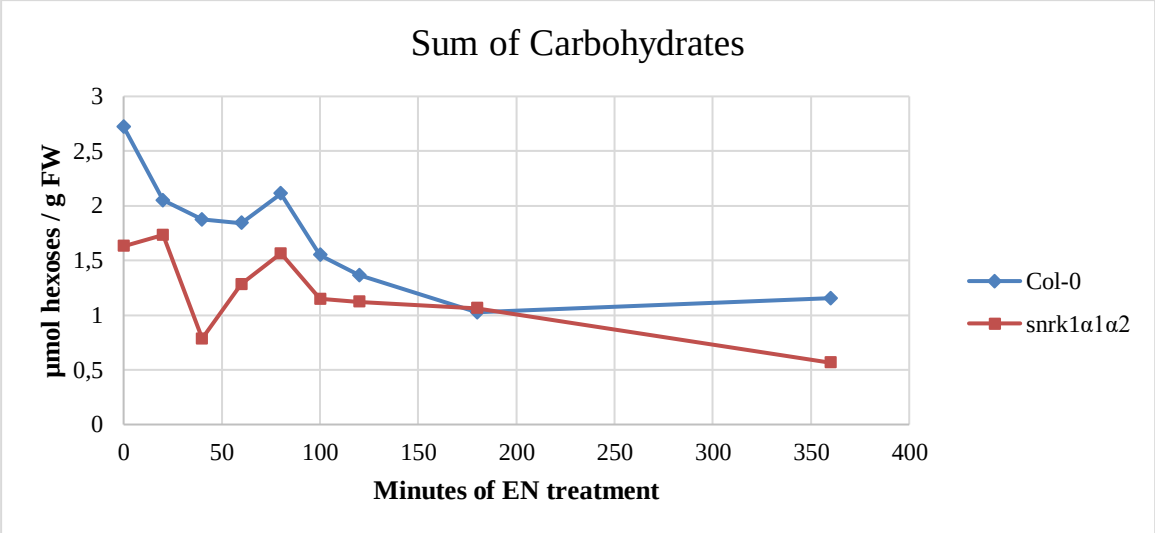

Figure 28 Comparison of carbohydrate content between Col-0 and *snrk1α1α2:* Sum of mean values of sucrose, glucose, fructose, and starch.

Cluster analysis proves different dynamics between genotypes within the first 20 minutes of the EN treatment

To reveal statistical similarities and differences of metabolic reprogramming in both analysed genotypes, cluster analysis was performed using the Euclidian distance information which was calculated for scaled data (zero mean/unit variance; scaled data are provided in the file *'Summary of experimental data'* in the e*lectronic supplements*[1]. Figure 29 shows the heatmap representations for each genotype. All time points were included, thus, G6P, F6P and UDPG were necessarily omitted.

In the wildtype, the first time point, which is the end of the regular night, clearly separated from the time points of the extended night treatment. Furthermore, the early time points (20-100min) and the late ones (120-360min) clustered together. During the first 20 minutes of EN, all enzymes measured showed an increased v_{max}. The metabolites sucrose, fructose and starch decreased in this period, only glucose concentration increased. This explains why glucose clustered together with the enzymes rather than the other metabolites. During the late time points (120-360min), all metabolites showed lower levels. In contrast, invertase activity increased consistently.

For the *snrk1α1α2* mutant, no clear separation of the time points was observed. During the first 20 minutes, enzyme activities and metabolites concentrations retained in many cases highly similar levels, which was contrasting the trend observed in the wildtype. While the metabolites glucose, sucrose, and fructose clustered together, also glucokinase was included as it displayed a trend resembling sucrose. Starch clustered together with the other enzymes, showing a pattern highly similar to invertase. Additionally, the time course of fructokinase activity resembled that of invertase.

[1] A collection of data files (including raw data, calculations, assay protocols and detailed results of the time series analysis) is provided on a USB-stick at the Department of Molecular Systems Biology (MoSys), University of Vienna

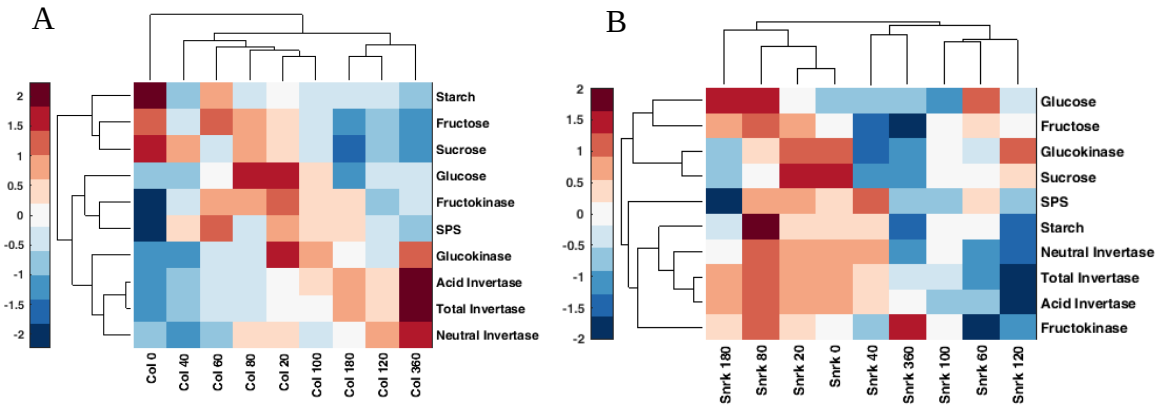

Figure 29 Heat maps of scaled (zero mean/unit variance) mean values of maximum enzyme activities (v_{max}) and the concentrations of sucrose, fructose, glucose, and starch. A: Col-0, B: *snrk1α1α2*

3.2 Functional Connection of Experimental Data with the Biochemical Network Structure

Differences between both genotypes in the central carbohydrate metabolism were analysed with regard to the involved enzymes and metabolites. A previously published algorithm was applied connecting experimental time series data with the biochemical network of central carbohydrate metabolism (the graphical network structure is provided in the *Introduction*; (Nägele et al. 2016)). The algorithm was applied within the Matlab®-based graphical user interface FEMTO (Nägele et al. 2016).

Figure 48 - Figure 61 (see *Appendix 6.4*) show the curves of cubic spline interpolation with selected weights for all metabolites measured, created via the curve fitting tool implemented in the FEMTO script. For optimized interpolation, the roughness of several spline functions had to be adjusted manually (spline settings are given on the figures). Further detailed information about the results of the time series analysis is provided in the *electronic supplements* (File '*Femto ratios'*).

To improve the interpretability of the results, all time series information related to one enzyme reaction was plotted together. For instance, in the case of sucrose biosynthesis catalysed by SPS, four different ratio functions, i.e. ω(t) functions, were summarized in context of experimental data: F6P"/F6P', UDPG"/UDPG', Suc"/UDPG' and Suc"/F6P'

(Figure 30). Each ratio indicated possible time-points of biochemical regulation, which, in context of the given example, could include a changed maximum activity of SPS. Further explanations for peaks of the ω(t) function, that could be discerned from the present dataset, were changes of substrate pools or concentration changes of effector metabolites, e.g. inhibitors or activators. Within the interconnected structure of the central carbohydrate metabolism, changes of further enzymes affecting a specific metabolite also need to be considered.

A decreased invertase activity falls together with high SPS activity at the beginning of the extended night in Col-0

After 30 minutes of extended night treatment, functional time-series analysis indicated the first peak of sucrose biosynthesis (Figure 30). It resulted from a decreasing first derivative of the interpolated sucrose concentration (Figure 31), while for the substrate UDPG no remarkable concentration changes were observed. Shortly beforehand, a significant (t-test, $p=0.006$) increase of SPS maximum activity was observed until 20 min (Figure 7). Furthermore, values of v_{max} for invertase decreased between 20 and 40 minutes of extended night (Figure 13).

Another peak occurred after 160 minutes, involving the second substrate, F6P. The sucrose decrease slowed down, while F6P levels remained constant. After 180 min, stable UDPG levels resulted in a peak. Indeed, SPS activity was slightly higher after 180 min (+15%).

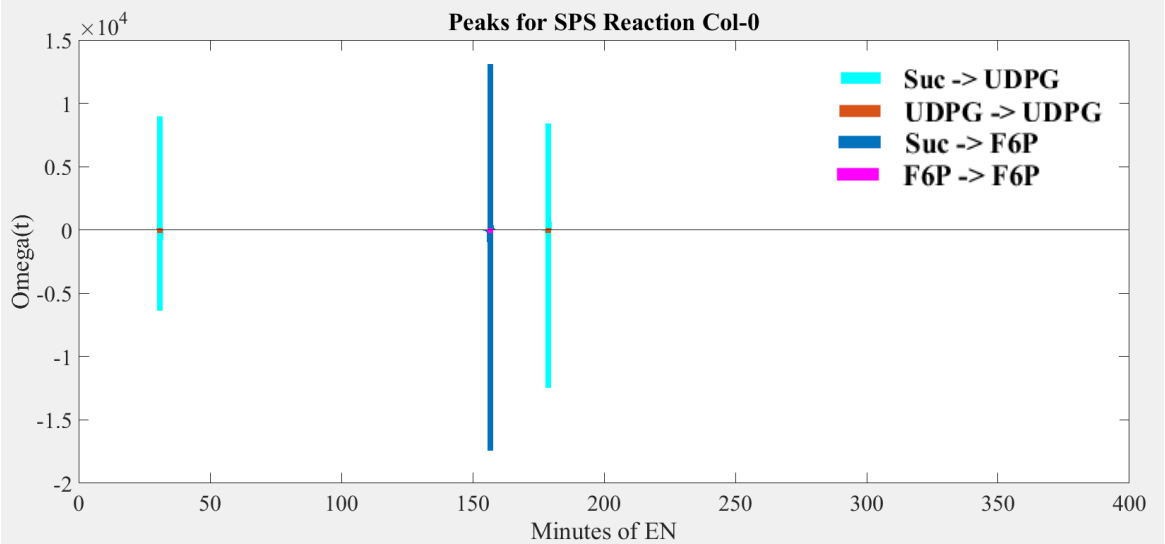

Figure 30 Results of functional time series analysis for sucrose biosynthesis in Col-0. Arrows "->" in the legend indicate that the second derivative of metabolite A's interpolation is divided by the first derivate of metabolite B's interpolation

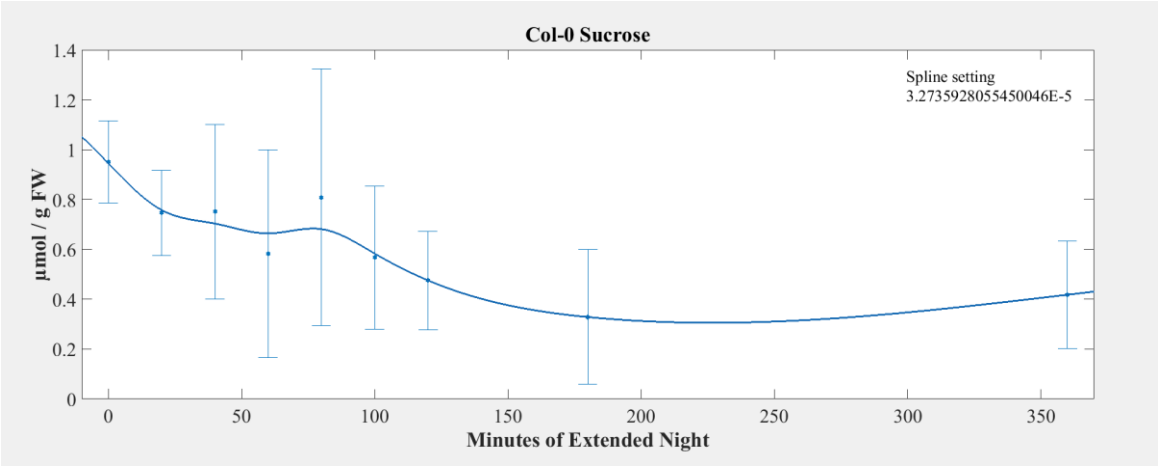

Figure 31 Cubic spline interpolation of sucrose concentrations in Col-0

At the level of v_{max}, no distinct changes in SPS activity occurred in the *snrk1α1α2* mutant over the extended night time course. The first related peaks occurred after 40 min (Figure 32), when sucrose concentration was at its momentary lowest (Figure 33), while F6P levels began to fall. SPS maximum activity did not change at that timepoint. After 55 min of EN treatment, when the second peak was indicated, UDPG glucose levels stopped falling and began to increase, while the rise in sucrose levels accelerated. Again, no changes in SPS activity were recorded. Interstingly, invertase maximum activity was downregulated between 40 and 60 min.

The peak after 160 min was caused by accumulation of UDPG glucose, while the sucrose level decreased. After ~215 min, F6P began to recover slightly while the decrease of

sucrose slowed down. A minor dynamic of SPS maximum activity was recorded for these late time points: From 120 to 180 min, activity slightly decreased, and until 360 min, it increased again to the same extent.

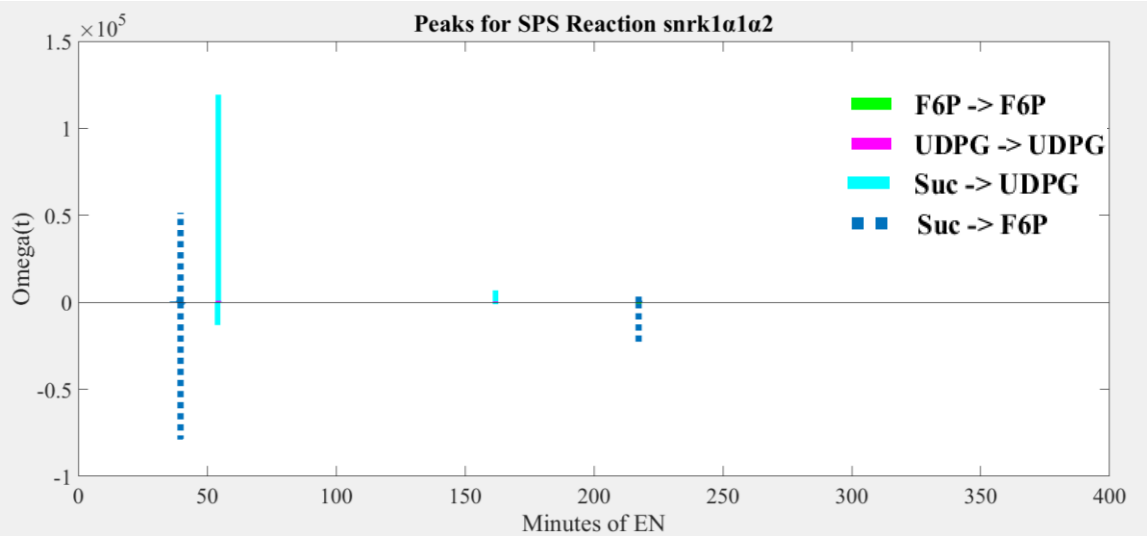

Figure 32 Results of functional time series analysis for sucrose biosynthesis in *snrk1α1α2*. Arrows "->" in the legend indicate that the second derivative of metabolite A's interpolation is divided by the first derivate of metabolite B's interpolation.

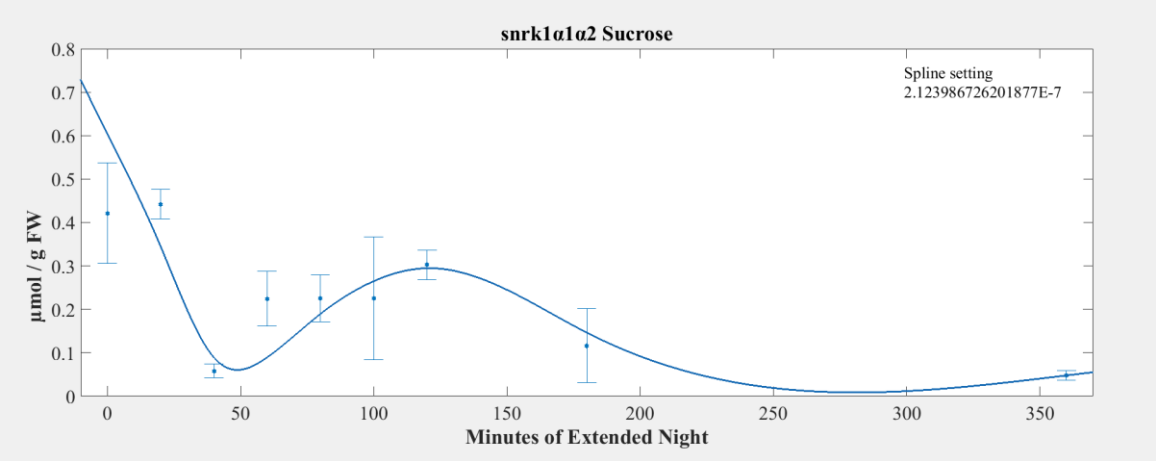

Figure 33 Cubic spline interpolation of sucrose concentrations in *snrk1α1α2*

Changes in the metabolic function of sucrose often coincide with shifts in invertase maximum activity in *snrk1α1α2*

Functional time series analysis indicated a peak for sucrose cleavage in the wildtype after 60 min (Figure 34), when sucrose levels stopped falling and subsequently started to rise slightly. Simultaneously, the rise in fructose levels slowed down, and glucose levels started to increase. The second peak was indicated for around 75 minutes into the EN

treatment. Sucrose stopped accumulating and started to decrease. Glucose accumulation slowed down at the same time. After 225 min (3rd peak), the sucrose level started to recover slightly according to the chosen interpolation. Invertase maximum activity increased in a linear manner from 40 min onwards. Between 60 and 80 min, SPS maximum activity distinctly decreased.

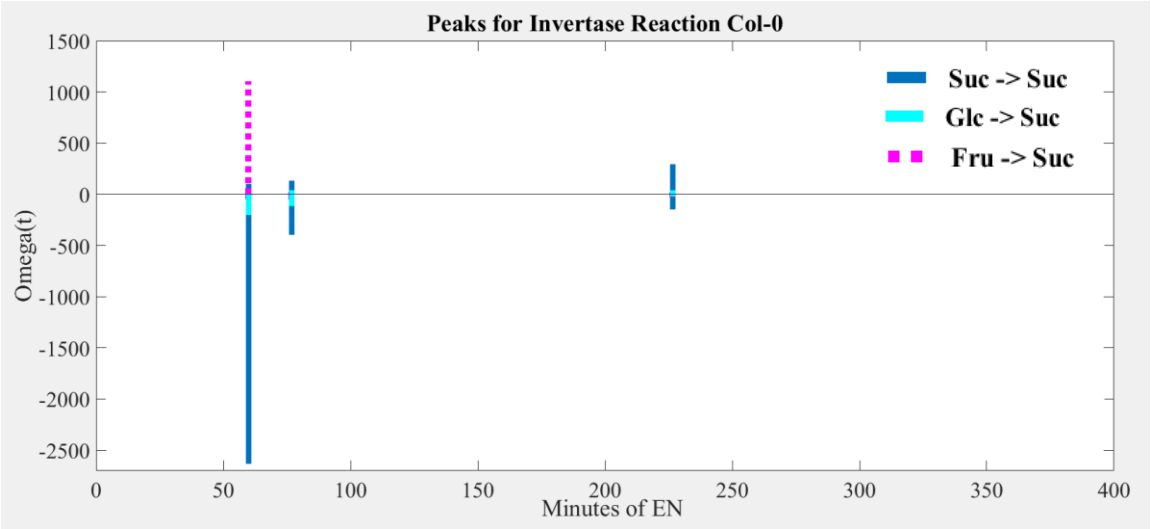

Figure 34 Results of functional time series analysis for sucrose cleavage in Col-0. Arrows "->" in the legend indicate that the second derivative of metabolite A's interpolation is divided by the first derivate of metabolite B's interpolation

The first peak for sucrose cleavage in *snrk1α1α2* occurred after 45 minutes of EN treatment (Figure 35), when the strong loss of sucrose ceased and levels quickly began to rise again. Fructose levels showed a very similar dynamic within the first hour, also having a minimum after 40 min. Glucose levels were at a minimum at the same time as well. A downregulation of invertase activity between 40 and 60 min was observed.

A next Peak ensued after 120 min, when sucrose levels started to decrease again. At the same time, glucose started to increase more strongly. Interestingly, invertase maximum activity was significantly upregulated between 120 and 180 min.

After 280 min, a third peak occurred as sucrose levels were at a low level and started to recover slightly. The mean value of invertase maximum activity moderately decreased in the second half of the extended night.

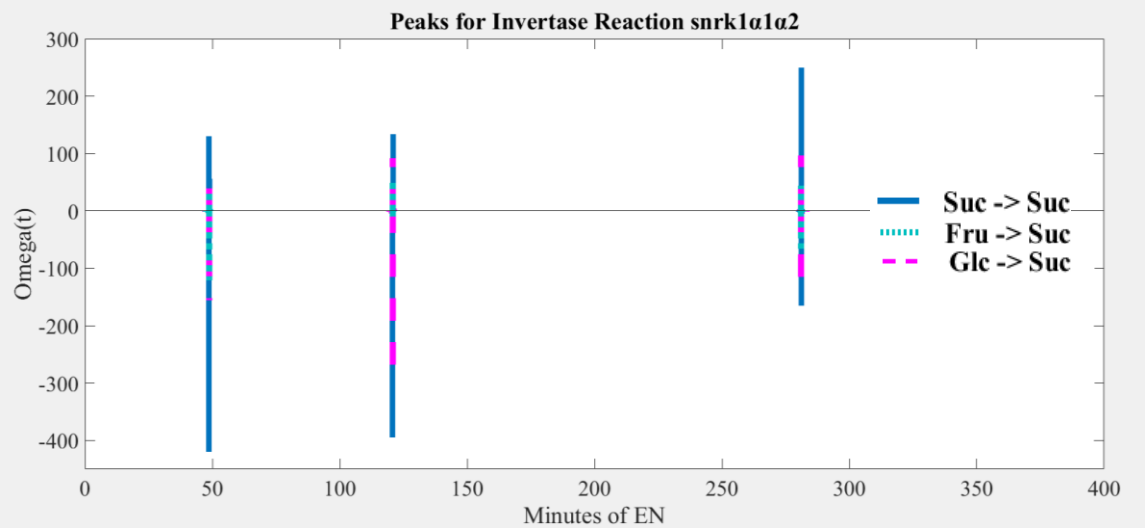

Figure 35 Results of functional time series analysis for sucrose cleavage in *snrk1α1α2*. Arrows "->" in the legend indicate that the second derivative of metabolite A's interpolation is divided by the first derivate of metabolite B's interpolation.

Glucose accumulation at the beginning of the extended night coincides with transiently increased glucokinase and invertase maximum activites in Col-0

After 20 min of EN, glucose levels stopped to increase and began to fall in the wildtype (Figure 37). The metabolic function of G6P also changed, as the metabolite no longer decreased. Indeed, glucokinase maximum activity was distinctly higher after 20 min, but it decreased again to a similar extent until 40 min. It can be noted that culmination of glucose levels coincided with high glucokinase activity, as well as high invertase activity.

The next peak, around 45 minutes in the EN (Figure 36), indicated that glucose levels ceased falling. No changes in v_{max} for glucokinase were observed at that time. After 80 min, another transient glucose peak occurred. Again, no change of glucokinase maximum activity correlated temporally.

The peak after 190 min indicates that glucose levels stopped to decrease. During the second half of EN (i.e. between 180 and 360 min), glucose concentration increased, while G6P levels declined. Glucokinase maximum activity slightly rose in that interval.

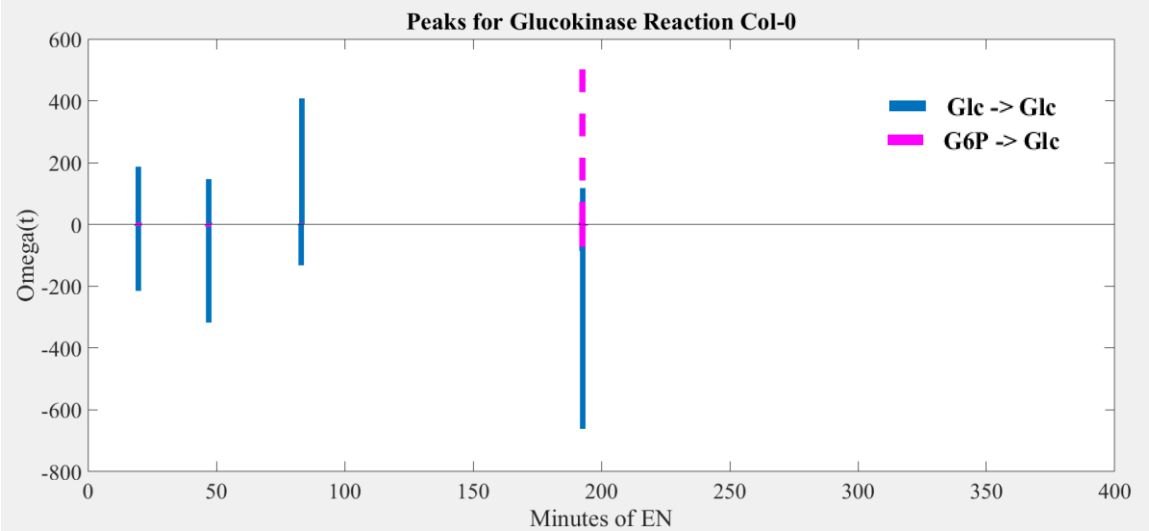

Figure 36 Results of functional time series analysis for glucose phosphorylation in Col-0. Arrows "->" in the legend indicate that the second derivative of metabolite A's interpolation is divided by the first derivate of metabolite B's interpolation

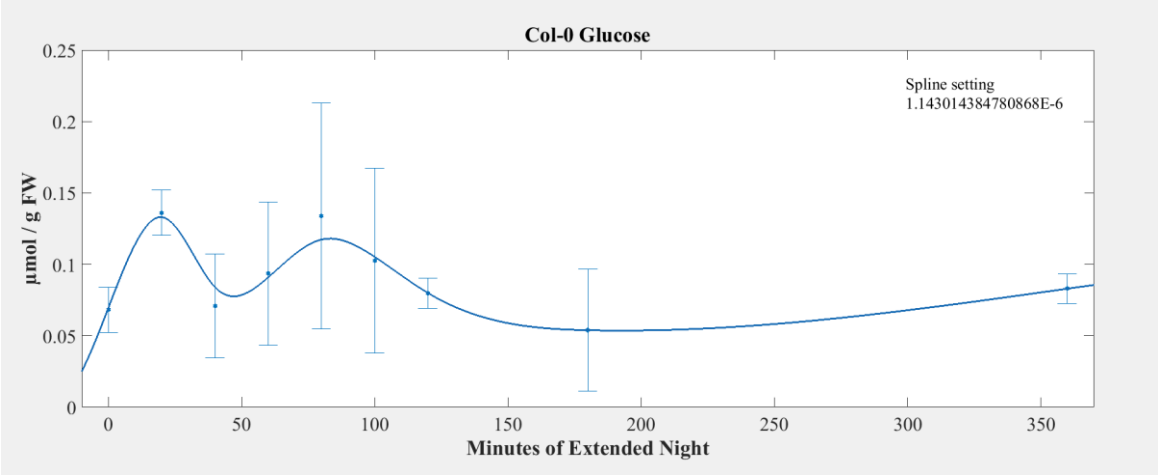

Figure 37 Cubic spline interpolation of glucose concentrations in Col-0.

The first Femto peak for glucokinase reaction in *snrk1α1α2* occurred around 10 min into the EN (Figure 38), as previously stable glucose levels started to decrease (Figure 39). At that time, no changes of glucokinase maximum activity are found. The second peak (after 35 min) indicates that the decrease of glucose ceased. In this case, a coinciding lower glucokinase activity after 40 min was found. After 75 minutes, glucose levels culminated and started to decrease again. A slight increase in glucokinase activity (+15%) between 60 and 80 min was observed. Conversely, a highly significant rise of invertase activity took place at that time.

After 100 min, glucose concentration reached a very low value (~0.042µmol/gFW). The metabolic function of glucose changed distinctly after 105 min, when the downfall ceased (4th peak). No noteable changes of glucokinase maximum activity were recorded at that time. Invertase activity significantly decreased between 80 and 120 min.

The last peak after 205 min indicated that glucose stopped to accumulate. Maximum activity of glucokinase was stable at that time, but a moderate decrease of invertase maximum activity was recorded.

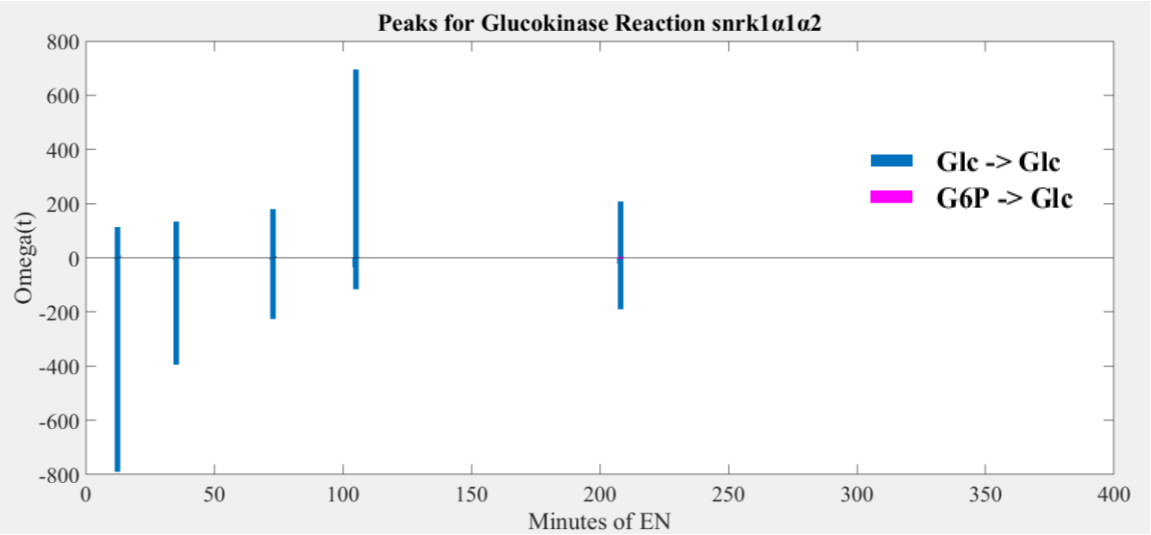

Figure 38 Results of functional time series analysis for glucose phosphorylation in *snrk1α1α2*. Arrows "->" in the legend indicate that the second derivative of metabolite A's interpolation is divided by the first derivate of metabolite B's interpolation.

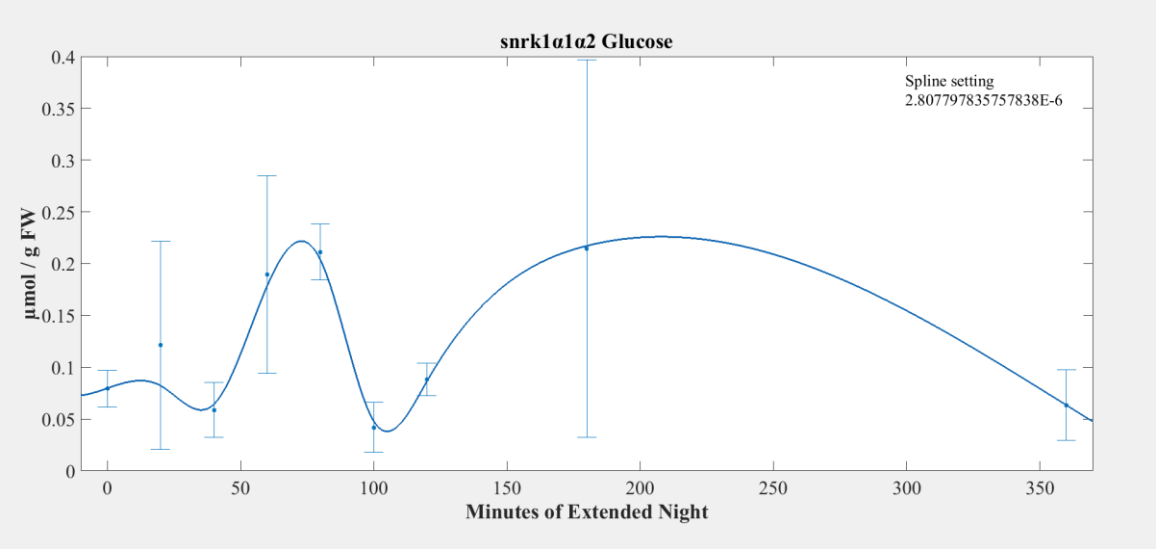

Figure 39 Cubic spline interpolation of glucose concentrations in *snrk1α1α2*.

Changes in the metabolic function of fructose often coincide with altered fructokinase and invertase activity in *snrk1α1α2*

After 35 min of EN, fructose levels in the wildtype stopped to decrease (Figure 41). According to the interpolation, F6P levels constantly fell during the first hour of the EN. At the beginning of EN, fructokinase showed a very similar regulation pattern when compared to glucokinase. It transiently increased within the first 20 minutes, followed by an again lower value after 40. Invertase activity showed a similar course of regulation. After 65 min, a second peak for fructose phosphorylation occurred (Figure 40). Fructose accumulation stopped and transitioned into a steady decrease in the second hour of the extended night. The decline of F6P levels slowed down in that interval. Fructokinase maximum activity showed relatively high values from 60 to 100 min.

After 150 minutes, and according to the chosen interpolation, F6P levels were stable. At that time, fructose concentration reached the lowest value after a strong decline during the second hour of the EN. The value of v_{max} for fructokinase was transiently lowered after 120 min, but subsequently recovered until 180 min. The last peak was indicated after 270 min, when the fructose concentration reached a stable plateau. In the second half of the extended night exposure, fructokinase maximum activity slightly decreased.

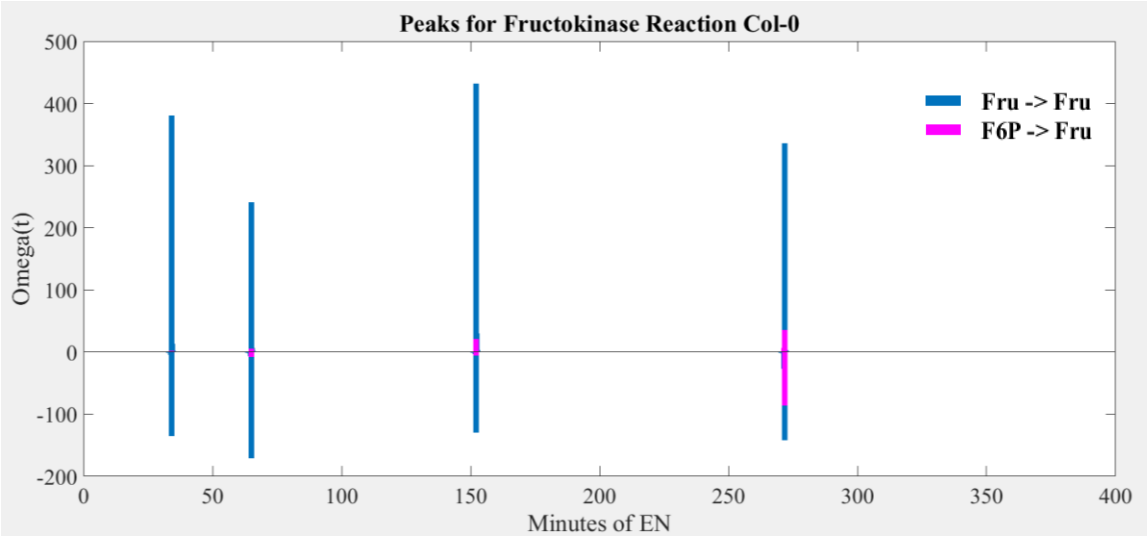

Figure 40 Results of functional time series analysis for fructose phosphorylation in Col-0. Arrows "->" in the legend indicate that the second derivative of metabolite A's interpolation is divided by the first derivate of metabolite B's interpolation.

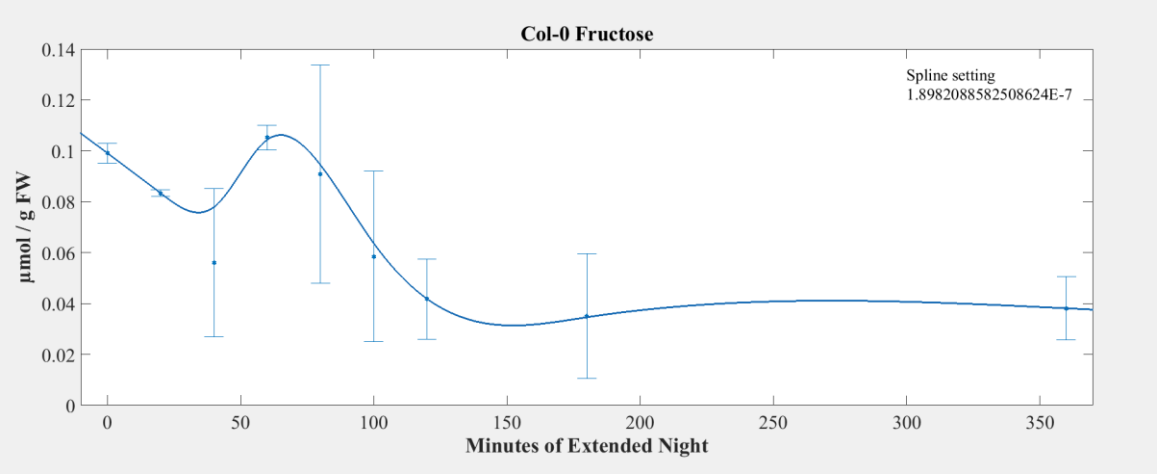

Figure 41 Cubic spline interpolation of fructose concentrations in Col-0.

As for glucose, fructose in *snrk1α1α2* accumulated after 10 min, exhibiting first changes of its metabolic function very early in the EN (Figure 43). No variations of fructokinase maximum activity were recorded for that time. The second peak (40 min) indicated that the decrease of fructose ended and levels began to recover (Figure 42). A decrease of fructokinase activity after 40 min had just started, but unlike glucokinase, further downregulation took place from 40 to 60 min. Invertase activity decreased simultaneously during that interval. After 75 min, the rise in fructose levels ceased. This coincided with rising hexokinase and invertase activity between 60 and 80 min. Subsequently, maximum activity of both enzymes decreased distinctly until 120 min. After 120 min, fructose levels stopped to decline and started to recover. Between 120 and 180 min, invertase v_{max} significantly increased.

The last peak, after 210 minutes of prolonged darkness, indicates that fructose levels started to decrease again. According to the chosen interpolation, F6P simultaneously increased in an inverted manner. No notable change of fructokinase maximum activity was recorded in the second half the EN.

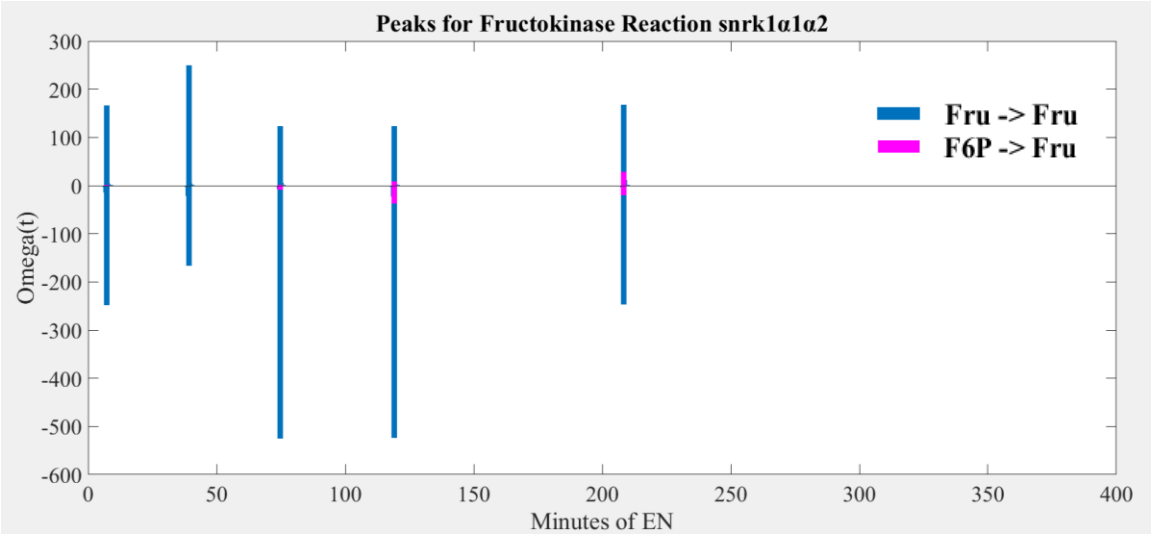

Figure 42 Results of functional time series analysis for fructose phosphorylation in *snrk1α1α2*. Arrows "->" in the legend indicate that the second derivative of metabolite A's interpolation is divided by the first derivate of metabolite B's interpolation.

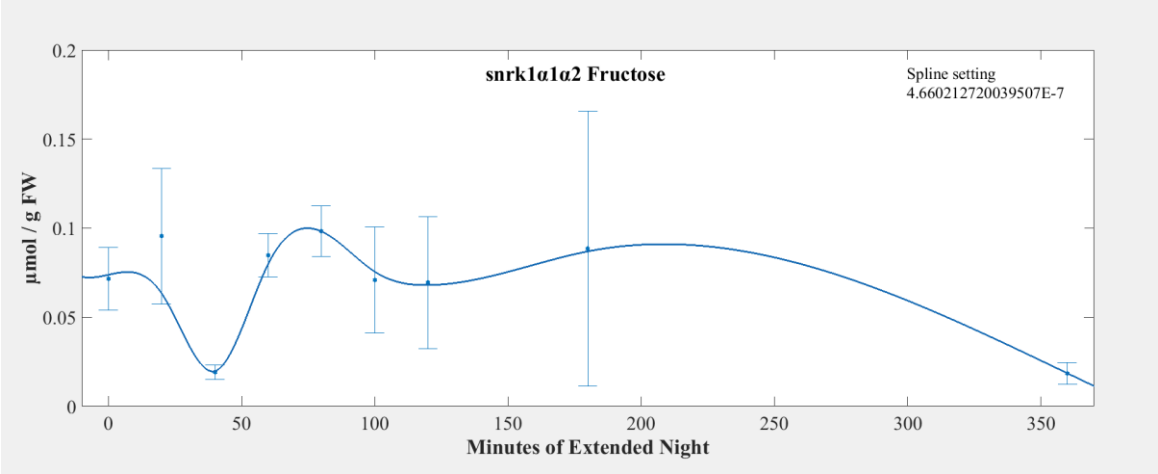

Figure 43 Cubic spline interpolation of fructose concentrations in *snrk1α1α2*.

4 Discussion

Stabilization of sucrose levels by SPS and invertase activity

The hypothesis that SnRK1 affects the central carbohydrate metabolism under energy limitation, emerging from strongly deviating sucrose levels reported by Nukarinen et al. (2016), was confirmed by the present study. Metabolite concentrations of the two genotypes showed different levels and dynamics during the exposure to extended night. Levels of glucose-6-phosphate were found to be consistently higher in Col-0. In contrast, transitory starch levels were notably higher in the *snrk1α1α2* mutant. But among all quantified metabolites, sucrose levels still showed the biggest divergence. Already at the end of the night, sucrose levels were 55% lower in *snrk1α1α2.*

Previously published data on extended night dynamics in Col-0 underpinned the specific pattern of sucrose levels during an extended night exposure. Pal and colleagues reported a drop of sucrose levels by 60% within 4 hours of an extended night treatment (Pal et al. 2013). Their plants were grown in a 12/12h light/dark cycle as the plants used in the present project, but at higher light intensity (180µmol m^{-2} s^{-1}). This was reflected in higher starch levels at the end of the regular night. Interestingly, sucrose levels were nearly identical at that timepoint: ~0.95µmol/gFW (Nukarinen et al. 2016) vs. 0.94µmol/gFW (Pal et al. 2013). Although the reported course of concentrations differed at the very beginning of the extended night, the values at which sucrose levels were stabilized after a few hours were again found to be very similar (0.42µmol/gFW Nukarinen et al. 2016, 6h EN) vs. 0.35µmol/gFW (Pal et al. 2013, 8 h EN). In another extended night experiment of Usadel et al. (2008), plants contained more than twice as much sucrose at the end of the regular night, as compared to the applied data and data from Pal et al. (2013). Within 2 hours of extended darkness, sucrose content decreased to 50%. In contrast to the present data, a continuous decrease of sucrose levels occurred during the first hours of EN. A potential reason for this prolonged decrease observed by Usadel et al. (2008) could lie in higher absolute concentrations, hence enabling longer supply with substrates for catabolism from the sucrose reserves. But still, after 6 hours of extended night, the sucrose level was at ~0.5µmol/gFW, which is not very different from the ~0.42µmol/gFW measured by Nukarinen et al. (2016).

Altogether, these data suggest a significant reduction of the sucrose pool, yet not a complete depletion, during the first six hours of extended night. A commonly observed level, to which sucrose decreased after a few hours of prolonged darkness, was 0.35-0.5µmol/gFW. The observed stabilization of sucrose levels after 3 hours, which was reported by Nukarinen et al. (2016), agrees with the data from Pal et al. (2013), indicating that synthesis and cleavage of sucrose are tightly regulated in Col-0. In contrast to the consistent picture of well-controlled sucrose levels in the wildtype, sucrose concentrations in *snrk1α1α2* fell to distinctly lower levels (see Figure 12). Lowest concentrations were observed after 40 min (~0.058µmol/gFW) and after 360 min (~0.048µmol/gFW). One explanation could be that *snrk1α1α2* plants were consuming too much sucrose, leading to these low levels. But considering the already distinctly lower value at the end of the normal night, the temporal course of concentrations revealed that *snrk1α1α2* was in fact consuming similar amounts of sucrose as the wildtype.

To explore the reasons for the different sucrose levels between Col-0 and *snrk1α1α2* plants, it is necessary to analyse the functional interplay between key enzymes in central carbohydrate metabolism. Enzyme activities of SPS and invertase might reveal explanations for the significantly diverging sucrose levels between wildtype and *snrk1α1α2* plants. The functional time series analysis indicated possible time points of altered substrate-product dynamics. The main difference between the genotypes with regards to SPS maximum activity consisted in a significantly lower value in Col-0 at the end of the night (see Figure 9). As indicated by the functional time series analysis, a regulatory event, beginning to stabilize the sucrose level, occurred after 30 min in the wildtype. Between 0 and 20 min, SPS activity was upregulated significantly. Although the peak appeared a bit later, a causal relationship between an increased v_{max} value for SPS and the stabilization of sucrose concentration seems plausible. The temporal accuracy of the applied functional time series analysis approach is in this case (SPS) confined by the interpolation exactness for UDPG and F6P levels. The low number of biological replicates and the lower number of time points set a limit on interpretability. However, in addition to elevated SPS activity, stabilization of the sucrose pool was also indicated by the decreased invertase activity after 40 min of extended night. A substantial contribution of reduced sucrose cleavage seems very probable, as fructose and glucose levels both went down in concordance between 20 and 40 min.

Functional time series analysis of sucrose levels indicated a possible alteration in the invertase reaction after 60 min in the wildtype. Invertase activity, however, increased linearly from 40 min onwards, which contrasts the increasing sucrose levels. Conversely, SPS activity distinctly decreased between 60 and 80 min. This controversial picture could be explained by degradation of the small amount of starch which was synthesised in the time period before. As SPS is allosterically activated by G6P (Huber, Huber 1996), increased levels of G6P resulting from starch remobilization could thus enhance sucrose synthesis despite decreasing levels of its substrate F6P. This assumption agrees with the observed increase of glucose levels (Figure 16). A raised enzyme activity through elevated levels of the activator G6P could subsequently require downregulation of SPS maximum activity to retain stable sucrose levels.

In contrast to the wildtype, v_{max} values for SPS of *snrk1α1α2* did not change during the first 80 min of extended night exposure. A slight downregulation was observed between 80 and 180 min (see Figure 9). These subtle changes of maximum activity cannot account for the strong dynamic of sucrose levels in *snrk1α1α2* during the first hour of EN. Functional time series analysis indicated a peak for sucrose biosynthesis after 40 min, when the substrate F6P started to decrease, while the drop of sucrose stopped. This combination of substrate and product behaviour would be consistent with an elevated sucrose biosynthesis, but at least maximum activity of SPS did not change. Interestingly, invertase activity was downregulated between 40 and 60 min, which could account for the recovery of sucrose levels. Functional time series analysis gave a peak for possible alterations in sucrose cleavage during this period of extended night. However, hexose levels also increased in parallel with sucrose, leading to a higher sum of main sugars, as depicted in Figure 28. This increase cannot fully be attributed to increased sucrose cleavage, and thus points to further regulatory events taking place after 40 min in the mutant. Possible explanations, like an additional influx of carbohydrates, will be discussed in detail later in context of SnRK1 activity.

Time-series analysis revealed another time point of deregulation of the invertase reaction in *snrk1α1α2* plants after 120 min, when sucrose levels decreased again (Figure 35). Simultaneously, glucose increased while fructose levels were stable. Due to the fact that invertase activity significantly increased between 120 and 180 min, these metabolite dynamics might be a direct consequence of invertase dynamics. However, invertase

dynamics in *snrk1α1α2* were not always reflected in sucrose levels. For instance, although the sucrose pool was stable between 60 and 120 minutes, significant up- and downregulation of invertase maximum activity still occurred.

The present study suggests that regulation of invertase activity plays an important role in controlling carbohydrate metabolism under energy limitation. Considering the high degree of interconnection within the central carbohydrate metabolism, it is not surprising that an influence of invertase maximum activity on other components was observed. Cluster analysis (Figure 29) revealed simultaneity in the regulation of invertase and fructokinase in *snrk1α1α*. After 80 min of extended night, invertase activity in the mutant line temporarily increased, while the sucrose level remained constant. Remarkably, fructokinase activity also increased by 38% between 60 and 80 min. The significantly lower v_{max} of invertase after 120 min again coincided with a likewise decreased fructokinase activity. The parallel regulation of fructokinase could contribute to stabilization of fructose levels to accommodate flux changes caused by altered sucrose cleavage. Invertase enzymes have a high potential to influence hexose levels and in this way trigger signalling events (Koch 2004). In a kinetic modelling approach, Nägele et al. (2010) observed that solely lowering invertase maximum activity led to a drainage of hexoses. Hence, they suggested that lowering hexokinase (respectively fructokinase) activity was a necessary response to stabilize metabolism when invertase activity is decreased.

In Col-0, simultaneous regulation of fructokinase and invertase took place only during the first hour of the extended night. After 120 min, fructokinase maximum activity decreased when fructose levels were at a low value of 0.042 µmol/g FW. In contrast, invertase activity was linearly increasing at that time. Hence, a direct functional linkage of both enzymes seems unlikely. The simultaneity, which was mainly observed in *snrk1α1α2*, probably results from corresponding changes in the fructose pool. But how this sensing is implemented on the molecular level remains open, as fructokinase was so far not shown to be involved in fructose sensing (Granot et al. 2014). Conversely, fructokinase did not always change in a way that retains fructose levels. Between 40 and 60 min, fructokinase maximum activity increased moderately in the wildtype (+27%). The activity then stayed high until 100 min. In that interval of high fructokinase activity, fructose levels dropped distinctly. This could indicate that fructose was needed to retain the F6P pool. As sucrose

levels remained stable, the fructose reserves were possibly exhausted on purpose to obtain substrate. Lowered fructokinase activity after 120 min then coincided with stabilization of the fructose level.

Cellular glucose concentration is signficantly affected by the dynamics of invertase activity. When the striking changes of invertase activity are not visible in the sucrose level, the underlying flux can still exhibit strong fluctuations. In the wildtype, glucose was the only sugar accumulating during the first 20 minutes of the extended night. This rise was also described in literature (Pal et al. 2013). After 40 min, glucose concentration again decreased to a lower value (~0.071µmol/gFW), comparable to the concentration at the end of the night. The glucose pool directly depends on supply by degradation of starch and sucrose, as well as on the interconversion rate to G6P via hexokinase. The high values at 20 min in the wildtype can be explained by increased sucrose cleavage, as well as starch degradation. Stagnation of this supplying processes would be a sufficient explanation for the change of the metabolic function of glucose after 20 min. Glucokinase activity showed the same pattern of up- and downregulation as fructokinase and invertase during the first hour of extended night, but also resembled the time course of glucose concentrations. Glucose levels rose during the first 20 min, although hexokinase activity increased as well. This contrasts the fructose-fructokinase interplay at that time, suggesting an additional influence of starch degradation on glucose levels.

Compared to the wild type, the analysis of *snrk1α1α2* samples revealed similar glucose levels at the very beginning of the extended night, but a distinctly higher peaking of glucose levels after 60 and 80 min. Similar glucose levels were contrasting the observation that starch remobilization at the beginning of extended night exposure was clearly decreased in the mutant (see Figure 27). The two genotypes showed similar starch levels at the end of the night, but noteworthy differences in degradation during the extended night treatment. AKIN10 is known to induce genes involved in starch degradation (Baena-Gonzalez et al. 2007). Consistently, transient leaf starch in Arabidopsis AKIN10/11 double mutants was found to stay high at the end of the night, pointing towards a role of SnRK1 in starch degradation (ibid.). These findings do not fully agree with similar starch levels at the end of the night, as found in the present experiment. But a trend of impaired starch mobilization due to lacking SnRK1 activity was observed congruently.

In context of starch metabolism in the *snrk1α1α2* mutant line**,** it is interesting to note that cluster analysis based on Euclidean distance revealed a similar pattern of starch levels and invertase activity (see Figure 29). When invertase v_{max} decreased between 80 and 120 min, starch was degraded. Invertase maximum activity was lowest after 120 min, and only at that time, starch levels in *snrk1α1α2* approached the generally lower wildtype levels. One possible explanation for this temporal correlation could be found within the glucose pool. The stabilization of sucrose via a decreased invertase maximum activity affects glucose levels, which could then be compensated by remobilization of starch. Glucose levels reached very low levels of 0.042 µmol/g FW after 100 min, and recovered slightly until 120 min, which would support this hypothesis. Alternatively, starch degradation between 80 and 120 min could be initiated by another mechanism. The decreased invertase maximum activity could constitute a reaction to rising substrate availability through mobilization of starch reserves, which would reach the sucrose pool via futile cycling. In both cases, invertase would play a central role in stabilizing sucrose levels.

Surprisingly, the present study also revealed a transient and slight increase of mean starch levels during the extended night for both genotypes (Col-0: 60min, *snrk1α1α2:* 80min). This phenomenon has not yet been reported in literature. But samples have been measured in a randomized order, which speaks against a technical artefact. One possible explanation for the missing reference in other datasets might be the lower number of time points in those studies (e.g. Usadel et al. 2008; Pal et al. 2013). The temporal increase of starch happened within 20 minutes, and was instantly degraded within the subsequent 20 minutes. Only a very dense temporal resolution can record this event. On the functional level, an accumulation of starch during the extended night requires the import of carbohydrates from the cytoplasm to the chloroplast. Alternatively, substrate for starch synthesis, e.g. in the form of maltose or TCA intermediates, could still remain in the plastids. In *A. thaliana,* G6P was suggested to be imported into the plastid through GPT2 (a glucose 6-phosphate/phosphate translocator), where it is used for starch synthesis (Dyson et al. 2015). This mechanism was discussed to play a role during acclimation to high light conditions, when it may buffer variations in carbon metabolism caused by elevated photosynthesis. In the present experiment, plants experienced an opposite situation. Nevertheless, this mechanism would make sense in context of the observed metabolic situation: In *snrk1α1α2,* increasing invertase activity between 60 and 80 min

produced more glucose. Yet, in contrast, glucose did not solely accumulate but was presumably converted to G6P and possibly imported into the chloroplast for starch synthesis.

In obvious contradiction to the present data, Huarancca Reyes et al. (2016) observed a positive correlation between rising sugar concentrations and increased invertase activity. In the present study, the opposite was the case. In Col-0, invertase activities increased steadily although sugar levels decreased over the extended night exposure. A possible explanation for the increase in activity might be an adaptation to decreasing substrate concentrations in order to sustain a specific flux into hexose pools. v_{max} modulations are a possibility to influence product dynamics, as already shown for vacuolar invertase (Nägele et al. 2010). In accordance with wildtype data from the present study, Gibon et al. (2006) measured moderately increasing acid invertase maximum activities for Col-0 plants during 6 hours of extended darkness, which deviated from the diurnal pattern. Additionally, transcript levels for acid invertase were shown to respond with an increase already during the first hours of an extended night treatment, as compared to diurnal conditions (Usadel et al. 2008). Altogether, these data support the hypothesis that elevated values of v_{max} for invertase are a typical reaction to extended darkness in *A. thaliana*.

In contrast to the (almost linear) increase in the wildtype, invertase activity in *snrk1α1α2* was highly dynamic. While all metabolites recovered between 40 and 60 min, invertase v_{max} decreased. Considering the higher sum of carbohydrates after 60 min, the downregulation of invertase maximum activity could be the output of a regulatory response to increasing substrate availability, preventing the newly gained sucrose from immediate cleavage caused by enhanced catalytic activity. Conversely, invertase activity increased significantly in the subsequent interval from 60 to 80 min, potentially contributing to the stabilization of hexose and sucrose levels. In summary, the time courses of v_{max} values convey the impression, that the stabilization of sucrose levels is exerted via distinct regulation of invertase in *snrk1α1α2*, while regulation of SPS maximum activity is hypothesised to play a more dominant role in the wildtype. A contribution of SPS to balancing the central carbohydrate metabolism has to be assumed even under non-photosynthetic conditions. Sucrose synthesis in context of sucrose cycling was shown to take place in heterotrophic tissue like potato tubers or *Ricinus*

cotyledons (Huber, Huber 1996). Decades ago, futile cycling of sucrose within plant cells was postulated to constitute a mechanism for tight regulation of sucrose levels (Huber 1989). Model simulations of the central carbohydrate metabolism in *A. thaliana* confirmed a stabilizing effect of sucrose cycling on hexose and hexose phosphate pools, as well as a role in sink-export control (Nägele et al. 2010). Hence, the present study indicates a dyadic interplay of SPS and invertase activity enabling rigid control over sucrose levels in the wildtype.

The impact of SnRK1 activity on extended night induced metabolic reprogramming

The measurement of maximum enzyme activities revealed a different pattern of regulation between genotypes at the beginning of the extended night treatment. In the wildtype plants, SPS, invertase, glucokinase and fructokinase started at lower levels and were upregulated within the first 20 minutes. After 20 min, activities were comparable to those of *snrk1α1α2*. Previous work has shown that SPS constitutes a target for phosphorylation by SnRK1, resulting in its inactivation (Sugden et al. 1999). This led to the assumption that the *snrk1α1α2* plants show higher SPS activities, as they lack this path of regulation. Indeed, SPS activity at the end of the night was lower in the wildtype, supporting this hypothesis. Yet, in contrast, for the other time points of the extended night exposure, no significant differences between the genotypes could be determined. Only between 60 and 80 min the v_{max} value of SPS decreased again moderately in the wildtype. This pattern of comparatively similar SPS v_{max} levels is not in full agreement with assumed steady differences of SnRK1 catalytic activity between the genotypes. Nukarinen and colleagues measured the SnRK1 specific phosphorylated T-loop peptide for Col-0 and *snrk1α1α2* for the extended night timepoints (Nukarinen et al. 2016). In *snrk1α1α2*, the abundance was in general reduced by more than 75%. In the wildtype, a decrease occurred during the first 20 min of the extended night treatment, which fits the rise in SPS maximum activity at that time. But until 40 min, AKIN 10/11 phosphopeptide abundance rose to output levels again, while no changes in SPS maximum activity corresponded. The lower v_{max} values at the end of the regular night in Col-0 concerned all enzymes measured. Except for SPS, the maximum activities decreased once more in the subsequent interval until 40 min of extended night. Controversially, the pattern of invertase, fructokinase and glucokinase maximum activities qualitatively coincided with the activation state of SnRK1 during the first hour of prolonged darkness. Just SPS, which

is known to be a target for direct phosphorylation by SnRK1, showed a deviating pattern. Thus, coordinated regulatory mechanisms, other than direct phosphorylation by SnRK1, seem plausible.

Due to the systematic increase of enzyme activities at the early extended night in Col-0, circadian clock processes might be involved. An influence of AKIN10 on the circadian clock in *A. thaliana* was recently discovered by Shin et al. (2017). The authors found that AKIN10 influences the expression of the evening clock gene GI (=GIGANTEA) under diurnal and constant light conditions. The period of GI was lengthened by 4 hours in plants overexpressing AKIN10. The period extending effect was found to be dependent on another central clock gene called TIC (Time for Coffee). In mutants lacking TIC function, AKIN10 overexpression did not alter the period of GI. The effect was also diminished under constant darkness. The molecular mechanism of interaction between AKIN10 and GI has not yet been examined, and, as a consequence, the reason for the light dependency and the type of interaction between TIC and AKIN10 remain unclear. The authors suggested a role of AKIN10 in the input pathways of the circadian network. As both, GI and TIC, were shown to be involved in starch metabolism and oxidative stress, the interaction with AKIN10 could contribute to the role of integrating energy sensing to the circadian clock (Shin et al. 2017).

Considering that experiments by Shin et al. (2017) revealed longer rhythms for GI under AKIN10 overexpression, the *snrk1α1α2* mutants might analogously go along with altered circadian cycles of GI. In consequence of the high complexity of the circadian signalling network, possible alterations on circadian timing in the *snrk1α1α2* mutant cannot be simply reconstructed from the present data and need further experimental analysis. As enzyme activities were lower in the wildtype compared to *snrk1α1α2* at the end of the night, a down-regulating component might be inactive in *snrk1α1α2* plants.

Regardless of a possible influence of SnRK1 on the circadian clock, Choudhary and colleagues suggested a circadian mediated regulation of the enzyme SPS in *A. thaliana* (Choudhary et al. 2015). Three distinctively phosphorylated peptides belonging to SPS showed circadian oscillations. Circadian phosphoregulation of SPS was already shown before for tomato plants (Jones, Ort 1997). These authors revealed the rhythmic transcription of a SPS phosphatase (dephosphorylation = activation), that could account

for the circadian pattern of SPS activities they measured under constant low light. Controversially, the rhythmic changes in activity only occurred under substrate limiting conditions and not in v_{max} measurements. This implicates that the assumed change in phosphorylation state would only change the enzymes substrate affinity but does not restrict the enzymes maximum capacity under optimal conditions. Analogous to findings of Jones and Ort (1997), the phosphorylation of spinach SPS by SnRK1 was suggested to only affect the enzyme's activity under substrate limiting conditions (Sugden et al. 1999). This points to the need to critically reflect the interpretability of v_{max} measurements with regards to regulatory events like phosphorylation. But still, kinetic properties and regulatory mechanisms for functionally identical enzymes can vary strongly between species, which might prevent a direct transfer of regulatory cascades from tomato and spinach to *A. thaliana*.

The other way around, phosphorylation levels of enzymes should not be over-interpreted in context of activation or inactivation of enzymes quantified by v_{max} levels. For example, for INV1, which is an *A. thaliana* cytosolic alkaline invertase, Nukarinen et al. (2016, suppl. data) found a consistently higher abundance of one phosphopeptide of the enzyme in *snrk1α1α2* for all time points. The mean values differed significantly between genotypes after 0, 20 and 360 min. However, while v_{max} at the early time points was lower in the wildtype, it was higher at the end of the extended night. Thus, the different levels of v_{max} for this invertase isoform cannot fully be explained by the dynamics of phosphopeptide abundance.

So far, little is known about potential interactions of SnRK1 and invertase enzymes. Lin and colleagues found that the main isoform of vacuolar acid invertase in potato tubers, *StvacINV1*, is subject to a complex posttranslational regulatory mechanism involving SnRK1 (Lin et al. 2015). In their experiment, the invertase inhibitor *StInvInh2B* was deactivated by the beta-subunit of wild potato SnRK1 *(SbSnRK1β)*. But additional presence of the phosphorylated form of the alpha subunit *(SbSnRK1α)* abolished this inactivation. The group found a linear correlation between rising amounts of phosphorylated *SbSnRK1α* and decreasing *StvacINV1* activity. The effect was completely dependent on phosphorylation of *SbSnRK1α* at its Thr-175 residue. If the same complex mechanism was present in *A. thaliana*, this could partially explain the great differences in invertase activity between the genotypes in our experiment. If present, the reduced

abundance of alpha subunits in *snrk1α1α2* would lead to a strong deactivation of invertase inhibitors by SnRK1 β- subunits, which are not affected in the mutant. The result should be an elevated invertase activity, as observed for the beginning of the extended night. The transient increase of invertase activity after 20 min in the wildtype could also be explained by the discussed mechanism, as the abundance of SnRK1 specific phosphorylated T-loop peptide was reduced specifically at that time (Nukarinen et al. 2016). Further research on a putative regulatory role of SnRK1 on invertase activity in *A. thaliana* will be needed. Moreover, transient but distinct downregulation of invertase activity in *snrk1α1α2* was observed after 60 min and between 80 and 120 min. It should be considered that the used *snrk1α1α2* knock-down mutant shows residual SnRK1 catalytic activity, which may provide potential for metabolic regulation. Nevertheless, other regulatory mechanisms for fine tuning invertase maximum activity are of interest, as transient downregulation seems to provide control over sucrose levels under energy limitation.

Within the first 20 minutes of EN, sugar concentrations are relatively stable in *snrk1α1α2* (see Figure 28). Also in this context the question arises, if other energy saving mechanisms besides residual SnRK1 activity remain active in the mutant. As sucrose levels were significantly lower at the end of the regular night in *snrk1α1α2*, transcriptional reprogramming as a consequence to the carbohydrate limitation seems plausible. Sugar depletion in the later night period, as observed for a starchless Arabidopsis *pgm* mutant, leads to global changes in gene expression (Gibon et al. 2004). In consequence, growth restriction and a vast reduction of carbohydrate consumption occur at the beginning of the subsequent day. A similar transcriptional reprogramming was found to take place in Col-0 wildtype plants after a 6-hours extension of the night (ibid.).

The constantly lower sucrose levels in the mutant plants coincide with persistently lowered G6P levels. G6P is, together with UDP-glucose, substrate for the enzyme TPS producing trehalose-6-phosphate (Ruan 2014). T6P is known to follow up sucrose levels across a great range of physiological concentrations (Lunn et al. 2014). Thus, it can be assumed that T6P levels might differ between Col-0 and *snrk1α1α2 in vivo*. It has been discussed recently if T6P signalling constitutes a separate pathway for reaction to sucrose availability, overlapping with functionalities of the SnRK1 pathway, or if its function is

limited to being an allosteric inhibitor for the kinase (Lunn et al. 2014). Hence, T6P levels could constitute an important remaining mechanism for sucrose sensing in the *snrk1α1α2* mutant.

If metabolic reprogramming already occurred in *snrk1α1α2* in response to lowered sucrose levels during the regular night, this could also explain the reduced carbohydrate consumption during the first 20 minutes of the extended night treatment (see Figure 28). Interestingly, from 20 to 40 min, a sharp decline of major carbohydrate levels finally occurred in *snrk1α1α2*, while maximum enzyme activities remained unaltered. As reported previously (Nukarinen et al. 2016), TCA cycle intermediates were also affected at that time point. One reason for the decrease of sugar levels could be the anticipation of dusk, leading to an adjustment of physiology for the following photoperiod (Dodd et al. 2005). But due to the disruption of the SnRK1 pathway, and a possible activity of other energy saving mechanisms, the induction of catabolic processes might be retarded in comparison to the wildtype. The major carbohydrates also dropped beyond distinctly lower levels as compared to the wildtype, indicating a role of SnRK1 in the fine tuning of these processes. This is further suggested by the fact that decreasing AKIN10/11 phosphopeptide abundance in Col-0 coincided with higher consumption of metabolites within the first 20 min of prolonged darkness (Nukarinen et al. 2016 & Figure 28).

Between 40 and 60 minutes of extended night, sucrose and hexose levels recovered, i.e. increased, in the *snrk1α1α2* mutant. Functional time series analysis revealed an accumulation of peaks around 40 min, when sucrose, glucose, and fructose concentrations were at a minimum and increased simultaneously. Comparing these dynamics to the enzyme activity data revealed a contradicting picture: Invertase maximum activity decreased distinctly between 40 and 60 min (-14%), which could eventually account for the change in the metabolic function of sucrose. Interestingly, fructose and glucose levels also began to rise despite a reduction in the maximum capacity of the reaction producing them. Partially, a decrease of hexokinase reaction rates could be responsible for this rise in hexoses. But the sum of carbohydrates (Figure 28) indicated a generally higher amount of sugars circulating. Interestingly, levels of TCA intermediates were likewise restored, as reported by Nukarinen et al. (2016). Potential acquiring of carbohydrates from alternative sources at that time point in the extended night seems plausible. Genes involved in degradation of lipids, amino acids, structural carbohydrates, and genes concerned with

gluconeogenesis show elevated transcript levels very early in the extended night in Col-0 plants (Usadel et al. 2008). Their transcription was suggested to respond to different stages of carbon depletion. But only if the change in transcript levels results in rapid adjustment of the encoded protein, this occurs in favour of quick adaptations. In the case of protein degradation, which was transcriptionally induced, it correlated with a reduced protein content and increased level of amino acids already after 2 hours of extended night exposure (Usadel et al. 2008). Considering the results from Nukarinen et al. (2016), who measured a distinct decrease of TCA intermediates in *snrk1α1α2* after 40 min, it seems plausible that autophagy was involved in the recovery of sugars, TCA intermediates and other metabolite levels until 60 min. The induction of autophagy is suggested to be based on the lacking supply of the mitochondria with substrates for respiration (Aubert et al. 1996). To shed light on the actual processes providing carbohydrates, measurement of F6P levels after 40 minutes would be interesting, as this metabolite is at the direct entrance point into glycolysis. Additionally, total protein levels and structural carbohydrate measurements should be considered in a future approach. However, as the amount of additional carbohydrates is quite small (~0.78µmol hexoses/gFW), revealing the source might be challenging.

5 Conclusion & Outlook

The present study indicates points of regulatory interaction between SnRK1 and the central carbohydrate metabolism in *A. thaliana*. The findings pointed to an effect of SnRK1 activity on the known target enzyme SPS, yet only to a moderate degree. The presented results also highlight the importance of SnRK1 activity for regulation of transitory starch degradation. In a future approach, choosing higher light intensity, e.g. 150 µmol m^{-2} s^{-1}, for plant growth might lead to stronger dynamics in sucrose and starch metabolism which might emphasize the suggested regulatory impact.

The significant differences between invertase activity in Col-0 and *snrk1α1α2* plants point towards a crucial role in stabilizing sucrose levels under energy limitation. Further, it is tempting to speculate if SnRK1 and (cytosolic) invertase interact directly (protein-protein) or indirectly via transcriptional or metabolic control. Finally, physiological parameters like rates of respiration and sucrose export to sink tissue, are promising candidates for future studies to unambiguously resolve the regulatory role of SnRK1 during energy deprivation.

6 Appendix

6.1 Abstract

The protein kinase SnRK1 is a key player in plant energy homeostasis. During energy limitation, for instance due to extended night conditions, plants with hampered SnRK1 activity suffer from carbohydrate shortfall. Although a role of SnRK1 in low energy signalling is well established, knowledge about specific biochemical interactions within the central carbohydrate metabolism is limited. This study intends to reveal possible reasons for the significantly lowered sucrose levels of *snrk1α1α2* double mutants of *A. thaliana*, being defective in SnRK1 activity, in an extended night experiment.

The study covered 6 hours of prolonged darkness with 20 minutes sampling intervals at the beginning. Maximum enzyme activities of sucrose-phosphate synthase, acid and neutral soluble invertase, glucokinase and fructokinase were measured by biochemical assays under optimum conditions. Hexose phosphates and UDP-glucose were quantified via ion chromatography coupled to triple quadrupole mass spectrometry, whereas glucose moieties of leaf starch were analysed via gas chromatography coupled to time-of-flight mass spectrometry. To functionally interpret metabolite and enzyme data in context of the network structure of the central carbohydrate metabolism, a recently published algorithm for functional time series analysis was applied.

Main differences between the genotypes were observed for the beginning of the extended night, when levels of v_{max} for all measured enzymes simultaneously increased in the wildtype. The most prominent effect was found for invertase activity, as *snrk1α1α2* showed a completely different course of regulation. Additionally, starch degradation was impaired in the mutant.

The present study underpins the importance of invertase enzymes for the stabilization of sucrose levels under carbohydrate limitation. It provides initial indications for a putative interaction between SnRK1 and invertase enzymes. Moreover, the simultaneous regulation of key enzymes in the wildtype is indicative of a potential function of SnRK1 in circadian clock processes.

6.2 Kurzfassung

Die Proteinkinase SnRK1 spielt in der Regulation des pflanzlichen Energiestoffwechsels eine große Rolle. Unter Energielimitation, welche zum Beispiel durch eine verlängerte Nacht induziert wird, zeigt sich in Pflanzen mit einem Defekt der SnRK1 Aktivität eine verstärkte Kohlenhydratlimitation. Obwohl die Rolle von SnRK1 in der Signalisierung von Energiemangel bereits gut ergründet wurde, ist das Wissen über spezifische biochemische Interaktionen des Enzyms innerhalb des zentralen Kohlenhydratstoffwechsels sehr beschränkt. Ziel dieser Arbeit ist es, mögliche Gründe für signifikant niedrigere Saccharose Konzentrationen in *snrk1α1α2* Doppelmutanten, welche einen Defekt der SnRK1 Aktivität aufweisen, im Zuge eines Experiments mit verlängerter Nacht zu ermitteln.

Die Studie umfasst eine Verlängerung der Nacht um 6 Stunden, mit 20-minütigen Probenahmeintervallen zu Beginn. Die maximalen Enzymaktivitäten von Saccharose-Phosphat-Synthase, saurer und neutraler löslicher Invertase, Glucokinase und Fructokinase wurden mittels biochemischer Verfahren unter optimalen Bedingungen bestimmt. Hexosephosphate und UDP-Glukose wurden mittels Ionenchromatographie und Massenspektrometrie quantifiziert, während die Dynamik der transitorischen Blattstärke durch Analyse mittels Gaschromatografie und Massenspektrometrie bestimmt wurde. Um die Metabolit- und Enzymdaten im Kontext der Netzwerkstruktur des zentralen Kohlenhydratstoffwechsels funktional interpretieren zu können, wurde ein Algorithmus zur funktionellen Zeitserienanalyse verwendet.

Die größten Unterschiede zwischen den Genotypen wurden zu Beginn der verlängerten Nacht beobachtet, als die maximalen Aktivitäten aller gemessenen Enzyme im Wildtypen gleichzeitig anstiegen. Der am stärksten ausgeprägte Effekt wurde für die Invertaseaktivität gefunden, da die *snrk1α1α2* Mutante einen komplett andersartigen Verlauf aufwies. Zusätzlich war der Stärkeabbau in der Mutante beeinträchtigt.

Die vorliegende Arbeit unterstreicht die Bedeutung von Invertase-Enzymen hinsichtlich der Stabilisierung von Saccharosekonzentrationen unter Kohlenhydratlimitation. Sie liefert erste Hinweise für eine mögliche Interaktion zwischen SnRK1 und Invertase-Isoformen. Darüber hinaus indiziert die anfängliche gleichzeitige Regulation der

wichtigsten Enzyme im Wildtyp eine potenzielle Beteiligung von SnRK1 an Prozessen der circadianen Rhythmik.

6.3 Separate Data for Acid and Neutral Invertase

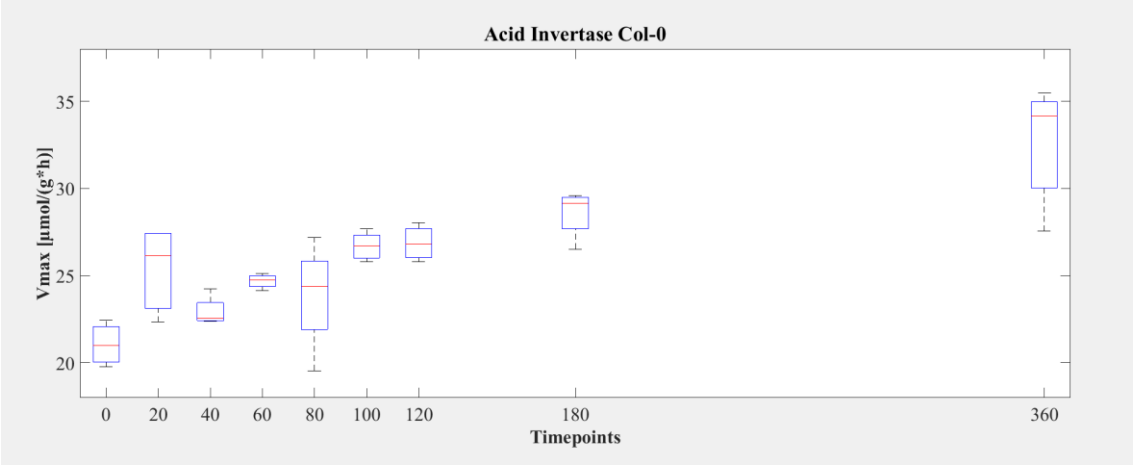

Figure 44 Time series of acid invertase maximum activity (v_{max}) for Col-0

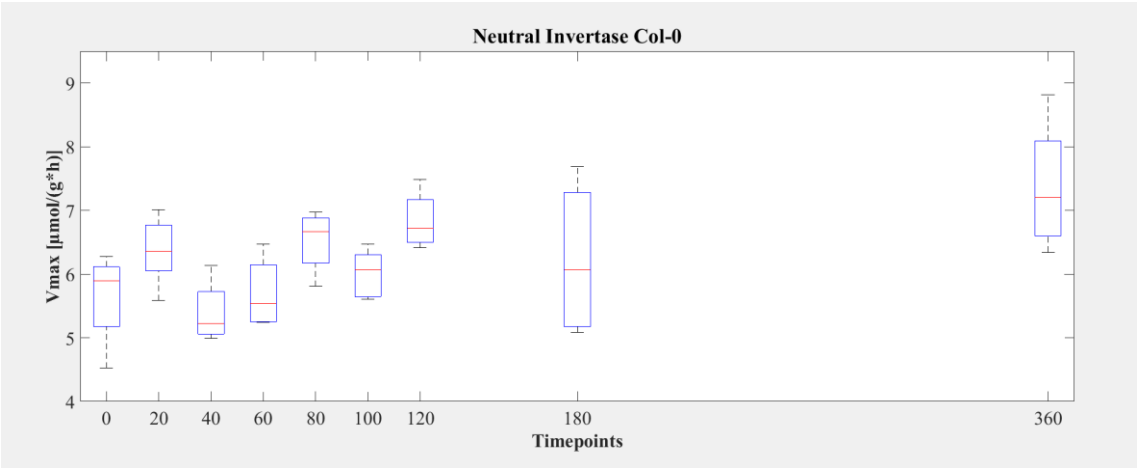

Figure 45 Time series of neutral invertase maximum activity (v_{max}) for Col-0

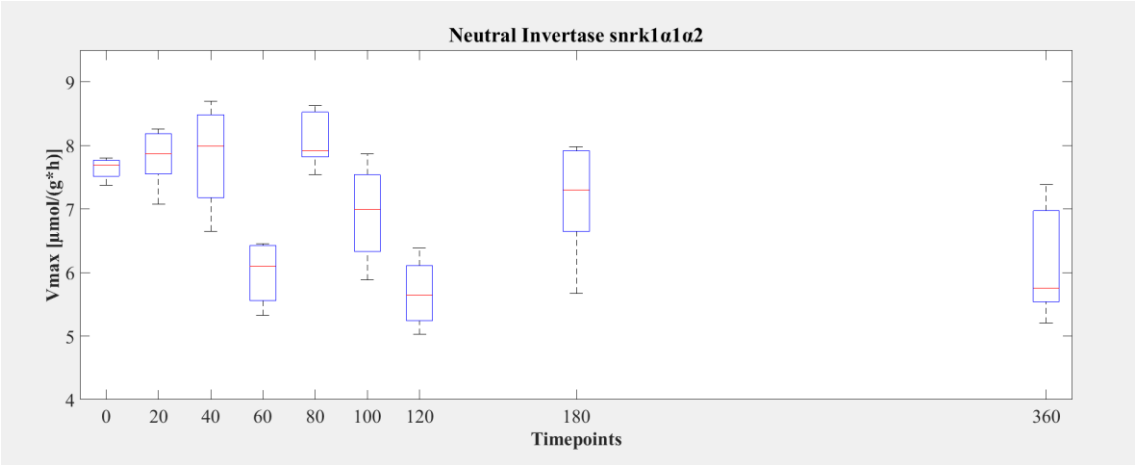

Figure 46 Time series of neutral invertase maximum activity (v_{max}) for *snrk1α1α2*

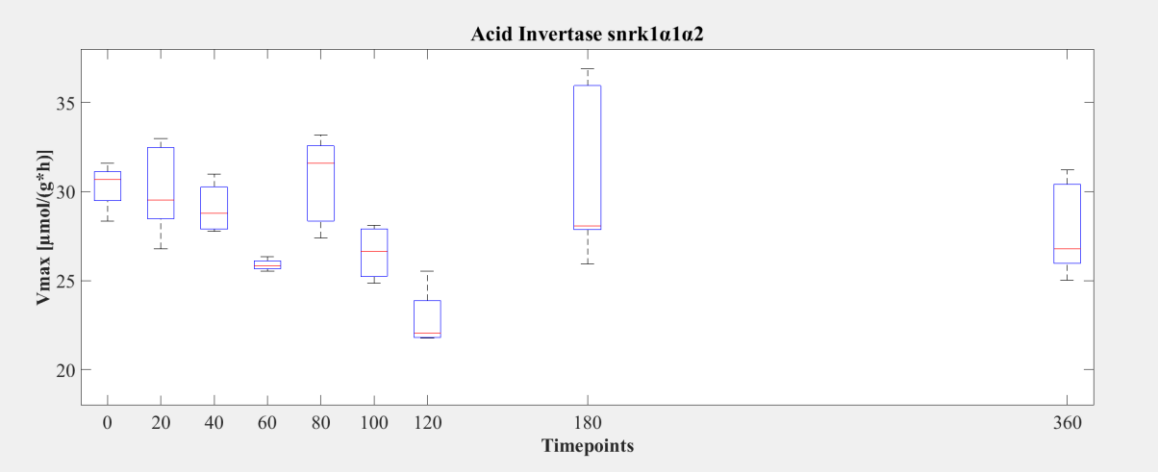

Figure 47 Time series of acid invertase maximum activity (v_{max}) for *snrk1α1α2*

6.4 Cubic Spline Interpolation of All Metabolites

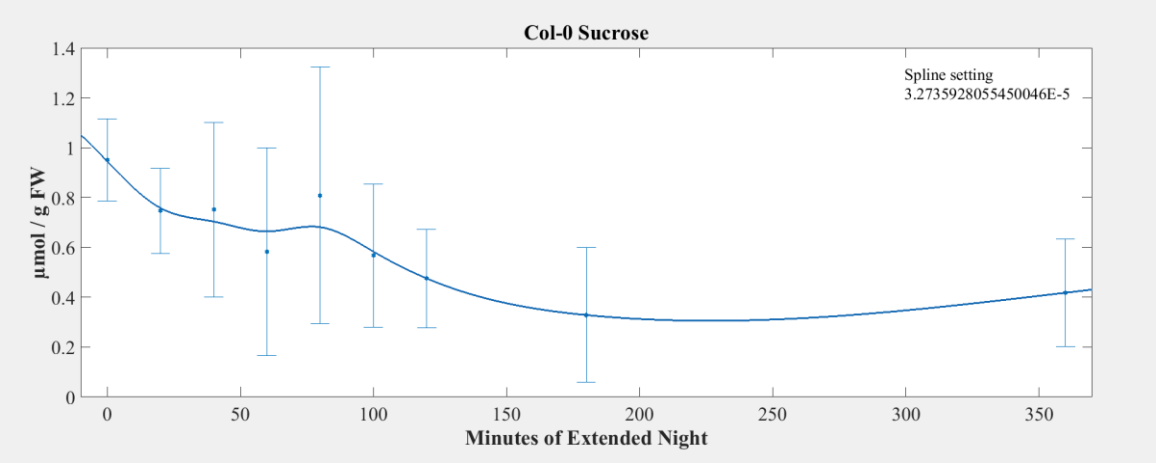

Figure 48 Cubic spline interpolation of sucrose concentrations in Col-0.

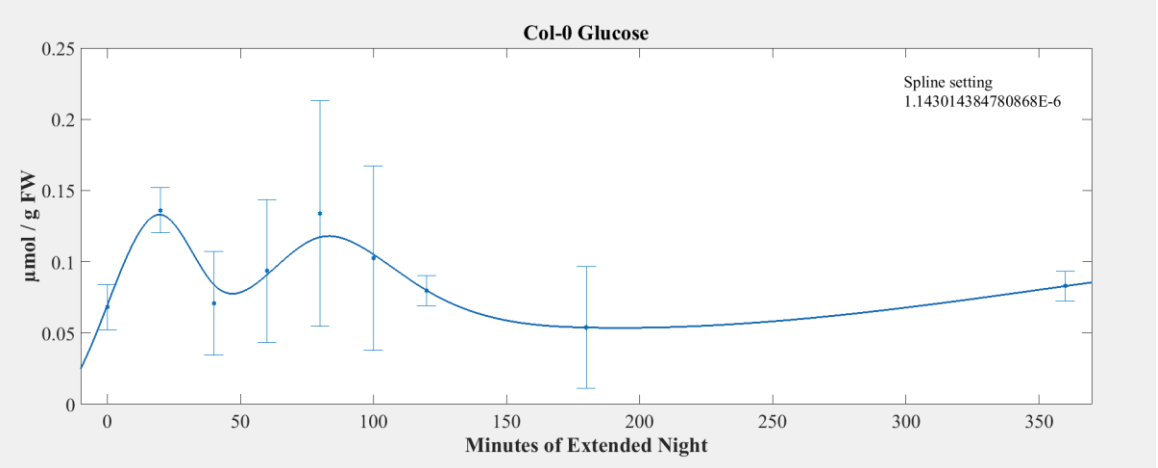

Figure 49 Cubic spline interpolation of glucose concentrations in Col-0.

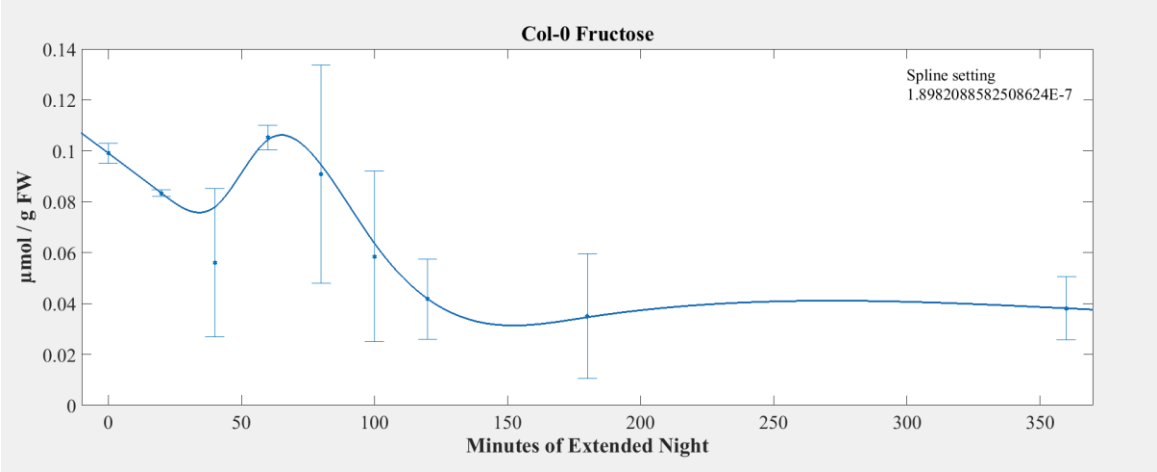

Figure 50 Cubic spline interpolation of fructose concentrations in Col-0.

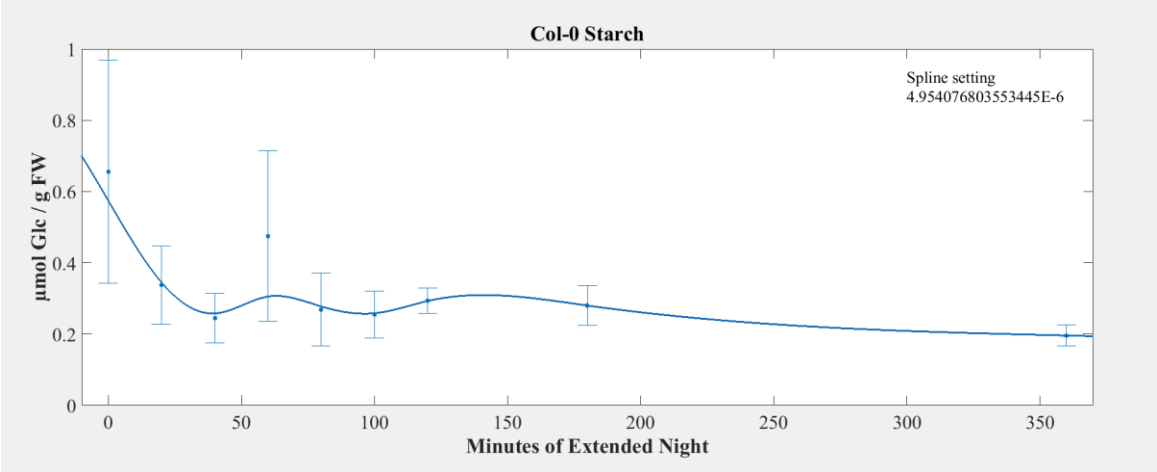

Figure 51 Cubic spline interpolation of starch concentrations in Col-0.

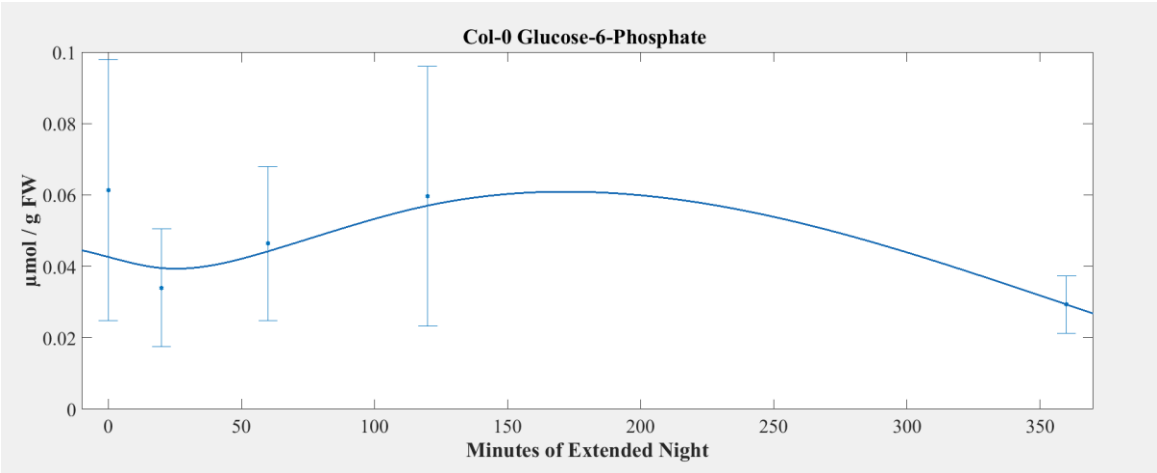

Figure 52 Cubic spline interpolation of glucose-6-phosphate concentrations in Col-0.

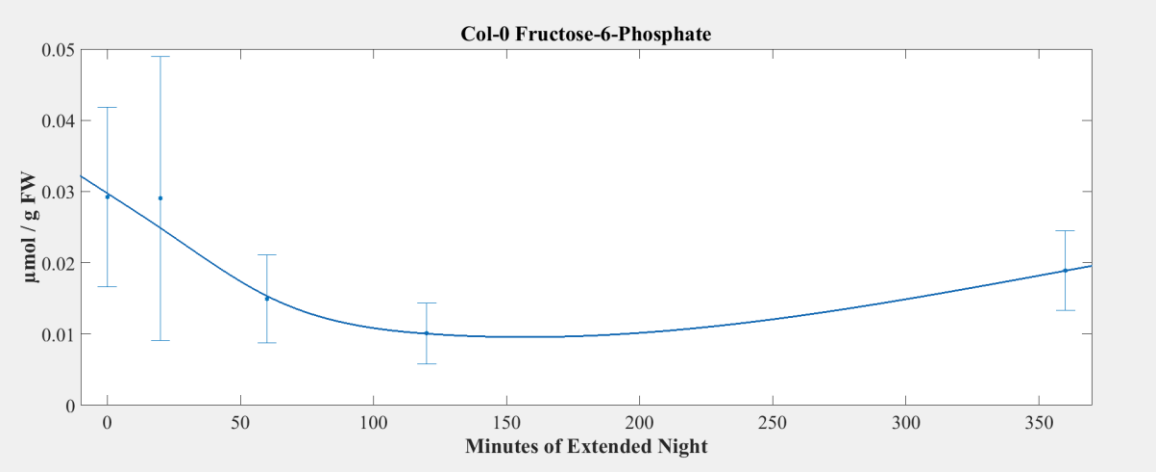

Figure 53 Cubic spline interpolation of fructose-6-phosphate concentrations in Col-0.

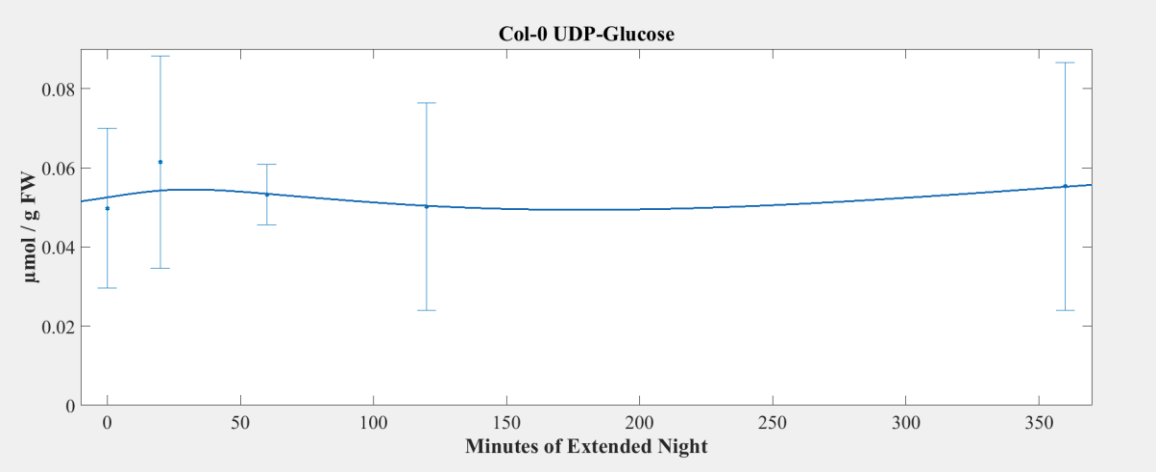

Figure 54 Cubic spline interpolation of UDP-glucose concentrations in Col-0.

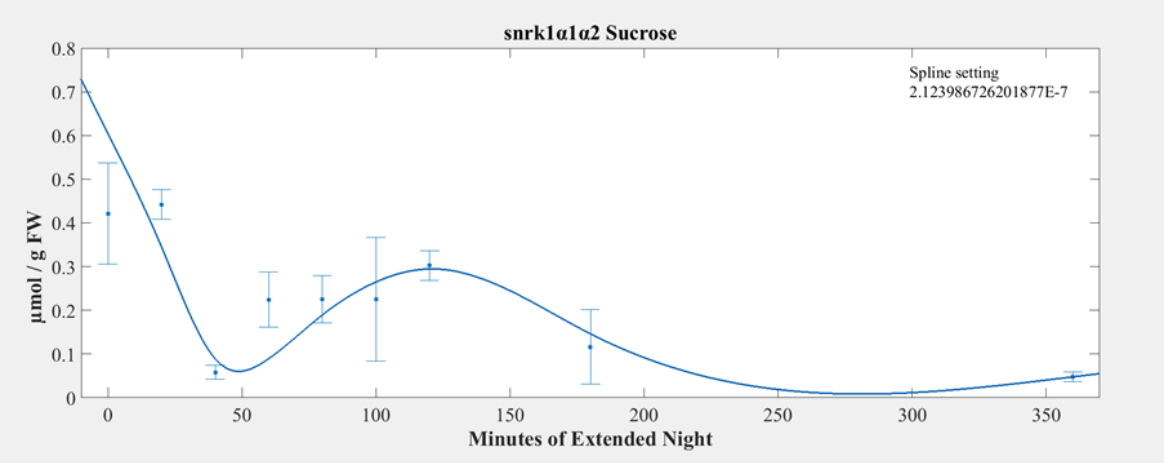

Figure 55 Cubic spline interpolation of sucrose concentrations in *snrk1α1α2*

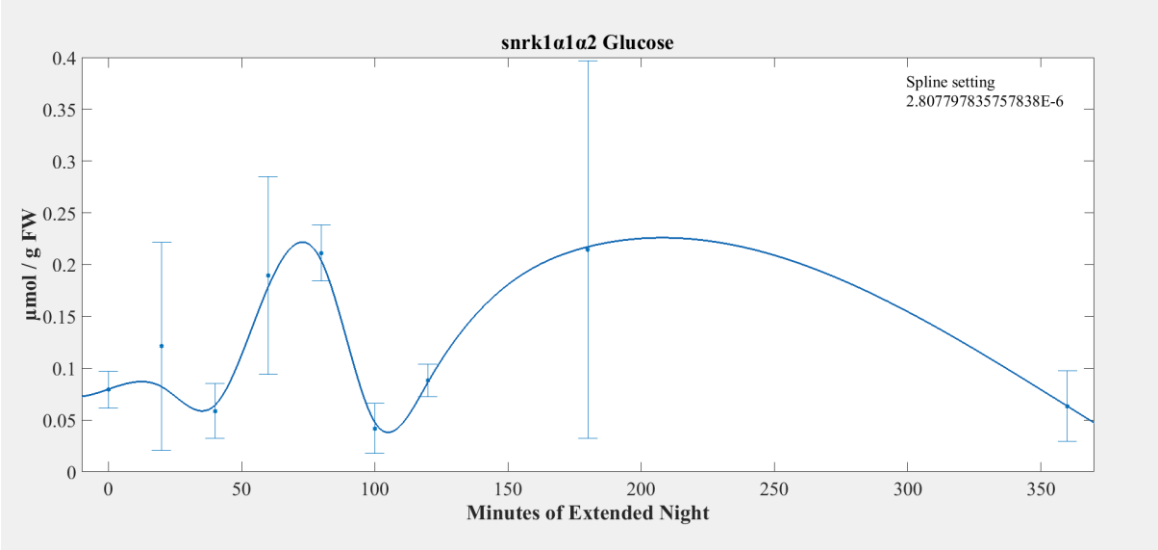

Figure 56 Cubic spline interpolation of glucose concentrations in snrk1α1α2.

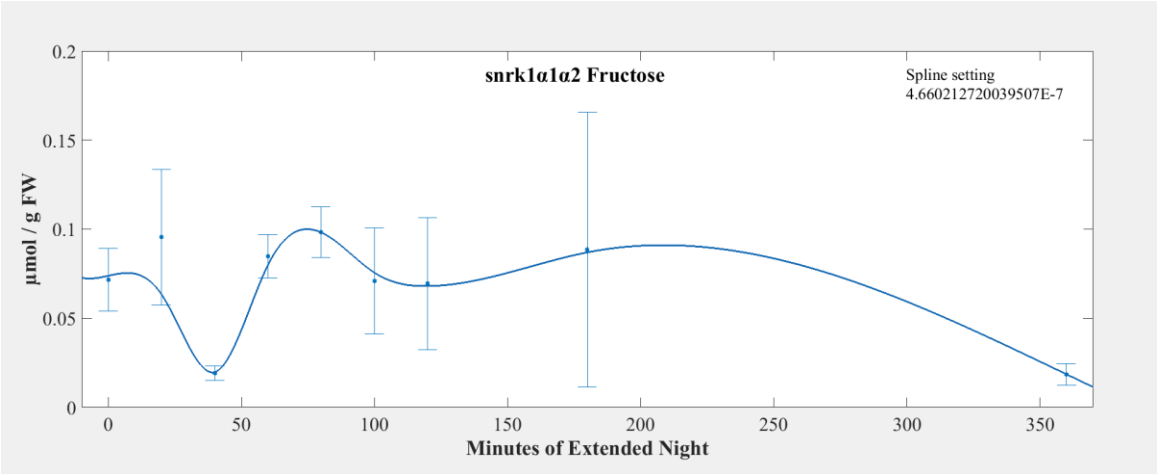

Figure 57 Cubic spline interpolation of fructose concentrations in snrk1α1α2.

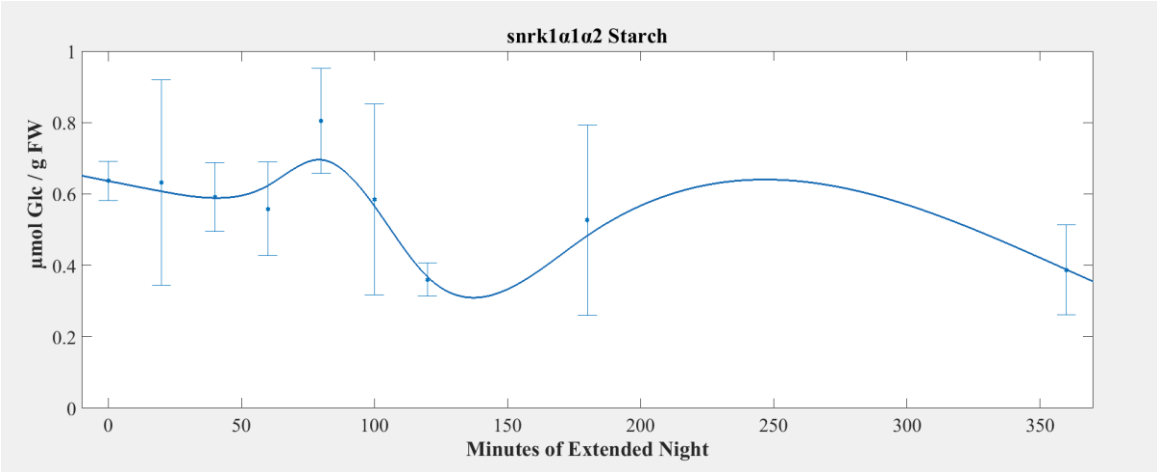

Figure 58 Cubic spline interpolation of starch concentrations in snrk1α1α2.

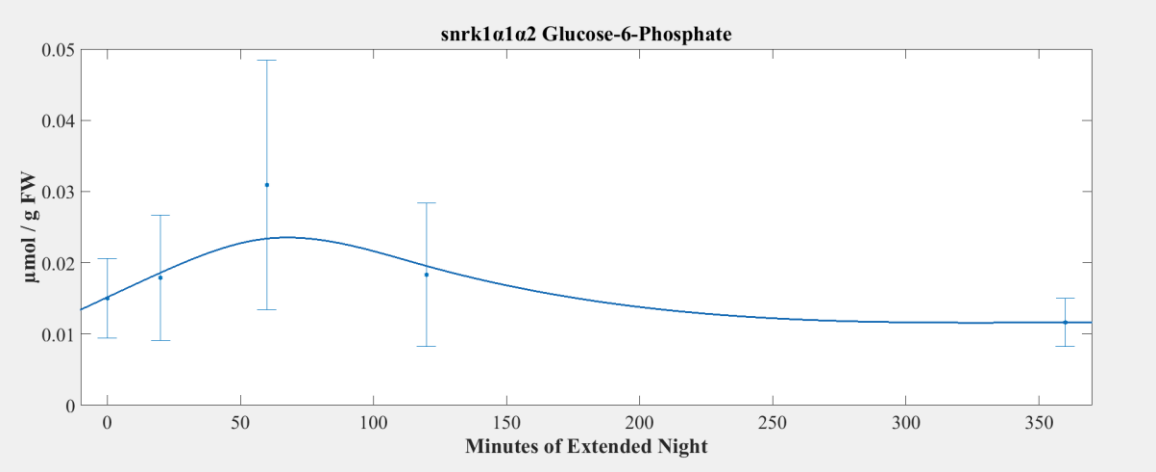

Figure 59 Cubic spline interpolation of glucose-6-phosphate concentrations in snrk1α1α2.

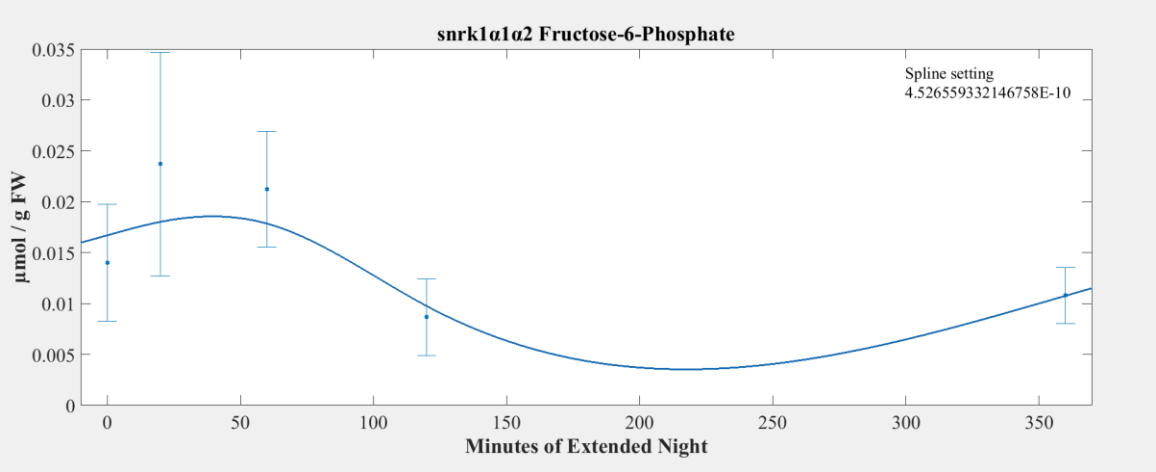

Figure 60 Cubic spline interpolation of fructose-6-phosphate concentrations in snrk1α1α2.

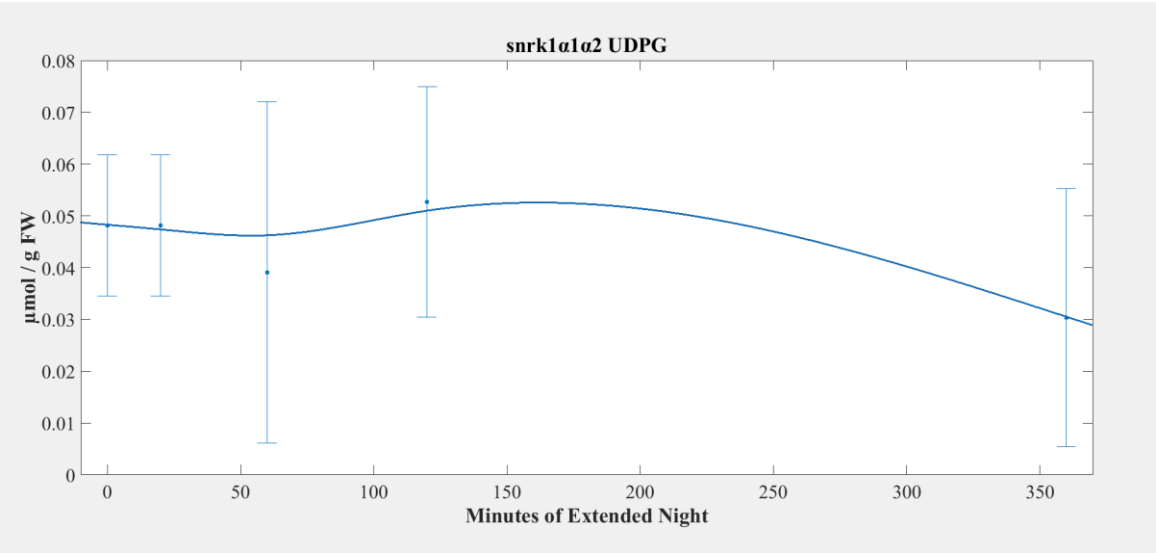

Figure 61 Cubic spline interpolation of UDP-glucose concentrations in snrk1α1α2.

Register of Figures and Tables

Bibliography

Albi, Tomas; Ruiz, M. Teresa; Los Reyes, Pedro de; Valverde, Federico; Romero, Jose M. (2016): Characterization of the Sucrose Phosphate Phosphatase (SPP) Isoforms from Arabidopsis thaliana and Role of the S6PPc Domain in Dimerization. In *PloS one* 11 (11), e0166308. DOI: 10.1371/journal.pone.0166308.

Alderson, Alison; Sabelli, Paolo A.; Dickinson, Richard; Cole, Deborah; Richardson, Michael; Kreis, Martin et al. (1991): Complementation of snf1, a mutation affecting global regulation of carbon metabolism in yeast, by a plant protein kinase cDNA. In *Proceedings of the National Academy of Sciences of the United States of America* 88, pp. 8602–8605.

Amir, Jacob; Preiss, Jack (1982): Kinetic Characterization of Spinach Leaf Sucrose-Phosphate Synthase. In *Plant physiology* (69), pp. 1027–1030.

Aubert, Serge; Gout, Elisabeth; Bligny, Richard; Marty-Mazars, Danièle; Barrieu, Francois; Alabouvette, Josianne et al. (1996): Ultrastructural and Biochemical Characterization of Autophagy in Higher Plant Cells Subjected to Carbon Deprivation: Control by the Supply of Mitochondria with Respiratory Substrates. In *The Journal of Cell Biology* 133, pp. 1251–1263.

Baena-Gonzalez, Elena; Rolland, Filip; Thevelein, Johan M.; Sheen, Jen (2007): A central integrator of transcription networks in plant stress and energy signalling. In *Nature* 448, pp. 938–942. DOI: 10.1038/nature06069.

Baena-Gonzalez, Elena; Sheen, Jen (2008): Convergent energy and stress signaling. In *Trends in plant science* 13 (9), pp. 474–482. DOI: 10.1016/j.tplants.2008.06.006.

Baroja-Fernandez, Edurne; Munoz, Francisco Jose; Li, Jun; Bahaji, Abdellatif; Almagro, Goizeder; Montero, Manuel et al. (2012): Sucrose synthase activity in the sus1/sus2/sus3/sus4 Arabidopsis mutant is sufficient to support normal cellulose and starch production. In *Proceedings of the National Academy of Sciences of the United States of America* 109 (1), pp. 321–326. DOI: 10.1073/pnas.1117099109.

Bisswanger, Hans (2012): Practical enzymology. 1st repr, 2nd, compl. rev. ed. Weinheim: Wiley-Blackwell.

Bläsing, Oliver E.; Gibon, Yves; Gunther, Manuela; Hohne, Melanie; Morcuende, Rosa; Osuna, Daniel et al. (2005): Sugars and circadian regulation make major contributions to the global regulation of diurnal gene expression in Arabidopsis. In *The Plant cell* 17 (12), pp. 3257–3281. DOI: 10.1105/tpc.105.035261.

Bouly, Jean-Pierre; Gissot, Lionel; Lessard, Philippe; Kreis, Martin; Thomas, Martine (1999): Arabidopsis thaliana proteins related to the yeast SIP and SNF4 interact with AKINalpha1, an SNF1-like protein kinase. In *The Plant Journal* 18 (5), pp. 541–550. DOI: 10.1046/j.1365-313X.1999.00476.x.

Choudhary, Mani Kant; Nomura, Yuko; Wang, Lei; Nakagami, Hirofumi; Somers, David E. (2015): Quantitative Circadian Phosphoproteomic Analysis of Arabidopsis Reveals Extensive Clock Control of Key Components in Physiological, Metabolic, and Signaling Pathways. In *Molecular & cellular proteomics : MCP* 14 (8), pp. 2243–2260. DOI: 10.1074/mcp.M114.047183.

Claeyssen, Eric; Rivoal, Jean (2007): Isozymes of plant hexokinase: occurrence, properties and functions. In *Phytochemistry* 68 (6), pp. 709–731. DOI: 10.1016/j.phytochem.2006.12.001.

Confraria, Ana; Martinho, Claudia; Elias, Alexandre; Rubio-Somoza, Ignacio; Baena-Gonzalez, Elena (2013): miRNAs mediate SnRK1-dependent energy signaling in Arabidopsis. In *Frontiers in plant science* 4, 197. DOI: 10.3389/fpls.2013.00197.

Crozet, Pierre; Jammes, Fabien; Valot, Benoit; Ambard-Bretteville, Francoise; Nessler, Sylvie; Hodges, Michael et al. (2010): Cross-phosphorylation between Arabidopsis thaliana sucrose nonfermenting 1-related protein kinase 1 (AtSnRK1) and its activating kinase (AtSnAK) determines their catalytic activities. In *The Journal of biological chemistry* 285 (16), pp. 12071–12077. DOI: 10.1074/jbc.M109.079194.

Crozet, Pierre; Margalha, Leonor; Butowt, Rafal; Fernandes, Noemia; Elias, Carlos A.; Orosa, Beatriz et al. (2016): SUMOylation represses SnRK1 signaling in Arabidopsis. In *The Plant journal : for cell and molecular biology* 85 (1), pp. 120–133. DOI: 10.1111/tpj.13096.

Crozet, Pierre; Margalha, Leonor; Confraria, Ana; Rodrigues, Americo; Martinho, Claudia; Adamo, Mattia et al. (2014): Mechanisms of regulation of SNF1/AMPK/SnRK1 protein kinases. In *Frontiers in plant science* 5, 190. DOI: 10.3389/fpls.2014.00190.

Dodd, Antony N.; Salathia, Neeraj; Hall, Anthony; Kevei, Eva; Toth, Reka; Nagy, Ferenc et al. (2005): Plant circadian clocks increase photosynthesis, growth, survival, and competitive advantage. In *Science (New York, N.Y.)* 309, pp. 630–633. DOI: 10.1126/science.1115581.

Doerfler, Hannes; Lyon, David; Nägele, Thomas; Sun, Xiaoliang; Fragner, Lena; Hadacek, Franz et al. (2013): Granger causality in integrated GC-MS and LC-MS metabolomics data reveals the interface of primary and secondary metabolism. In *Metabolomics : Official journal of the Metabolomic Society* 9 (3), pp. 564–574. DOI: 10.1007/s11306-012-0470-0.

Dyson, Beth C.; Allwood, J. William; Feil, Regina; Xu, Yun; Miller, Matthew; Bowsher, Caroline G. et al. (2015): Acclimation of metabolism to light in Arabidopsis thaliana: the glucose 6-phosphate/phosphate translocator GPT2 directs metabolic acclimation. In *Plant, cell & environment* 38 (7), pp. 1404–1417. DOI: 10.1111/pce.12495.

Emanuelle, Shane; Hossain, Mohammed Iqbal; Moller, Isabel E.; Pedersen, Henriette L.; van de Meene, Allison M. L.; Doblin, Monika S. et al. (2015): SnRK1 from Arabidopsis thaliana is an atypical AMPK. In *The Plant journal : for cell and molecular biology* 82 (2), pp. 183–192. DOI: 10.1111/tpj.12813.

Flugge, Ulf-Ingo (1999): PHOSPHATE TRANSLOCATORS IN PLASTIDS. In *Annual Review of Plant Physiology and Plant Molecular Biology* 50, pp. 27–45. DOI: 10.1146/annurev.arplant.50.1.27.

Fu, Y.; Ballicora, M. A.; Leykam, J. F.; Preiss, J. (1998): Mechanism of Reductive Activation of Potato Tuber ADP-glucose Pyrophosphorylase. In *Journal of Biological Chemistry* 273 (39), pp. 25045–25052. DOI: 10.1074/jbc.273.39.25045.

Gibon, Yves; Blasing, Oliver E.; Palacios-Rojas, Natalia; Pankovic, Dejana; Hendriks, Janneke H. M.; Fisahn, Joachim et al. (2004): Adjustment of diurnal starch turnover to short days: depletion of sugar during the night leads to a temporary inhibition of carbohydrate utilization, accumulation of sugars and post-translational activation of ADP-glucose pyrophosphorylase in the following light period. In *The Plant journal : for cell and molecular biology* 39 (6), pp. 847–862. DOI: 10.1111/j.1365-313X.2004.02173.x.

Gibon, Yves; Usadel, Bjoern; Blaesing, Oliver; Kamlage, Beate; Hoehne, Melanie; Trethewey, Richard; Stitt, Mark (2006): Integration of metabolite with transcript and enzyme activity profiling during diurnal cycles in Arabidopsis rosettes. In *Genome Biology* 7 (8), R76.

Gissot, Lionel; Polge, Cecile; Jossier, Mathieu; Girin, Thomas; Bouly, Jean-Pierre; Kreis, Martin; Thomas, Martine (2006): AKINbetagamma contributes to SnRK1 heterotrimeric complexes and interacts with two proteins implicated in plant pathogen resistance through its KIS/GBD sequence. In *Plant physiology* 142 (3), pp. 931–944. DOI: 10.1104/pp.106.087718.

Gissot, Lionel; Polge, Cécile; Bouly, Jean-Pierre; Lemaitre, Thomas; Kreis, Martin; Thomas, Martine (2004): AKINb3, a plant specific SnRK1 protein, is lacking domains present in yeast and mammals non-catalytic b-subunits. In *Plant Molecular Biology* 56, pp. 747–759.

Graf, Alexander; Schlereth, Armin; Stitt, Mark; Smith, Alison M. (2010): Circadian control of carbohydrate availability for growth in Arabidopsis plants at night. In *Proceedings of the National Academy of Sciences of the United States of America* 107 (20), pp. 9458–9463. DOI: 10.1073/pnas.0914299107.

Granot, David (2008): Putting plant hexokinases in their proper place. In *Phytochemistry* 69 (15), pp. 2649–2654. DOI: 10.1016/j.phytochem.2008.08.026.

Granot, David; Kelly, Gilor; Stein, Ofer; David-Schwartz, Rakefet (2014): Substantial roles of hexokinase and fructokinase in the effects of sugars on plant physiology and development. In *Journal of experimental botany* 65 (3), pp. 809–819. DOI: 10.1093/jxb/ert400.

Gross, Jürgen (2013): Massenspektrometrie. Ein Lehrbuch. Berlin-Heidelberg: Springer Spektrum.

Guérinier, Thomas; Millan, Laurine; Crozet, Pierre; Oury, Celine; Rey, Francois; Valot, Benoit et al. (2013): Phosphorylation of p27(KIP1) homologs KRP6 and 7 by SNF1-related protein kinase-1 links plant energy homeostasis and cell proliferation. In *The Plant journal : for cell and molecular biology* 75 (3), pp. 515–525. DOI: 10.1111/tpj.12218.

Halford, N. G.; Hey, S.; Jhurreea, D.; Laurie, S.; McKibbin, R. S.; Paul, M.; Zhang, Y. (2003): Metabolic signalling and carbon partitioning. Role of Snf1-related (SnRK1) protein kinase. In *Journal of experimental botany* 54 (382), pp. 467–475. DOI: 10.1093/jxb/erg038.

Halford, Nigel G.; Hardie, Grahame D. (1998): SNF1-related protein kinases: global regulators of carbon metabolism in plants? In *Plant Molecular Biology* 37, pp. 735–748.

Hardie, D. Grahame (2007): AMP-activated/SNF1 protein kinases: conserved guardians of cellular energy. In *Nature reviews. Molecular cell biology* 8 (10), pp. 774–785. DOI: 10.1038/nrm2249.

Hardy, Rolletschek; Heinzel, Nicolas (2010): Primary Metabolite Analysis of Plant Material Using a Triple Quadrupole MS Coupled to a Monolith Anion-Exchange Column. Available online at https://appslab.thermofisher.com/App/2379/can-109-primary-metabolite-analysis-plant-material-using-a-triple-quadrupole-ms-coupled-a-monolith-anionexchange-column, checked on 5/25/2017.

Hrabak, Estelle M.; Chan, Catherine W. M.; Gribskov, Michael; Harper, Jeffrey F.; Choi, Jung H.; Halford, Nigel et al. (2003): The Arabidopsis CDPK-SnRK superfamily of protein kinases. In *Plant physiology* 132 (2), pp. 666–680. DOI: 10.1104/pp.102.011999.

Huarancca Reyes, Thais; Scartazza, Andrea; Lu, Yu; Yamaguchi, Junji; Guglielminetti, Lorenzo (2016): Effect of carbon/nitrogen ratio on carbohydrate metabolism and light energy dissipation mechanisms in Arabidopsis thaliana. In *Plant physiology and biochemistry : PPB* 105, pp. 195–202. DOI: 10.1016/j.plaphy.2016.04.030.

Huber, Steven C. (1989): Biochemical Mechanism for Regulation of Sucrose Accumulation in Leaves during Photosynthesis. In *Plant Physiol.* 91 (2), pp. 656–662.

Huber, Steven C.; Huber, Joan L. (1996): ROLE AND REGULATION OF SUCROSE-PHOSPHATE SYNTHASE IN HIGHER PLANTS. In *Annual Review of Plant Physiology and Plant Molecular Biology* 47, pp. 431–444.

Iglesias, Alberto A.; Barry, Gerard F.; Meyer, Christopher; Bloksberg, Leonard; Nakata, Paul A.; Greene, Thomas et al. (1993): Expression of the Potato Tuber ADP-glucose Pyrophosphorylase in Escherichia coli. In *The Journal of biological chemistry* 268 (2), pp. 1081–1086.

Jones, Tamara L.; Ort, Donald R. (1997): Circadian Regulation of Sucrose Phosphate Synthase Activity in Tomato by Protein Phosphatase Activity. In *Plant Physiol.* 113, pp. 1167–1175.

Kim, Donggiun; Park, So Yun; Chung, Youngjae; Park, Jongbum; Lee, Sukchan; Lee, Taek-Kyun (2010): Biochemical characterization of soluble acid and alkaline invertases from shoots of etiolated pea seedlings. In *Journal of integrative plant biology* 52 (6), pp. 536–548. DOI: 10.1111/j.1744-7909.2010.00937.x.

Kingston-Smith, Alison H.; Walker, Robert P.; Pollock, Christopher J. (1999): Invertase in leaves: conundrum or control point? In *Journal of experimental botany* 50, pp. 735–743.

Koch, Karen (2004): Sucrose metabolism: regulatory mechanisms and pivotal roles in sugar sensing and plant development. In *Current opinion in plant biology* 7 (3), pp. 235–246. DOI: 10.1016/j.pbi.2004.03.014.

Kolbe, Anna; Tiessen, Axel; Schluepmann, Henriette; Paul, Matthew; Ulrich, Silke; Geigenberger, Peter (2005): Trehalose 6-phosphate regulates starch synthesis via posttranslational redox activation of ADP-glucose pyrophosphorylase. In *Proceedings of the National Academy of Sciences of the United States of America* 102 (31), pp. 11118–11123. DOI: 10.1073/pnas.0503410102.

Kolling, Katharina; Thalmann, Matthias; Muller, Antonia; Jenny, Camilla; Zeeman, Samuel C. (2015): Carbon partitioning in Arabidopsis thaliana is a dynamic process controlled by the plants metabolic status and its circadian clock. In *Plant, cell & environment* 38 (10), pp. 1965–1979. DOI: 10.1111/pce.12512.

Laurie, S. (2003): Antisense SNF1-related (SnRK1) protein kinase gene represses transient activity of an alpha-amylase (alpha-Amy2) gene promoter in cultured wheat embryos. In *Journal of experimental botany* 54 (383), pp. 739–747. DOI: 10.1093/jxb/erg085.

Lin, Yuan; Liu, Tengfei; Liu, Jun; Liu, Xun; Ou, Yongbin; Zhang, Huiling et al. (2015): Subtle Regulation of Potato Acid Invertase Activity by a Protein Complex of Invertase, Invertase Inhibitor, and SUCROSE NONFERMENTING1-RELATED PROTEIN KINASE. In *Plant physiology* 168 (4), pp. 1807–1819. DOI: 10.1104/pp.15.00664.

Lunn, John Edward; Delorge, Ines; Figueroa, Carlos Maria; van Dijck, Patrick; Stitt, Mark (2014): Trehalose metabolism in plants. In *The Plant journal : for cell and molecular biology* 79 (4), pp. 544–567. DOI: 10.1111/tpj.12509.

Mair, Andrea; Pedrotti, Lorenzo; Wurzinger, Bernhard; Anrather, Dorothea; Simeunovic, Andrea; Weiste, Christoph et al. (2015): SnRK1-triggered switch of bZIP63 dimerization mediates the low-energy response in plants. In *eLife. DOI:* 10.7554/eLife.05828.001.

Margalha, Leonor; Valerio, Concetta; Baena-González, Elena (2016): Plant SnRK1 Kinases: Structure, Regulation, and Function. In Mario D. Cordero, Benoit Viollet (Eds.): AMP-activated Protein Kinase. Switzerland: Springer International Publishing (Experientia Supplementum, 107), pp. 403–440.

Moore, Brandon; Zhou, Li; Rolland, Filip; Hall, Qi; Cheng, Wan-Hsing; Liu, Yan-Xia et al. (2003): Role of the Arabidopsis glucose sensor HXK1 in nutrient, light, and hormonal signaling. In *Science (New York, N.Y.)* 300 (5617), pp. 332–336. DOI: 10.1126/science.1080585.

Myers, Alan M.; Morell, Matthew K.; James, Martha G.; Ball, Steven G. (2000): Recent Progress toward Understanding Biosynthesis of the Amylopectin Crystal. In *Plant Physiol.* 122 (4), pp. 989–998. DOI: 10.1104/pp.122.4.989.

Nägele, Thomas; Furtauer, Lisa; Nagler, Matthias; Weiszmann, Jakob; Weckwerth, Wolfram (2016): A Strategy for Functional Interpretation of Metabolomic Time Series Data in Context of Metabolic Network Information. In *Frontiers in molecular biosciences* 3, 6. DOI: 10.3389/fmolb.2016.00006.

Nägele, Thomas; Henkel, Sebastian; Hormiller, Imke; Sauter, Thomas; Sawodny, Oliver; Ederer, Michael; Heyer, Arnd G. (2010): Mathematical modeling of the central carbohydrate metabolism in Arabidopsis reveals a substantial regulatory influence of vacuolar invertase on whole plant carbon metabolism. In *Plant physiology* 153 (1), pp. 260–272. DOI: 10.1104/pp.110.154443.

Nägele, Thomas; Weckwerth, Wolfram (2014): Mathematical modeling reveals that metabolic feedback regulation of SnRK1 and hexokinase is sufficient to control sugar homeostasis from energy depletion to full recovery. In *Frontiers in plant science* 5, 365. DOI: 10.3389/fpls.2014.00365.

Niittyla, Totte; Messerli, Gaelle; Trevisan, Martine; Chen, Jychian; Smith, Alison M.; Zeeman, Samuel C. (2004): A previously unknown maltose transporter essential for starch degradation in leaves. In *Science (New York, N.Y.)* 303 (5654), pp. 87–89. DOI: 10.1126/science.1091811.

Nukarinen, Ella; Nägele, Thomas; Pedrotti, Lorenzo; Wurzinger, Bernhard; Mair, Andrea; Landgraf, Ramona et al. (2016): Quantitative phosphoproteomics reveals the role of the AMPK plant ortholog SnRK1 as a metabolic master regulator under energy deprivation. In *Scientific reports* 6, 31697. DOI: 10.1038/srep31697.

Nunes, Catia; Primavesi, Lucia F.; Patel, Mitul K.; Martinez-Barajas, Eleazar; Powers, Stephen J.; Sagar, Ram et al. (2013): Inhibition of SnRK1 by metabolites: tissue-dependent effects and cooperative inhibition by glucose 1-phosphate in combination with trehalose 6-phosphate. In *Plant physiology and biochemistry : PPB / Societe francaise de physiologie vegetale* 63, pp. 89–98. DOI: 10.1016/j.plaphy.2012.11.011.

Pal, Sunil Kumar; Liput, Magdalena; Piques, Maria; Ishihara, Hirofumi; Obata, Toshihiro; Martins, Marina C. M. et al. (2013): Diurnal changes of polysome loading track sucrose content in the rosette of wild-type arabidopsis and the starchless pgm mutant. In *Plant physiology* 162 (3), pp. 1246–1265. DOI: 10.1104/pp.112.212258.

Polge, Cecile; Thomas, Martine (2007): SNF1/AMPK/SnRK1 kinases, global regulators at the heart of energy control? In *Trends in plant science* 12 (1), pp. 20–28. DOI: 10.1016/j.tplants.2006.11.005.

Pribil, M.; Leister, D. (2016): Photosynthesis. In Brian Thomas, Denis J. Murphy, Brian G. Murray (Eds.): Encyclopedia of Applied Plant Sciences. 2nd ed. Saint Louis: Elsevier Science, pp. 90–95.

Purcell, Patrick C.; Smith, Alison M.; Halford, Nigel G. (1998): Antisense expression of a sucrose non-fermenting-1-related protein kinase sequence in potato results in decreased expression of sucrose synthase in tubers and loss of sucrose-inducibility of sucrose synthase transcripts in leaves. In *The Plant Journal* 14 (2), pp. 195–202.

Radchuk, Ruslana; Emery, R. J. Neil; Weier, Diana; Vigeolas, Helene; Geigenberger, Peter; Lunn, John E. et al. (2010): Sucrose non-fermenting kinase 1 (SnRK1) coordinates metabolic and hormonal signals during pea cotyledon growth and differentiation. In *The Plant journal : for cell and molecular biology* 61 (2), pp. 324–338. DOI: 10.1111/j.1365-313X.2009.04057.x.

Robaglia, Christophe; Thomas, Martine; Meyer, Christian (2012): Sensing nutrient and energy status by SnRK1 and TOR kinases. In *Current opinion in plant biology* 15 (3), pp. 301–307. DOI: 10.1016/j.pbi.2012.01.012.

Rodrigues, Americo; Adamo, Mattia; Crozet, Pierre; Margalha, Leonor; Confraria, Ana; Martinho, Claudia et al. (2013): ABI1 and PP2CA phosphatases are negative regulators of Snf1-related protein kinase1 signaling in Arabidopsis. In *The Plant cell* 25 (10), pp. 3871–3884. DOI: 10.1105/tpc.113.114066.

Roitsch, Thomas; Gonzalez, Mari-Cruz (2004): Function and regulation of plant invertases: sweet sensations. In *Trends in plant science* 9 (12), pp. 606–613. DOI: 10.1016/j.tplants.2004.10.009.

Ruan, Yong-Ling (2014): Sucrose metabolism: gateway to diverse carbon use and sugar signaling. In *Annual review of plant biology* 65, pp. 33–67. DOI: 10.1146/annurev-arplant-050213-040251.

Santelia, Diana; Kotting, Oliver; Seung, David; Schubert, Mario; Thalmann, Matthias; Bischof, Sylvain et al. (2011): The phosphoglucan phosphatase like sex Four2 dephosphorylates starch at the C3-position in Arabidopsis. In *The Plant cell* 23 (11), pp. 4096–4111. DOI: 10.1105/tpc.111.092155.

Schopfer, Peter; Brennicke, Axel (2010): Pflanzenphysiologie. 7.Auflage. Freiburg/Ulm: Springer Spektrum.

Sekiguchi, Yoko; Mitsuhashi, Naoto; Inoue, Yoshinori; Yagisawa, Hitoshi; Mimura, Tetsuro (2004): Analysis of sugar phosphates in plants by ion chromatography on a titanium dioxide column with pulsed amperometric detection. In *Journal of Chromatography A*, pp. 71–76. DOI: 10.1016/j.chroma.2004.02.015.

Sheen, Jen (2014): Master Regulators in Plant Glucose Signaling Networks. In *Journal of plant biology* 57 (2), pp. 67–79. DOI: 10.1007/s12374-014-0902-7.

Shin, Jieun; Sanchez-Villarreal, Alfredo; Davis, Amanda M.; Du, Shen-Xiu; Berendzen, Kenneth W.; Koncz, Csaba et al. (2017): The metabolic sensor AKIN10 modulates the Arabidopsis circadian clock in a light-dependent manner. In *Plant, cell & environment. DOI:* 10.1111/pce.12903.

Smith, Alison M.; Stitt, Mark (2007): Coordination of carbon supply and plant growth. In *Plant, cell & environment* 30 (9), pp. 1126–1149. DOI: 10.1111/j.1365-3040.2007.01708.x.

Stitt, M. (1990): Fructose-2,6-Bisphosphate As A Regulatory Molecule In Plants. In *Annual Review of Plant Physiology and Plant Molecular Biology* 41 (1), pp. 153–185. DOI: 10.1146/annurev.arplant.41.1.153.

Stitt, Mark; Gibon, Yves; Lunn, John E.; Piques, Maria (2007): Multilevel genomics analysis of carbon signalling during low carbon availability. Coordinating the supply and utilisation of

carbon in a fluctuating environment. In *Functional Plant Biol.* 34 (6), pp. 526–549. DOI: 10.1071/FP06249.

Stitt, Mark; Lunn, John; Usadel, Bjorn (2010): Arabidopsis and primary photosynthetic metabolism - more than the icing on the cake. In *The Plant journal : for cell and molecular biology* 61 (6), pp. 1067–1091. DOI: 10.1111/j.1365-313X.2010.04142.x.

Strand, Asa; Zrenner, Rita; Trevanion, Stephen; Stitt, Mark; Gustafsson, Petter; Gardestrom, Per (2000): Decreased expression of two key enzymes in the sucrose biosynthesis pathway, cytosolic fructose-1,6-bisphosphatase and sucrose phosphate synthase, has remarkably different consequences for photosynthetic carbon metabolism in transgenic Arabidopsis thaliana. In *Plant J* 23 (6), pp. 759–770. DOI: 10.1046/j.1365-313x.2000.00847.x.

Streb, Sebastian; Zeeman, Samuel C. (2012): Starch metabolism in Arabidopsis. In *The Arabidopsis book* 10, e0160. DOI: 10.1199/tab.0160.

Sturm, A. (1999): Invertases. Primary Structures, Functions, and Roles in Plant Development and Sucrose Partitioning. In *Plant physiology* 121 (1), pp. 1–8. DOI: 10.1104/pp.121.1.1.

Sugden, Christopher; Donaghy, Paul G.; Halford, Nigel G.; Hardie, D. Grahame (1999): Two SNF1-Related Protein Kinases from Spinach Leaf Phosphorylate and Inactivate 3-Hydroxy-3-Methylglutaryl-Coenzyme A Reductase, Nitrate Reductase, and Sucrose Phosphate Synthase in Vitro. In *Plant Physiol.* 120 (1), pp. 257–274. DOI: 10.1104/pp.120.1.257.

Sulpice, Ronan; Flis, Anna; Ivakov, Alexander A.; Apelt, Federico; Krohn, Nicole; Encke, Beatrice et al. (2014): Arabidopsis coordinates the diurnal regulation of carbon allocation and growth across a wide range of photoperiods. In *Molecular plant* 7 (1), pp. 137–155. DOI: 10.1093/mp/sst127.

Szecowka, Marek; Heise, Robert; Tohge, Takayuki; Nunes-Nesi, Adriano; Vosloh, Daniel; Huege, Jan et al. (2013): Metabolic fluxes in an illuminated Arabidopsis rosette. In *The Plant cell* 25 (2), pp. 694–714. DOI: 10.1105/tpc.112.106989.

Takeda, Y.; Hizukuri, S. (1981): Re-examination of the action of sweet-potato beta-amylase on phosphorylated (1->4)-α-D-glucan. Takeda, Y., and Hizukuri, S. In *Carbohydrate Research* 89, pp. 174–178.

Tiessen, Axel; Prescha, Katrin; Branscheid, Anja; Palacios, Natalia; McKibbin, Rowan; Halford, Nigel G.; Geigenberger, Peter (2003): Evidence that SNF1-related kinase and hexokinase are involved in separate sugar-signalling pathways modulating post-translational redox activation of ADP-glucose pyrophosphorylase in potato tubers. In *Plant J* 35 (4), pp. 490–500. DOI: 10.1046/j.1365-313X.2003.01823.x.

Tome, Filipa; Nägele, Thomas; Adamo, Mattia; Garg, Abhroop; Marco-Llorca, Carles; Nukarinen, Ella et al. (2014): The low energy signaling network. In *Frontiers in plant science* 5, 353. DOI: 10.3389/fpls.2014.00353.

Tymowska-Lalanne, Z.; Kreis, M. (1998): Expression of the Arabidopsis thaliana invertase gene family. In *Planta* 207 (2), pp. 259–265. DOI: 10.1007/s004250050481.

Usadel, Bjorn; Blasing, Oliver E.; Gibon, Yves; Retzlaff, Kristin; Hohne, Melanie; Gunther, Manuela; Stitt, Mark (2008): Global transcript levels respond to small changes of the carbon status during progressive exhaustion of carbohydrates in Arabidopsis rosettes. In *Plant physiology* 146 (4), pp. 1834–1861. DOI: 10.1104/pp.107.115592.

van Handel, E.; Haeger, J. S.; Hansen, C. W. (1972): The Sugars of Some Florida Nectars. In *American Journal of Botany* 59 (10), pp. 1030–1032.

Velickovic, Tanja; Ognjenovic, Jana; Mihajlovic, Luka (2012): Separation of Amino Acids, Peptides, and Proteins by Ion Exchange Chromatography. In Inamuddin, Mohammad Luqman (Eds.): Ion Exchange Technology II. Applications, pp. 1–34.

Zeeman, Samuel C.; Smith, Steven M.; Smith, Alison M. (2007): The diurnal metabolism of leaf starch. In *The Biochemical journal* 401 (1), pp. 13–28. DOI: 10.1042/BJ20061393.

Zhang, Yuhua; Primavesi, Lucia F.; Jhurreea, Deveraj; Andralojc, P. John; Mitchell, Rowan A. C.; Powers, Stephen J. et al. (2009): Inhibition of SNF1-related protein kinase1 activity and regulation of metabolic pathways by trehalose-6-phosphate. In *Plant physiology* 149 (4), pp. 1860–1871. DOI: 10.1104/pp.108.133934.